NASA
Technical
Paper
1850

1987

Straight Cylindrical Seal for High-Performance Turbomachines

Robert C. Hendricks

Lewis Research Center
Cleveland, Ohio

National Aeronautics
and Space Administration

**Scientific and Technical
Information Office**

Contents

	Page
Summary	1
Introduction	1
Symbols	2
Apparatus, Instrumentation, and Procedure	3
Theoretical Background	3
Results and Discussion	5
Concentric Configuration—Simulating Normal Operation	6
Fully Eccentric Configuration—Simulating Point of Rub	7
Some Effects of Backpressure Control	10
Flow Coefficient Analogy	11
Summary of Results	11
Appendixes	
A—Fanno-Raleigh Relations	12
B—Gas Injection	12
C—Model—Including Vapor Production at Wall	13
References	14
Figures	15
Tables	
I.—Pressure Tap Locations for Straight Cylindrical Seal	48
II.—Critical Constants Used in Reducing Parameters	48
III.—Flow Rate and Pressure Drop Data for Straight Cylindrical Seal, Concentric Position	49
IV.—Flow Rate and Pressure Drop Data for Straight Cylindrical Seal, Fully Eccentric Position	65
V.—Flow Rate and Pressure Drop Data for Straight Cylindrical Seal With Backpressure Control, Partially Eccentric Position	70
VI.—Hydrogen Choked-Flow Data	72

Summary

A straight cylindrical seal configuration representing the seal for a high-performance turbopump (e.g., the space shuttle main engine fuel pump) was tested under static (*nonrotating*) conditions. The test data included critical mass flux and pressure profiles over a wide range of fluid conditions at concentric and fully eccentric seal positions.[1] The critical mass fluxes (or leakage rates) for the concentric and fully eccentric configurations were nearly the same when based on stagnation conditions upstream of the seal inlet. The fully eccentric configuration pressure profiles of the gas and liquid were different. Further, the pressure differences between the maximum- and minimum-clearance positions were highly dependent on the geometric conditions, the temperature, and the pressure at both the inlet and the exit, with the greatest pressure differences in the inlet region with profile crossover within the passage. These differences are most important to the dynamic stability of a turbomachine.

Critical mass flux and pressure profiles for hydrogen flowing through a shaft seal offset by one-third of the nominal clearance indicated a suppression of two-phase choked flow as the backpressure at the exit reached the thermodynamic critical pressure. Injecting gaseous helium near the seal exit plane (close to the region where two-phase flow begins) substantially increased upstream pressure. Injecting gas into fluids[2] (gas or liquid) within the seal could control turbomachine instabilities. High-pressure, high-temperature hydrogen gas could be used for this purpose in an alternative design.

Some tests with fluid nitrogen demonstrated an anomalous pressure rise near the seal exit along the maximum-clearance position. The unusual pressure profile crossovers are characteristic of a skewed geometry and could represent a shaft under large bending loads or passing through critical speeds. However, the geometric position could not be verified and these profiles remain unexplained.

Data were taken over a range of inlet pressures and temperatures with fluid nitrogen and fluid hydrogen. The results, although complex, tend to follow the corresponding-states principles for critical flows. The mass flux profiles of this annular configuration can be roughly compared with those of an orifice; the pressure profiles can be compared with those characteristic of a long tube.

Introduction

In the early phases of the space shuttle main engine program excessive leakage and vibrations engendered catastrophic turbomachine failures that in many cases destroyed the entire apparatus. From the accident investigations it was postulated that the excessive vibrations were caused by the seals. However, the seal geometry and fluid conditions leading to such unstable operations were unknown.

Although there are many reports on the design of shaft seals for perfect gas flows (e.g., refs. 1 and 2), little information, experimental or theoretical, is available to guide the designer when the shaft seal must accommodate a real fluid over a wide range of thermodynamic states. Four fundamental problems exist:

(1) How can the leakage rate be determined?

(2) How do the pressure profiles respond to eccentric positioning?

(3) How can these results be applied to other working fluids?

(4) What is the role of backpressure?

In many hydrodynamically similar cases, critical flow rates through openings can be adequately described by using one-dimensional flow equations. The results can be parametrized in terms of inlet stagnation conditions as long as the stagnation-to-backpressure ratio is sufficiently large to choke the flow. (In these tests the simulated turbopump shaft does not rotate in the housing; the design simulation is a static configuration.)

A program was thus begun to evaluate seals for the space shuttle main engine fuel turbopump. The first purpose of this program was to establish the mass fluxes (leakage rates) for a straight cylindrical, a three-step cylindrical, and a three-step labyrinth shaft seal in both the concentric and eccentric positions. Although the primary purpose of a seal is to control leakage, an equally important purpose is to control dynamics. Eccentric positioning of the shaft can lead to nonuniform pressure profiles, which imply nonuniform loadings, which in turn affect shaft dynamics and seal leakage rates.

[1]All of the data and information obtained from these tests was released for general use in May 1977.

[2]Fluid refers to a thermodynamic state independent of temperature, pressure, or density – the use of the terms liquid and gaseous herein are redundant but convenient for may readers. In this sense the fluid enters the test section nominally in the liquid state. And in most cases two-phase flow can and probably does occur within the test section much of the time.

Thus the second purpose of this program was to determine the pressure profiles in the simulated seal configuration with the centerbody set in both concentric and eccentric positions. The fully eccentric position permitted a 0.2692-mm (0.0106-in.) gap at 180°, the maximum-clearance position, but touched the housing at 0°, the point of rub. This provided insight into seal dynamics, which significantly affect turbomachine dynamics.

The third purpose was to establish the credibility of the corresponding-states approach, which minimizes testing with hazardous and expensive fluids such as liquid oxygen and parahydrogen. If established, this approach could provide designers of both hydrogen and liquid oxygen seals with leakage rate data and pressure profiles. These results could then be extended to seal designs for any fluid obeying the corresponding-states principles.

One philosophy of seal design is that when the backpressure is above the thermodynamic critical pressure, two-phase flow within the seal is not possible. Although this is generally an incorrect assumption for stagnation entropies less than the thermodynamic critical entropy in simple geometries such as a venturi, the thesis that two-phase flow can also occur in a seal must be demonstrated for these complex geometries. Thus the fourth purpose was to investigate the effects of backpressure on mass flux and pressure profiles.

The results for the straight cylindrical seal are given in this report. Complementary data and results for a three-step cylindrical seal and a three-step labyrinth seal in a similar configuration are given in references 3 and 4.

Symbols

A	area, cm^2 (in.^{2})
C	damping, N s/m (lbf s/in.)
C_f	flow coefficient, $G_R/G_{R,v}$
C_p	specific heat at constant pressure, J/g K (Btu/lbm °R)
c	clearance, cm (in.)
D	diameter, cm (in.)
F	response (or forcing) function, N(lbf)
f	Fanning friction factor
G	mass flux, g/cm^2 s (lbm/in.^{2} s)
G_R	reduced mass flux, $G/G^*(1 + \psi_Q)$
G^*	flow-normalizing parameter (6010 g/cm^2 s (85.5 lbm/in.^{2} s) for nitrogen), $\sqrt{P_c\rho_c/Z_c}$
h	enthalpy, J/g (Btu/lbm)
K	stiffness, N/m (lbf/in.)
K_T	isothermal compressibility factor, $-(\partial \ln V/\partial P)_T$, MPa^{-1} (psia^{-1})
k	slip ratio (set to unity)
L	length, cm (in.)
M	mass, g (lbm)
P	pressure, MPa (psi)
R	gas constant, MPa cm^3/g K (psi in.^{3}/lbm °R)
Re	Reynolds number
S	entropy, J/g K (Btu/lbm °R)
T	temperature, K (°R)
u	velocity, cm/s (in./s)
V	specific volume, cm^3/g (in.^{3}/lbm)
$\dot{w}$	mass flow rate, g/s (lbm/s)
x	mass fraction of vapor
Z	PV/RT compressibility
z	axial position, cm (in.)
β	volumetric expansion coefficient, $(\partial \ln V/\partial T)_P$, K^{-1} (°R^{-1})
μ	viscosity, Pa s (psi s)
ρ	density, g/cm^3 (lbm/in.^{3})
τ	shear stress, Pa (psi)
φ	thermodynamic isoproperty path
ψ_Q	quantum correction factor

Subscripts:

c	thermodynamic critical value
e	exit
ecc	eccentric
g	gas
h	hydraulic
i	arbitrary axial position
ℓ	liquid
m	mean, for two-phase flow
max	maximum
o	inlet stagnation conditions
PG	perfect gas
R	reduced by corresponding-states parameter
sat	saturation value
t	throat
v	venturi
w	wall
x,y	reference positions
0	particular point in inlet (see fig. 23)
180°	180° to reference position

Superscripts:

—	average value

Apparatus, Instrumentation, and Procedure

The system of reference 5 was used, but a variety of hardware changes were required to accommodate the proposed interstage seal configurations for the space shuttle main engine fuel pump.

Selective modifications are described to indicate some of the difficulties in adapting these proposed designs to a real system. The facility installation (fig. 1) choked in the "plumbing" somewhere downstream of the seal – presumably in the exit mixing chamber of the flow system. From preliminary testing it became quite apparent that the flow rates were going to be higher than the predicted maximum of 115 g/s (1/4 lbm/s) for parahydrogen. Thus the downstream piping was too small and had to be enlarged (fig. 2) to permit operation with fluid hydrogen or fluid nitrogen. This modified configuration, consisting of an exhaust tube 7.62 cm (3 in.) in diameter, demonstrated that the choked condition could be maintained within the seal.

To demonstrate choking, the system was operated in three stages: (1) with gas flowing without a vent, (2) with gas or liquid flowing through the restricted 7.62-cm- (3-in.-) diameter exhaust tube, and (3) with the system reconnected to the vents above the roof. The 7.62-cm- (3-in.-) diameter exhaust tube had a 5.72-cm- (2¼-in.-) diameter flange connection, which served as an orifice type of restriction. The pressures at the exit flange for these three stages of system operation were typically 0.103, 0.134, and 0.383 MPa (15, 19.5, and 55.5 psia), respectively. However, although the flow rate remained invariant, the slope of the pressure profiles changed at the exit plane, similar to what would be expected with a long tube. The system was again modified (fig. 3) to permit operation with fluid hydrogen. The fluids were discharged through dual 5-cm- (2-in.-) diameter vent stacks with four exhaust ports 9 m (28 ft) above the roof. The straight cylindrical seal configuration was installed as the test section in the modified test facility (fig. 4). The venturi differential-pressure transducer range was increased to approximately 2 MPa (300 psid) to accommodate the higher flow rates, and the allowable facility abortable flow rate was increased to 300 g/s (2/3 lbm/s) for 45 s maximum. For these high flow rates the exhaust ports were carefully monitored for the dispersion and direction of plume flow. The cold hydrogen often approached, but did not touch, the roof. In general, the dissipation was very good. The key safety requirements were that all elements of the flow system be grounded and that no possible sources of arcs, sparks, or open flames be permitted in the test facility area.

In the straight cylindrical seal configuration (fig. 5) the seal centerbody was 8.4244 cm (3.3167 in.) in diameter and the housing was 8.4513 cm (3.3273 in.) in diameter, providing a cylindrical annular passage about 4.13 cm (1⅝ in.) long and 0.0135 cm (0.0053 in.) high. The centerbody was concentrically positioned in the housing to within 0.00127 cm (0.0005 in.). The conical inlet and exit flanges served as adaptors to our system and were not part of the seal.

A simulated shaft, a straight cylindrical centerbody, and a housing were used to represent a straight cylindrical seal configuration for a high-performance turbopump (e.g., the space shuttle main engine fuel pump). All tests were conducted under static (*nonrotating*) conditions. Pressure taps (fig. 6) were installed along the centerbody at seven distances from the seal inlet plane, one set at the 0° circumferential position and a similar set diametrically opposite at 180°, as shown in table I. At the 3.9980-cm (1.574-in.) axial position additional taps were provided at 90° and 270° (fig. 6). The seal and housing are shown in figure 7.

Pressure and temperature were also monitored in the conical inlet and exit reservoirs. These temperatures, however, were measured by insertion thermocouples and are included for reference only. The inlet temperature was measured by platinum thermometry in the inlet mixing chamber. Prior to a run series the system was capped off by removing the 7.62-cm- (3-in.-) diameter exhaust tube and placing a plate over the exhaust port; the system was then pressurized with nitrogen gas. Next the pressure transducers were calibrated by setting all of them to read the same pressure at two different levels. This ensured consistency of the readings while sacrificing perhaps ±0.014 MPa (±2 psia) in the absolute level. The transducers were electronically set to zero prior to pressurization.

The backpressure was controlled by injecting gas into the conical exit reservoir and adjusting a small valve at the exhaust port. Further details are given in reference 3, which describes the results of the three-step cylindrical seal tests.

Data were taken in the following sequence: (1) concentric position, (2) eccentric position, and (3) concentric and eccentric positions with backpressure control. The system was modified and upgraded during the sequence. Thus not all data points contain the same amount of information. General system accuracies follow those of reference 5.

Theoretical Background

Much of the theoretical and experimental work on two-phase choked flows and applications of the corresponding-states principles and other principles of similarity to choked flows is discussed in references 6 to 10 with additional material in references 11 to 14. Most of these studies deal with flows through nozzles, orifices, or slits; however, reference 15 deals with two-phase choked flows in a long tube with a length-to-diameter ratio L/D of 16 200. Thermophysical properties used in the computations in reference 15 and in this report were obtained from the computer code of reference 16. For a review of the Fanno-Rayleigh relations that were used, see appendix A.

In a duct such as that illustrated in figures 5 and 6, one-dimensional flow may be assumed and the two-phase momentum equation written as

$$
\begin{aligned}
-A\,dP - \tau_w\,dA_w &= \dot{w}\,du \\
&= \dot{w}^2\,d\left(\frac{V_m}{A}\right) \\
&= d\left[(\dot{w}u)_g + (\dot{w}u)_\ell\right] \\
&= d\left[\dot{w}u_\ell\left(x\frac{u_g}{u_\ell} + (1-x)\right)\right]
\end{aligned}
\tag{1}
$$

where

$$\dot{w} = \frac{\dot{w}_g}{x} = \frac{\dot{w}_\ell}{1-x} = \text{constant} \tag{2}$$

and

$$\dot{w}_g = (\rho u A)_g \qquad \dot{w}_\ell = (\rho u A)_\ell \qquad \dot{w} = \rho u A \tag{3}$$

From these latter relations we may write

$$\frac{A_g}{A} = \frac{x\dot{w}}{\rho_g u_g A} = 1 - \frac{(1-x)\dot{w}}{\rho_\ell u_\ell A} \tag{4}$$

and, solving for u_ℓ in terms of u_g/u_ℓ,

$$u_\ell = \frac{\left(\frac{\dot{w}}{A}\right)}{\left(\frac{u_g}{u_\ell}\right)}\left[\frac{x}{\rho_g} + \frac{1-x}{\rho_\ell}\left(\frac{u_g}{u_\ell}\right)\right] \tag{5}$$

Thus we find that the mean or average specific volume V_m can be written in terms of specific volumes as

$$V_m = \left[\frac{xV_g + (1-x)V_\ell\left(\frac{u_g}{u_\ell}\right)}{\frac{u_g}{u_\ell}}\right]\left[x\left(\frac{u_g}{u_\ell}\right) + (1-x)\right] \tag{6}$$

Defining the hydraulic diameter as

$$D_h = 4A\frac{dz}{dA_w} \tag{7}$$

and

$$f = \frac{2\tau_w}{\rho u^2} \tag{8}$$

which is the Fanning friction factor, we assume $k = u_g/u_\ell = 1$ in order to use standard friction factor charts.

We now write the governing equations in terms of V, A, and P:

$$-V\,dP = \dot{w}^2\frac{V}{A}\,d\left(\frac{V}{A}\right) + \dot{w}^2\frac{4f}{2D_h}\left(\frac{V}{A}\right)^2\frac{dz}{dP}\,dP \tag{9}$$

Integrating yields

$$\dot{w}^2 = \frac{-2\left(\frac{A}{V}\right)_i^2\int_{P_o}^{P_i} V\,dP}{\left\{1 - \left[\frac{\left(\frac{V}{A}\right)_o}{\left(\frac{V}{A}\right)_i}\right]^2\right\} + \left(\frac{A}{V}\right)_i^2\int_{P_o}^{P_i}\frac{4f}{D_h}\left(\frac{V}{A}\right)^2\frac{dz}{dP}\,dP}$$

or

$$G_i^2 = \frac{-\frac{2}{V_i^2}\int_{P_o}^{P_i} V\,dP}{1 - \left(\frac{u_{P_o}}{u_{P_i}}\right)^2 + \left(\frac{A}{V}\right)^2\int_{P_o}^{P_i}\frac{4f}{D_h}\left(\frac{V}{A}\right)^2\frac{dz}{dP}\,dP} \tag{10}$$

Differentiating equation (10) with respect to the exit pressure ($P_i \to P_e \to P_t$), assuming $u_{P_o}/u_P << 1$, and using the criterion for choked flows

$$\left.\frac{dG}{dP}\right|_e = 0 \tag{11}$$

yields the maximum value of mass flux, which becomes

$$-G_{\max}^2 = \frac{1 - \frac{2}{V}\frac{dV}{dP}\int_{P_o}^{P} V\,dP}{\left[A\frac{dA}{dP} - \left(\frac{A}{V}\right)^2\frac{dV}{dP}\right]\left[\int_{P_o}^{P_t}\frac{4f}{D_h}\left(\frac{V}{A}\right)^2\frac{dz}{dP}\,dP + \frac{4fV}{D_h}\frac{dz}{dP}\right]_e} \tag{12a}$$

Substituting equation (10) for G_{max} and following some algebra yields

$$-G_{max}^{-2} = \frac{dV}{dP} + A\frac{dA}{dP}\Big|_{P_o}^{P_t} \frac{4f}{D_h}\left(\frac{V}{A}\right)^2 \frac{dz}{dP}dP + V\frac{4f}{D_h}\frac{dz}{dP}\Bigg|_e \quad (12b)$$

Near the choking plane, $(dz/dP) \rightarrow 0$ and for these flows $(dA/dP) \rightarrow 0$; further, the effect of friction over very short distances is negligible. Thus equation (12) becomes

$$-G_{max}^2 = \left(\frac{dP}{dV}\right)_e \quad (13)$$

where G_{max} is a function of thermodynamic state parameters.

For isothermal flows

$$-G_{max}^{-2} = \left(\frac{K_T}{V}\right)_e \quad (14)$$

where K_T is the isothermal bulk modulus and, as such, is established by thermodynamic state conditions independently of fluid or flow conditions.

For isentropic flows

$$-G_{max}^2 = \frac{V}{K_T} - \frac{V^2T}{C_p}\beta^2 \quad (15a)$$

where β is the volumetric expansion coefficient and C_p is specific heat. Again G_{max} is established by thermodynamic state conditions, and at the thermodynamic critical point

$$G_{max} \rightarrow 0 \quad (15b)$$

To determine the exit conditions, we need to solve for the pressure profile. Since $A = A(z)$ with $V = V(P,\varphi)$, where φ represents the thermodynamic isoproperty path the expansion is assumed to follow (e.g., isentropic), equation (9) may be rewritten as follows:

$$-\frac{dP}{G^2} = \frac{dV}{dP}dP - \frac{V}{A}\frac{dA}{dz}dz + V\frac{4f}{2D_h}dz \quad (16)$$

and solving for dP,

$$dP = \left[\frac{V\left(\frac{1}{A}\frac{dA}{dz} - \frac{4f}{2D_h}\right)}{\frac{1}{G^2} + \frac{dV}{dP}}\right]dz \quad (17)$$

The pressure profile is determined from equation (17), and the mass flux is determined from equation (10) and is subject to the constraint equation (13).

Once the mass flux has been determined, we can use the principles of corresponding states to normalize the flux

$$G_R = \frac{G}{G^*} \quad (18)$$

where

$$G^* = \sqrt{\frac{P_c\rho_c}{Z_c}} \quad (19)$$

and to produce design charts. For an example see figures 8 and 9, which are reproduced from reference 8. The mass flux and pressure profiles of various fluids are compared, using the corresponding-states principles, in figures 10 and 11, respectively (from ref. 7). The normalizing parameters and critical constants for several fluids are given in table II. The applicability of the corresponding-states principles was conclusively demonstrated in reference 6 for nozzles, was more recently discussed in references 17 and 18, and is demonstrated in this report for coaxial geometries. The theoretical predictions, equations (10), (13), and (17), are not a priori in this report because inlet and exit effects were not known; rather the constants or levels were established empirically and the trends followed, as in the flow coefficient technique. This in no way affected the reduced experimental data results or trends.

The data for this investigation are presented using the theoretical material in this section as background information.

Results and Discussion

This section discusses (1) the concentric position, simulating normal operation; (2) the applicability of the principles of corresponding states to this configuration; (3) the fully eccentric position, simulating rotor dynamics to the point of rub; (4) the effects of backpressure on flow and pressure profiles; and (5) the flow coefficient analogy.

The data were taken in four stages—where the working fluids were gaseous nitrogen, liquid nitrogen, gaseous normal hydrogen, and liquid parahydrogen—as part of a systematic approach to achieving valid data while minimizing operations with hydrogen. The data taken with the straight cylindrical seal are tabulated in this report, and data for the three-step cylindrical and labyrinth seals are tabulated in references 3 and 4, respectively.

Concentric Configuration—Simulating Normal Operation

The experimental data for the straight cylindrical seal in the concentric configuration are given in table III.

Gaseous data.—The reduced critical mass flux and pressure profiles for gaseous nitrogen flowing through the straight seal (figs. 12 and 13, respectively) were taken without the conical exit flange. This configuration provided the minimum backpressure necessary to confirm choking. Data for a venturi (ref. 6) are included for comparison. Comparisons with previous pressure profiles and mass fluxes (i.e., those with the conical exit flange and exhaust lines in place) showed that these results represented critical flow through the seal. Further, the pressure drop at the exit satisfied that of choked flow for gases (i.e., ~ 2:1). Note that although these mass fluxes were large for this system, they were about one-sixth that for liquid nitrogen. Note further that the pressure profile curvature[3] was negative downward (parabolic), a characteristic of friction pressure drop with fluid acceleration, and dropped quite sharply right at the seal exit plane.

The locus representing the gaseous oxygen data for a venturi was approximately 1.4 times higher than the data of figure 12. Because these flow rates deviated approximately the same amount as those between an orifice and a venturi, a simplistic way of referencing these data is to consider this configuration to behave like an orifice. Such an analogy proved to be valid for the mass flux but invalid for the pressure profiles. The pressure distributions at 0°, 90°, 180°, and 270° (fig. 13) were uniform around the simulated shaft to within 5 percent; these pressure differences were extremely sensitive to small changes in eccentricity and could be used as position monitors.

Liquid data.—The critical reduced mass fluxes and the pressure profiles for liquid nitrogen flowing through the seal are illustrated in figures 14 and 15, respectively. In three separate operations the effective backpressure was physically changed to convince the author that the system was choked at the seal and not elsewhere in the system (as discussed in the **Apparatus, Instrumentation, and Procedure** section). The alterations necessary to prove that changes in backpressure did not significantly affect the mass flow also provided information on this seal configuration. The data appeared quite consistent for a range of reduced pressures at a reduced temperature $T_{R,o}$ of 0.7. The normalizing parameters for various fluids are given in table II and figure 16.

Also plotted in figure 14 is the locus representing the liquid oxygen data of reference 6 for a venturi. Multiplying the venturi results by 0.61 closely simulates orifice data. Further, the orifice locus closely parallels the data for this seal configuration. These results reinforced the simplistic view of the leakage of this seal—as that of an orifice. However, note that the slope of the pressure profiles in figure 15 is positive near the exit. Such profiles are characteristic of two-phased choked flows in long tubes (ref. 15). This illustrates the complexity of these flow patterns; thus the simplistic view is useful only as a simple reference tool. It will also become apparent that small changes in eccentricity effect large changes in circumferential pressure distribution.

Although mass flux and pressure profiles have been established for the straight seal in the concentric position, the application of the corresponding-states principles remains to be demonstrated.

Fluid hydrogen and corresponding states.—As the original goal was to determine hydrogen leakage through the seal, it became of paramount importance to run hydrogen (1) to demonstrate the applicability of the corresponding-states principles to this configuration and (2) to determine some basic flow (or leakage) data for this configuration with hydrogen.

The critical mass flux and pressure profiles for liquid hydrogen flowing through the straight cylindrical seal (figs. 17 and 18, respectively) at first appeared to be significantly lower than those for gaseous nitrogen (figs. 12 and 14). Hence it might have been concluded that the corresponding-states principles do not apply. However, when the reduced inlet stagnation temperature ($T_{R,o} = T_o/T_c$), namely, of the order of 8 for hydrogen and 2 for nitrogen, was taken into account, the gaseous data properly correlated as

$$G_R \frac{\sqrt{T_{R,o}}}{P_{R,o}} = \frac{C_f}{5} \tag{20}$$

where C_f is the flow coefficient. To provide further evidence, several points were taken at the termination of a liquid hydrogen run; the $T_{R,o}$ was of the order of 2.2 and was considered gaseous. A point in reduced T,P (temperature, pressure) coordinates was found that corresponded almost precisely to a nitrogen point. The two plots fell directly together on the plot (fig. 17).

The liquid hydrogen data of figures 17 and 18 fell almost directly on the liquid nitrogen data (fig. 14).[4] It might now have been concluded that the corresponding-states principles could be applied and that prediction of flows at higher pressures would follow the theoretical model. This appeared to be a valid premise until a second set of hydrogen data were acquired that fell 12 percent below the previous hydrogen results. Subsequent checks of the transducers and records revealed that the inlet temperatures might have been off by 1 to 2 deg K. To resolve this dilemma, a third set of hydrogen mass flux data were taken (fig. 19) that revealed how highly sensitive the locus was to small changes in inlet temperature. The corresponding pressure profiles are given in figure 20. From previous experimental and theoretical work on the application of the corresponding-states principles to two-phase choked flows (e.g., refs. 6 to 15) and from data herein, the

[3]Curvature is defined with respect to the pressure-axial position axis of the pressure profile plot.

[4]At the lower values of $T_{R,o}$ it was necessary to use the quantum correction factor ψ_Q, illustrated in figure 16(a), in addition to the theoretical model developed in the section **Theoretical Background.**

author felt that the nitrogen and hydrogen results followed the corresponding-states principles to within ± 5 percent depending somewhat on friction and inlet effects, which are irreversible losses.

The helium injection pattern, tap, and pressure transducers are discussed in appendix B.

Finally, the nature of the mass flux and pressure profiles was demonstrated at inlet temperatures to and above the thermodynamic critical temperature. Because hydrogen profiles are highly sensitive to temperature (further discussed in the section **Fully Eccentric Configuration—Simulating Point of Rub**), only the data for fluid nitrogen are presented in figure 21. The data for the several isotherms are quite distinct even though the isotherm variations are small. Isothermal data above the reduced value of unity are limited.

Gas injection.—A system was then conceived and tested whereby the pressure profile through the seal would become more uniform, thereby significantly increasing seal dynamic stiffness. Injecting gaseous helium[5] upstream but close to the region where the pressure equaled the cavitation pressure increased the pressure upstream of the injection point. In short, the characteristic concave downward profile for liquids became concave upward (e.g., compare fluid hydrogen runs 820 and 824). Injecting helium gas into nitrogen gas significantly increased the pressure upstream and rapidly decreased it downstream. (See fig. 22 and appendix B for further details.) Properly controlled gaseous injection could provide seal dynamic stability and in turn effectively control turbomachine stability.

Summary for concentric position.—The following is a summary for the straight cylindrical seal in normal operation, where the nonrotating centerbody on a shaft was set concentrically in the housing.

(1) Hydrogen and nitrogen mass flux and pressure profiles over a range of inlet pressures and temperatures were acquired and tabulated. In this configuration the flow area was a concentric annulus 4.13 cm (1⅝ in.) long by 0.0135 cm (0.0053 in.) high with a 0.357-cm^2 (0.0553-in.^{2}) cross-sectional area.

(2) The corresponding-states principles can be applied to these data, and extrapolation of basic design charts and theoretical calculations to higher pressures or temperatures should result in mass flux errors no greater than ± 10 percent. However, the effects of friction must be properly handled in the theoretical calculation, and it should be realized that fluid[6] hydrogen is sensitive to small changes in inlet stagnation conditions because of its low thermodynamic critical point. Simplistically one may consider the liquid flow leakage to behave like that for an orifice and the pressure profile to behave like that for a long tube.

(3) Injecting gaseous helium immediately upstream of the seal exit plane substantially flattened the pressure profile and could be used as a dynamic control mechanism.

[5]Helium was injected through pressure tap 5. See appendix B.

[6]See footnote 2.

Fully Eccentric Configuration—Simulating Point of Rub

In this section the results are presented in three parts: (1) mass flux data, (2) pressure profiles, and (3) assessment of circumferential pressure differences for the fully eccentric case, including examples. The seal was placed in its fully eccentric position (fig. 23). A subsequent investigation of the seal revealed that the eccentric position of the pressure taps was a maximum of 17° off the centerline of the true fully eccentric position. Although the difference between pressures at 0° and 17° should be small, it must be realized and considered when interpreting the pressure data of subsequent tables and figures. Data for the cylindrical seal in its fully eccentric position are given in table IV.

Mass flux data.—The critical reduced mass fluxes (leakage rates) for gaseous and fluid nitrogen through the straight seal in the fully eccentric position are shown in figure 24. The initial observations for gaseous nitrogen indicated the flows to be the same as those through the straight seal in the concentric configuration (based on the same flow area, as described in the previous section). This observation also appeared to be valid for liquid nitrogen and for those data where $T_{R,o} > 1$. In the previous section it was found that the hydrogen data were quite sensitive to inlet temperature; the nitrogen data of figure 24 appeared to be equally sensitive. This does not imply that the nitrogen data for the concentric configuration were not as sensitive: isotherm separations of 1 percent or better must be made in the data in order to distinguish the sensitivity. The critical reduced mass flux data for the fully eccentric and concentric configurations appeared to follow the same reduced isotherms when the reduced pressure was based on the stagnation pressure at the 0° position (fig. 23).

Likewise, the critical reduced mass fluxes for gaseous and fluid hydrogen (fig. 25) were nearly the same for the fully eccentric configuration, as they were for the concentric configuration of the previous section. The quantum correction factor $(1 + \psi_Q)$, figure 16(a), had to be evaluated at each isotherm in order to reduce these data in a corresponding-states manner. Comparing these data and those of figure 24 for the same isotherms again indicated that fluid nitrogen data could be used to predict fluid hydrogen flow rates (and vice versa). These results suggested a further extension of the applicability of the corresponding-states principles to flows through eccentric passages as well as to those through concentric passages and simple geometries such as the venturi and the orifice.

Pressure profiles.—Although the mass fluxes for the concentric and fully eccentric configurations appeared to be similar, the pressure profiles were quite different. Simplistically the dynamics may be pictured as a spring-damper-mass system excited by an external force:

$$F = KX + C\dot{X} + M\ddot{X} \tag{21}$$

Realistically K, C, and M are matrices whose components are coupled to the fluid and the structure, and F and X are force

and displacement vectors, respectively. Usually $\boldsymbol{F}$ and $\boldsymbol{X}$ are described by two coordinates or in complex form, for example, $\boldsymbol{F} = F_x + iF_y$, where $i = \sqrt{-1}$. Here $\boldsymbol{F}$ is the response (or forcing) function, K the stiffness, C the damping, and M the mass. As the system did not rotate, the only term that can be approximated is the direct stiffness coefficient of the K matrix, which is directly related to the difference in pressure at the 0° and 180° positions along the seal axis of rotation.

Gaseous nitrogen: Typical gaseous nitrogen pressure profiles for the fully eccentric configuration (fig. 26) show the pressure at the inlet to be higher at 0° than at 180°. However, about three-fourths of the way through the seal the profiles crossed over, and near the exit the pressure at 180° was significantly higher than the pressure at 0°. The pressure differences at these positions exert a significant force on seal configurations. In fact the pressure difference-eccentricity ratio is a measure of the direct stiffness of the seal, and a positive stiffness implies stability. Although the total stiffness is positive, the crossover represents a region of negative stiffness and is not only undesirable but unavoidable.[7] Subsequent measurements of the centerbody indicated a 0.0005- to 0.001-mm (0.0002- to 0.0004-in.) divergence in the clearance diameters from the inlet to the exit. Although not a significant factor in the mass flux, such a divergence can cause negative stiffness. However, a convergence from inlet to exit would enhance the region of positive stiffness.[8]

Liquid nitrogen: As for gaseous nitrogen typical liquid nitrogen pressure profiles for the fully eccentric configuration (fig. 27) show the pressure at the inlet to be significantly higher at 0° than at 180°. However, these profiles converged in the same region where the gaseous nitrogen profiles tended to cross over and diverge. This may be due to vapor production, which may force uniformity as did gas injection (appendix C).

Gaseous hydrogen: The typical gaseous hydrogen pressure profiles shown in figure 28 are quite similar to those for gaseous nitrogen (fig. 26). The crossover in both cases implies regions of positive and negative stiffness.

Liquid hydrogen: The liquid hydrogen pressure profiles shown in figure 28 are also similar to those for liquid nitrogen (fig. 27). The crossover region is subdued or moved to the exit plane. For both fluids the liquid pressure profiles at 0° and 180° are separated at the inlet and tend to merge near the exit. The problem now becomes how to assess and predict these pressure differences.

Circumferential pressure differences.—A second look at the gaseous pressure profile data (figs. 26 and 28) indicated that at 3.998 cm (1.574 in.) from the inlet plane pressures at 0°, 90°, and 270° were similar but differed from those at 180°. Since 180° was the only axial pressure-tap location between 90° and 270°, the "cosine variation" in the circumferential profiles can only be inferred.

A similar examination of the liquid data (figs. 27 and 28) indicated comparatively little difference between the 0°, 90°, 180°, and 270° pressure readings at 3.998 cm (1.574 in.) from the seal inlet.

Describing the reduced inlet pressure differences between 0° and 180° yields

$$\left.\frac{\Delta P_{ecc}}{P_0}\right|_{in} = \frac{P_{0°} - P_{180°}}{P_{0°}} \tag{22}$$

In a sense $\Delta P_{ecc}/P_0|_{in}$ is a measure of seal direct stiffness. The greater the $\Delta P_{ecc}/P_0|_{in}$ for a seal in an eccentric position, the greater the seal stiffness. Here the seal is fully eccentric.

Fluid nitrogen: For fluid nitrogen the reduced inlet pressure differences $\Delta P_{ecc}/\Delta P_0|_{in}$ (fig. 29) were constant at 0.09 for reduced inlet stagnation temperatures $T_{R,o} > 1$, dipped to a minimum near $T_{R,o} = 1$, and rose steeply for $T_{R,o} < 1$. Note that at one point the inlet conditions were quite close to the thermodynamic critical point, indicating that the profile differences may dip as low as 0.06. Although at first this may appear to be incongruous, a model discussed in appendix C points to the decrease in flow resistance as the reason for the positive curvature and the merger of the axial pressure profiles. Properties change rapidly in the thermodynamic critical region, and the static conditions at the point where these profiles merged tended to prevail also at the inlet. This is, however, the first evidence that near-critical thermophysical properties affect either the mass fluxes or the pressure profiles in an anomalous way. Such nonlinear profile variations can produce a significant load variation, which in turn affects turbomachine dynamics, especially for systems that operate near or must pass through the thermodynamic critical point en route to the operating condition.

Fluid hydrogen: Applying the criterion of equation (22) to the hydrogen data produced figure 30. Figures 29 and 30 are substantially different near $T_{R,o} = 1$ and are similar at $T_{R,o} >> 1$ and $T_{R,o} < 1$. However, because the outer casing of this seal configuration is subject to ambient conditions that could lead to a "smoothing" of the region near $T_{R,o} = 1$, lower density fluid may be produced near the walls and ingested into the seal configuration. Such ingestion of low-density fluids in liquids has been observed photographically in the study of reference 12. The lower density material may only serve to increase the difference in pressures at 0° and 180°. However, an experiment more sensitive to inlet temperature and environmental heat input might produce distinct changes in both flow and pressure. This is partially evidenced by the nitrogen data, where environmental heat input was significantly lower.

Although it would be difficult to accurately assess the pressure difference defined by equation (22) for an arbitrary isotherm, it should be quite apparent from figures 29 and 30 that at low or high values of $T_{R,o}$ the pressure level $P_{R,o}$ does not significantly alter this pressure difference.

[7]Negative stiffness could be controlled via gas injection as discussed in the section ***Gas injection***.

[8]Single-phase flows; multi-phase flows can have opposite trends.

For those not familiar with reduced parameters a few examples are now given.

Example 1: If the seal inlet conditions for fluid hydrogen at the 0° position are approximately 10.0 MPa (1450 psia)[9] at 26.4 K (47.5 °R) or $T_{R,o} = 0.8$, determine the pressure at the 180° position (seal diameter, 8.4244 cm (3.3167 in.)). From figure 10

$$\left.\frac{P_0 - P_{180°}}{P_0}\right|_{in} = \left.\frac{\Delta P_{ecc}}{P_0}\right|_{in} = 0.17 \tag{23}$$

The pressure at the 180° position becomes

$$P_{180°} = P_0 \times 0.83 = 8.3 \text{ MPa (1200 psia)} \tag{24}$$

a difference of 1.7 MPa (250 psia). This represents a restoring force *per unit of axial length* of 0.143 MN/m-axial (830 lb/in.-axial) acting at the inlet of the cylindrical seal configuration described herein, and a stiffness of $K \sim F/c \sim (0.143\times10^6/1.346\times10^{-4}) \sim 10^9$ N/m m-axial (0.16×10^6 lb/in. in.-axial), for a 0.01346-cm (0.0053-in.) clearance. The pressure profile similar to that of figure 27 (i.e., triangular) has a possible crossover at 3.75 cm (1.47 in.),with negligible stiffness (either positive or negative) generated downstream. Thus the force acts over the length (3.75−0.28 cm) (1.37 in.), or ~3.5 cm (see fig. 6), and the total restoring force becomes (note triangular area) $\frac{1}{2}\times10^9$ N/m m-axial×0.035 m-axial=18 MN m (0.11×10^6 lbf/in.).

Example 2: It may also be instructive to compute an average Reynolds number at 10 MPa and 26.4 K. From table III(b)

$$\left.\begin{aligned} P_{R,o} &= \frac{P_o}{P_c} = \frac{10}{1.2925} = 7.74 \\ T_{R,o} &= \frac{T_o}{T_c} = \frac{26.4}{32.976} = 0.8 \\ G^* &= 1158 \text{ g/cm}^2\text{ s (16.4 lbm/in}^2\text{ s)} \end{aligned}\right\} \tag{25}$$

From figure 16, $\psi_Q = -0.04$. As $P_{R,o}$ is far beyond the data, an extrapolation of the classic venturi solution (eq. (10)) and the mass flux data for the straight seal is necessary. By using data given herein for the concentric and eccentric positions and the flow through a classic venturi, figure 31 was constructed. At $P_{R,o} = 7.74$

$$G_R = \begin{cases} 3.9 & \text{for the classic venturi} \\ 1.85 & \text{for the classic venturi times 0.47} \\ 2.0 & \text{for extrapolation of data herein} \end{cases} \tag{26}$$

Since the extrapolated data and the curve for classic venturi flow times 0.47 are within 7 percent deviation, it would seem reasonable to use one-half of the classic venturi flow rates as flow rates for the straight seal configuration in the extrapolated regions. The Reynolds number now becomes

$$\begin{aligned} \rho u = G &= \frac{1}{2} G_R G^*(1 + \psi_Q) \\ &= \left(\frac{3.9}{2}\right)(1158)(1 - 0.04) \\ &= 2168 \text{ g/cm}^2\text{ s} \end{aligned} \tag{27}$$

$$\begin{aligned} \overline{Re} &= \frac{\rho u (D_{outside} - D_{inside})}{\mu} \\ &= \frac{2168(0.02692)}{0.168\times10^{-3}} = 0.35\times10^6 \end{aligned} \tag{28}$$

The average Reynolds number is high enough so that the flow is probably turbulent even though the acceleration terms are quite large. But it must be appreciated that the Reynolds number in the minimum-clearance region is very small and that the effects of secondary flows are not known. The question of turbulence in such small passages remains an open issue.

Summary for fully eccentric position.—The following is a summary for the straight cylindrical seal where the non-rotating centerbody was set in its fully eccentric position.

(1) Mass flux and pressure profile data for fluid nitrogen and fluid hydrogen flowing through the seal were acquired and tabulated. In the fully eccentric position the passage height at 180° was 0.02692 cm (0.0106 in.), but the shaft centerbody touched the housing at 0°.[10]

(2) The reduced mass flux data based on the inlet stagnation pressure at 0° for fluid hydrogen and fluid nitrogen were in agreement. Further, these data did not differ significantly from those obtained for the concentric configuration.

(3) The pressure profiles differed significantly both axially and circumferentially from those for the concentric configuration. The inlet pressure differences were sensitive to reduced temperature. But once determined, the reduced inlet pressure difference level $\Delta P_{ecc}/P_0|_{in}$) at low and high values of $T_{R,o}$ did not appear to be significantly altered by the absolute pressure level. However, near the thermodynamic critical point, $T_{R,o} \approx 1$, such a simplistic relation does not appear reasonable. Differences between hydrogen and nitrogen profiles appeared to be related to the heat input resulting from testing the configuration in the ambient environment. This diabatic condition appears to be in concert with a model that permits vapor production at some point on the seal surface. These differences in pressure (inlet and exit) are the key to

[9] 1 MPa = (14.696/0.101325) psia.

[10] Note possible 17° offset; see p. 7.

dynamic turbomachine stability because they represent the forces available to restore a perturbed shaft to its unperturbed position.

(4) For gases the pressure profiles for 0° and 180° crossed over at about three-fourths of the seal length. For liquids the crossover moved to the exit and may not always exist.

Some Effects of Backpressure Control[11]

In the classical sense a flow is choked when changes in backpressure (pressure at the seal exit plane) no longer cause a change in the mass flux (eq. (13)). For a gas the pressure ratio P_t/P_o is approximately 1/2, but for a high-pressure, low-temperature liquid this ratio can be less than 0.05. The backpressure control data for the straight cylindrical seal are given in table V.

Backpressure control data are needed for the straight seal because most seals operate against some positive backpressure. Also in the *axisymmetric case* considerable backpressure (up to perhaps 40 percent of the inlet stagnation pressure) can be applied without altering the flow or the pressure profiles within the tube (ref. 20). The question also arises as to how backpressure applied to the concentric and eccentric configurations alters flow and axial and circumferential pressure profiles.

Prior to this series of tests several pressure taps had to be repaired. This may explain some of the problems detailed later in this section. In an attempt to obtain data at a partially eccentric position with controlled backpressure, the straight seal was set 40 percent eccentric. The experimental data are given in table V.

Fluid hydrogen.—Fluid hydrogen profiles (fig. 32(a)) indicate a substantial pressure change between 0° and 180° with and without the backpressure held close to the thermodynamic critical pressure of hydrogen. The profiles with elevated backpressure were quite linear and, as can be seen from figure 32(b), increasing the inlet-to-backpressure ratio did not alter the profile shape. For these profiles and this geometrical configuration, two-phase vapor generation seemed to be suppressed or confined to a region immediately downstream of the seal exit. Increasing the inlet temperature $T_{R,o}$ (figs. 32(b) and (c)) did not materially alter these results.

Fluid nitrogen.—The first run with fluid nitrogen revealed an unusually high pressure near the seal exit, as illustrated in figure 33(a). This unusual profile also appears in the gaseous data for nitrogen (fig. 33(b)) and again in the data of figure 33(c). Between the runs shown in figures 33(a) and (f) the transducers used to measure pressure were all changed, but the profiles remained similar. This is quite an important point because such a profile represents negative stiffness, which is highly detrimental to shaft stability.

Because of the small clearances moisture could reach various areas and be frozen by liquid nitrogen, or small particles could lodge in the flow passage. Therefore after the first liquid nitrogen runs the seal was warmed to ambient temperature, and the tap was purged with high-pressure helium gas. The pressure tap flowed freely and ambient temperature should have dispelled any "ice jam." However, the gaseous data also indicated the pressure hump (fig. 33(b)), and changing transducers did not alter the profile (fig. 33(c)).

Subsequent physical examinations of the hardware revealed that the centerbody had a 0.00050- to 0.00075-cm (0.00020- to 0.00030-in.) taper from the inlet to the exit (slightly convergent frustum of a cone (fig. 6)) and that the 0.0038- to 0.0050-cm (0.0015- to 0.0020-in.) off-center alignment could only be measured at the exit plane. The crossovers near the midplane in the pressure profiles of figures 33(a) and (c) indicated a nonuniform axial alignment, and a shock seemed to be formed near the exit plane. Clogged passages, skewed alignment due to some thermal expansion, and malfunctioning signal conditioners are all plausible explanations of these profiles. However, no residue, foreign matter, surface deformation, or malfunction of the signal conditioner was found. Another factor is a possible link between a weak signal conditioner and the minicomputer used to display data on the cathode-ray tube. Also, recall that the hydrogen profiles (fig. 32) did not exhibit this anomaly nor was it found at the 90° or 270° positions (pressure taps 5*j* and 5*k*[12]). (See figs. 5 and 6, tables I and III.) None of these situations could be proven and at this time the nonuniform axial profile remains unexplained.

A similar situation was encountered in running a modified seal (ref. 19); in that case a pressure tube had been mislabeled. It is not likely that the pressure tubes in this test were mislabeled since the nitrogen tests were conducted the day after a nighttime hydrogen run, with insufficient time for mechanical alteration—but it is a possibility as is improper value settings of the pressure transducer. As in all cases the anomaly pressure P_5 corresponded to the midseal value (i.e., the value of P_3).

Summary for backpressure control.—The following is a summary of the effects of backpressure control for the straight cylindrical seal with the nonrotating centerbody set approximately 40 percent eccentric, or 0.0038- to 0.0050-cm (0.0015- to 0.0020-in.) offset (the exact position of the centerbody within the housing could not be verified).

(1) Pressure profiles and mass flow rate data taken with controlled backpressure up to perhaps 30 percent of the inlet stagnation pressure indicated little effect of backpressure.

(2) Pressure profiles for fluid hydrogen with controlled backpressure indicated that the 0.0050-cm (0.0020-in.) offset was aligned axially. Further, these hydrogen data indicated a suppression of two-phase flow as the backpressure increased to the thermodynamic critical pressure.

[11]All test data were taken with a minimum backpressure greater than 1 atm absolute; the level was controlled by system friction losses and vent check valves. The pressures were controlled.

[12]Pressure tap 5 represents data tabulated at minimum/maximum clearance (0°/180° positions); taps 5*j* and 5*k* represent data tabulated at minimum/maximum clearance (90°/270° positions).

However, the nitrogen profiles demonstrated the unusually large pressure rise near the seal exit characteristic of a shock; further, the 0° and 180° pressure profiles, although separated at the inlet, crossed over at the seal midplane and slightly recrossed at the exit. Such behavior is characteristic of a skewed position, with the centerbody sufficiently close to the 180° surface to cause a shock. Although the nitrogen data remain geometrically unexplained, I believe that a shaft under large bending moments or passing through a critical speed could be skewed within its housing and have a similar pressure distribution. Such pressure distributions would probably cause a catastrophic turbomachine failure.

Flow Coefficient Analogy

A convenient method of presenting mass flow data for complex geometries is to relate these flows to those calculated and measured for the classic venturi. In references 6 to 14 two-phase choked flows in a venturi were calculated and related to experimental data for tubes with Borda and orifice inlets. Quantitative evaluation of a 53-L/D tube with a Borda inlet provided a locus of points representing the variation of flow coefficient C_f with reduced inlet stagnation temperature $T_{R,o}$. Here C_f is defined as

$$C_f \equiv \frac{G_{R,\ \text{complex geometry}}}{G_{R,\ \text{venturi}}} \tag{29}$$

The Borda-inlet data were weak functions of pressure. The orifice data were pressure dependent as should be anticipated since orifice flows do not fully choke. The seal data, however, were strongly pressure dependent near and above the thermodynamic critical point, as illustrated in figure 34. The pressure dependence is characterized by the deviation bars. To some extent the seal data followed trends established for the simple axisymmetric geometries (Borda and orifice inlets). In the absence of other data the baseline data for the 53-L/D tube with a Borda inlet could be used to determine flow through a seal. For the straight cylindrical seal an approximate relation could be used:

$$\frac{G_{R,\ \text{straight cylindrical seal}}}{G_{R,\ 53\text{-}L/D\ \text{Borda inlet tube}}} = 0.9 \tag{30}$$

Summary of Results

Critical mass flux and pressure profile data were taken for flow through concentric and fully eccentric cylindrical annuli in a configuration representing a straight cylindrical seal for a high-performance turbopump (e.g., the space shuttle main engine fuel pump). All tests were conducted in the static condition (*nonrotating centerbody*). The critical mass fluxes (or leakage rates) for the concentric and fully eccentric configurations were nearly the same when based on stagnation conditions ($P_{R,o}, T_{R,o}$) upstream of the seal inlet.

The gas and liquid axial pressure profiles were parabolic and linear, respectively, and were very sensitive to small variations in eccentricity. The pressure differences between the maximum- and minimum-clearance positions were highly dependent on the geometric conditions, the temperature, and the pressure at both the inlet and the exit. The greatest pressure differences were in the inlet region. For gases these pressure profiles crossed over at approximately three-fourths of the seal length; for liquids the crossover moved toward the exit. These differences are most important to the dynamic stability of turbomachines.

A maximum circumferential positioning error of 17° off true 0° position was found subsequent to testing and should be realized and considered when interpreting the pressure data: in most cases the effect should be small.

Critical mass flux and pressure profiles for hydrogen flowing through a shaft seal offset by one-third of the nominal clearance indicated a suppression of two-phase choked flow as the backpressure at the exit reached the thermodynamic critical pressure. Injecting gaseous helium near the seal exit plane (close to the region where two-phase flow begins) substantially increased upstream pressure. Injecting helium into fluids (gas or liquid) within the seal could control turbomachine instabilities. High-pressure, high-temperature hydrogen gas could be used for this purpose in an alternative SSME fuel pump design.

Some tests with nitrogen demonstrated an anomalous pressure rise near the seal exit along the maximum-clearance position. This pressure rise could not be verified and remains unexplained.

Data were taken over a range of inlet pressures and temperatures with fluid nitrogen and fluid hydrogen. The results, although complex, tended to follow the corresponding-states principles for critical flows. The mass flux profiles of this annual configuration are roughly comparable to those of an orifice, and the pressure profiles to those of a long tube.

Lewis Research Center
National Aeronautics and Space Administration
Cleveland, Ohio, October 16, 1986

Appendix A
Fanno-Rayleigh Relations

Recall that for the simplified one-dimensional flow a solution of the energy, continuity, and state equations leads to the Fanno line.

$$h_x + \frac{u_x^2}{2} = h_y + \frac{u_y^2}{2} = h_o \qquad \text{Energy} \tag{A1}$$

$$G = \rho_x u_x = \rho_y u_y \qquad \text{Continuity} \tag{A2}$$

$$\left.\begin{aligned} S &= S(P,\rho) \\ h &= h(S,\rho) \end{aligned}\right\} \qquad \text{State} \tag{A3}$$

For a given G, select u_y, calculate ρ_y, compute h_y, and find S_y from the state relation. A plot of such solutions forms the Fanno line, with Mach number being unity at S_{max}. Changes along the Fanno line result from frictional effects but do not represent heat transfer. If flow is initially subsonic, friction causes velocity and Mach number to increase; but if flow is initially supersonic, velocity and Mach number decrease. In both cases the limiting value is Mach 1.

For a similar flow the solution of the momentum, continuity, and state equations leads to the Rayleigh line, where the momentum equation is

$$P_x + \rho_x u_x^2 = P_y + \rho_y u_y^2 = P_o \tag{A4}$$

For a given G, select u_y, calculate ρ_y, compute P_y, and find S_y from the state relation. A plot of these solutions forms the Rayleigh line. As the equation of state is implicit, iteration is usually required to produce the point on either line. Because stagnation enthalpies are not restricted, the Rayleigh line represents heat transfer effects.

The line joining the intersection of the Fanno and Rayleigh lines represents an abrupt transition from supersonic to subsonic flow, as shown in the following sketch:

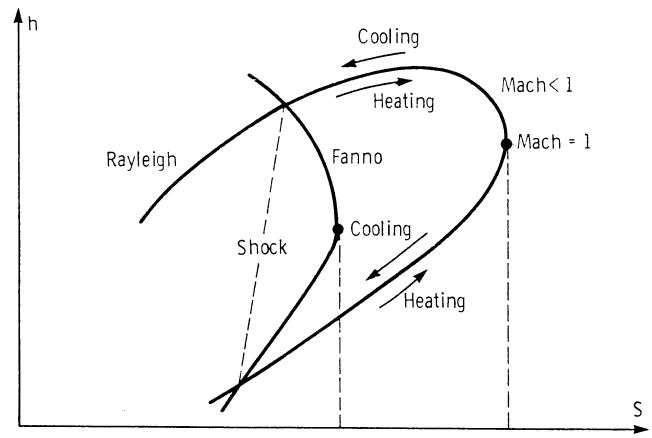

Appendix B
Gas Injection

The nature of the pressure profile is very important to shaft stability and housing loading. It was perceived that injecting gas into the region immediately ahead of the two-phase choke would substantially flatten the profile; that is, make it more gaslike than liquidlike (effect a negative-to-positive curvature change in the pressure profiles). Small quantities of helium gas were injected through three of the four pressure tap holes (0°, 90°, 270°; fig. 35) at a distance of 3.998 cm (1.574 in.) from the seal inlet plane (position P_5, figs. 5 and 6) and one (180°) at 4.623 cm (1.820 in.) from the seal inlet plane (position P_7). The resulting pressure profiles are shown in figure 22. As can be determined from the figure, the average slope changed from 0.40 to 0.23 MPa/cm (148 to 86 psi/in.). Such seal stiffening can produce significant changes in rotor dynamics.

In essence, the three injection ports at 270°, 0°, and 90° simulate an eccentrically positioned seal with accompanying circumferential flow toward and accelerated axial flow along the 180° position. Further, high-pressure, high-temperature fluid hydrogen is available for taking an enthalpy drop to drive the turbine, and an alternative design whereby gas is injected into the second and third seal stages of the SSME fuel pump could be realized.

Injection of a secondary gas, such as nitrogen or steam, could form a "freeze seal." As the compressive strength of ice is of the order of 14 to 21 MPa (2 to 3 ksi), fracture should not become a problem and the seal formed by the working fluid would remain intact during rub-in. Frozen material can act as a positive seal if a fluid can be frozen on the shaft and a minute amount of surface energy can be provided, prior to start, to melt a fraction of the seal surface. This would permit a minimum fluid loss if coolant to keep the ablative solid frozen were available. However, the power losses due to drag would be substantially increased.

Appendix C
Model – Including Vapor Production at Wall

A modification of the classic two-phase flow model is proposed herein although the details and range of applicability are not yet complete. The reason for inclusion at this time is that such modeling appears to explain some of the otherwise anomalous behavior observed in the studies of nozzles, orifices, long tubes, and straight seals. The basic outline of the model follows:

(1) Assume the flow to be homogeneous, single phase, and completely described by the classic equations of motion and state to the point X, which represents the point where the fluid can become saturated at the wall and is a function of h_o, P_{sat}, the bulk of the fluid being a function of h_{sat}, P_{sat}.

(2) Decreases in pressure caused by flow beyond this point result in a degree of superheat being applied to the microlayer adjacent to the wall and to the bulk fluid as well. Further decreases in pressure increase the degree of wall superheat until Hsu's nucleation criteria (ref. 21) for a flowing fluid are satisfied. At this point bubbles form – their size, number, and rapidity depending on the superheat, the surface conditions, and the fluid.

(3) The microlayer downstream becomes bubble laden, and its effective viscosity is substantially reduced.

(4) The liquid core tends to ride on the vapor layer with a reduction in pressure drop while at the same time being constricted by the vapor annulus. The slip becomes quite large and the assumption of $k = u_g/u_\ell = 1$, or a slip ratio of unity, is no longer valid. In fact, one technique is to set $k = 0$, that is, assume that a continuous annular static vapor layer exists and that the liquid flows through the resulting constricted opening. The thickness of the annular vapor layer is defined by the number of bubbles generated per unit area, and their size is determined by the Hsu criteria (ref. 21).

Such a model (items 1 to 3) permits vapor generation but never more than in an annulus since once vapor generation begins the effective viscosity is reduced to a parabolic shock profile at the exit irrespective of the tube length; this makes the problem elliptic. Decoupling may be permitted so long as the solutions are all matched at their respective interfaces. Note that all this should occur close to the exit.

This type of model is useful in explaining the positive and negative curvature changes in the axial pressure profiles of both the long tube and the seal. It is also useful in explaining why a decoupled solution for mass flux (eqs. (10) and (17)) overpredicts the data. However, one must also combine the modeling with the diabatic entrance effects, which can reduce the inlet temperature and thus lower the calculated mass flux.

References

1. Zuk, John; Ludwig, Lawrence P.; Johnson, Robert L.: Quasi-One-Dimensional Compressible Flow Across Face Seals and Narrow Slots. I—Analysis. NASA TN D-6668, 1972.
2. Zuk, J.; and Smith, P.J.: Quasi-One-Dimensional Compressible Flow Across Face Seals and Narrow Slots. II—Computer Program. NASA TN D-6787, 1972.
3. Hendricks, R.C.: Three-Step Cylindrical Seal for High-Performance Turbomachines. NASA TP-1849, 1987.
4. Hendricks, R.C.: Three-Step Labyrinth Seal for High-Performance Turbomachines. NASA TP-1848, 1987.
5. Hendricks, R.C.; Graham, R.W.; Hsu, Y.Y.; and Friedman, R.: Experimental Heat-Transfer Results for Cryogenic Hydrogen Flowing in Tubes at Subcritical and Supercritical Pressures to 800 Pounds Per Square Inch Absolute. NASA TN D-3095, 1966.
6. Hendricks, R.C.; Simoneau, R.J.; and Barrows, R.F.: Two-Phase Choked Flow of Subcooled Oxygen and Nitrogen. NASA TN D-8169, 1976.
7. Hendricks, R.C.; and Simoneau, R.J.: Application of the Principle of Corresponding States to Two-Phase Choked Flow. NASA TM X-68193, 1973.
8. Simoneau, R.J.; and Hendricks, R.C.: Generalized Charts for Computation of Two-Phase Choked Flow of Simple Cryogenic Liquids. Cryogenics, vol. 17, no. 2, Feb. 1977, pp. 73-76.
9. Simoneau, R.J.: Maximum Two-Phase Flow Rates of Subcooled Nitrogen Through a Sharp-Edged Orifice. Advances in Cryogenic Engineering, Vol. 21, K.D. Timmerhaus and D.H. Weitzel, ed., Plenum Press, 1975, pp. 299-306.
10. Hendricks, R.C.: Normalizing Parameters for the Critical Flow Rate of Simple Fluids Through Nozzles. Proceedings of the Fifth International Cryogenic Engineering Conference, ICEC5, K. Mendelssohn, ed., IPC Science and Technology Press, 1974, pp. 278-281.
11. Hendricks, R.C.; Simoneau, R.J.; and Ehlers, R.C.: Choked Flow of Fluid Nitrogen with Emphasis on the Thermodynamic Critical Region. Advances in Cryogenic Engineering, Vol. 18, K.D. Timmerhaus, ed., Plenum Press, 1973, pp. 150-161.
12. Hendricks, R.C.; Simoneau, R.J.; and Hsu, Y.Y.: A Visual Study of Radial Inward Choked Flow of Liquid Nitrogen. Advances in Cryogenic Engineering, Vol. 20, K.D. Timmerhaus, ed., Plenum Press, 1975, pp. 370-382.
13. Simoneau, R.J.: Two-Phase Choked Flow of Subcooled Nitrogen Through a Slit. Proceedings of the 10th Southeastern Seminar on Thermal Sciences, R.G. Watts and H.H. Sogin, eds., Tulane Univ., 1974, pp. 225-238.
14. Simoneau, R.J.: Pressure Distribution in a Converging-Diverging Nozzle During Two-Phase Choked Flow of Subcooled Nitrogen. Non-Equilibrium Two-Phase Flows, R.T. Lahey and G.B. Wallis, eds., ASME, 1975, pp. 37-45.
15. Hendricks, R.C.; and Simoneau, R.J.: Two-Phase Choked Flow in Tubes with Very Large L/D. Advances in Cryogenic Engineering, Vol. 23, K.D. Timmerhaus, ed., Plenum Press, 1977, pp. 265-275.
16. Hendricks, R.C.; Baron, A.K.; and Peller, I.C.: GASP—A Computer Code for Calculating the Thermodynamic and Transport Properties for Ten Fluids: Parahydrogen, Helium, Neon, Methane, Nitrogen, Carbon Monoxide, Oxygen, Fluorine, Argon, and Carbon Dioxide. NASA TN D-7808, 1975.
17. Simoneau, R.J.; and Hendricks, R.C.: Two-Phased Choked Flow of Cryogenic Fluids in Converging-Diverging Nozzles. NASA TP-1484, 1979.
18. Hendricks, R.C.; and Sengers, J.V.: Application of the Principle of Similarity to Fluid-Mechanics. Water and Steam, J. Straub and K. Scheffler, eds., Pergamon, 1980, pp. 322-325.
19. Hendricks, R.C.: Some Flow Characteristics of Conventional and Tapered High-Pressure-Drop Simulated Seals. ASLE Trans, vol. 24, no. 1, Jan. 1981, pp. 23-28.
20. Hendricks, R.C.; and Stetz, T.T.: Some Flow Phenomena Associated with Aligned, Sequential Apertures with Borda-Type Inlets. NASA TP-1792, 1980.
21. Hsu, Y.Y.; and Graham, R.W.: Transport Processes in Boiling Two-Phase Systems. McGraw-Hill, 1976.

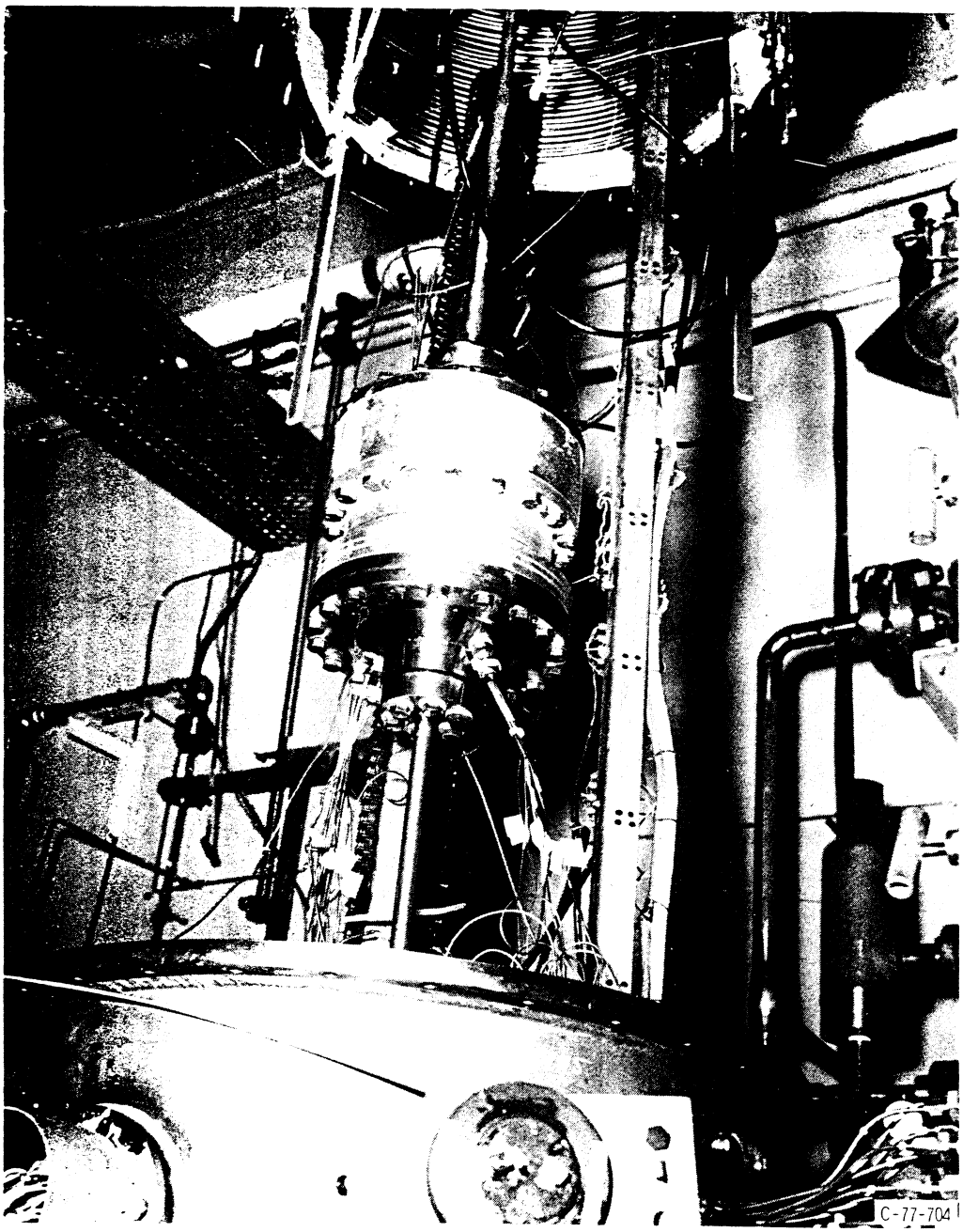

Figure 1.—Seal test installation, 1.91-cm- (3/4-in.-) diameter exhaust tube.

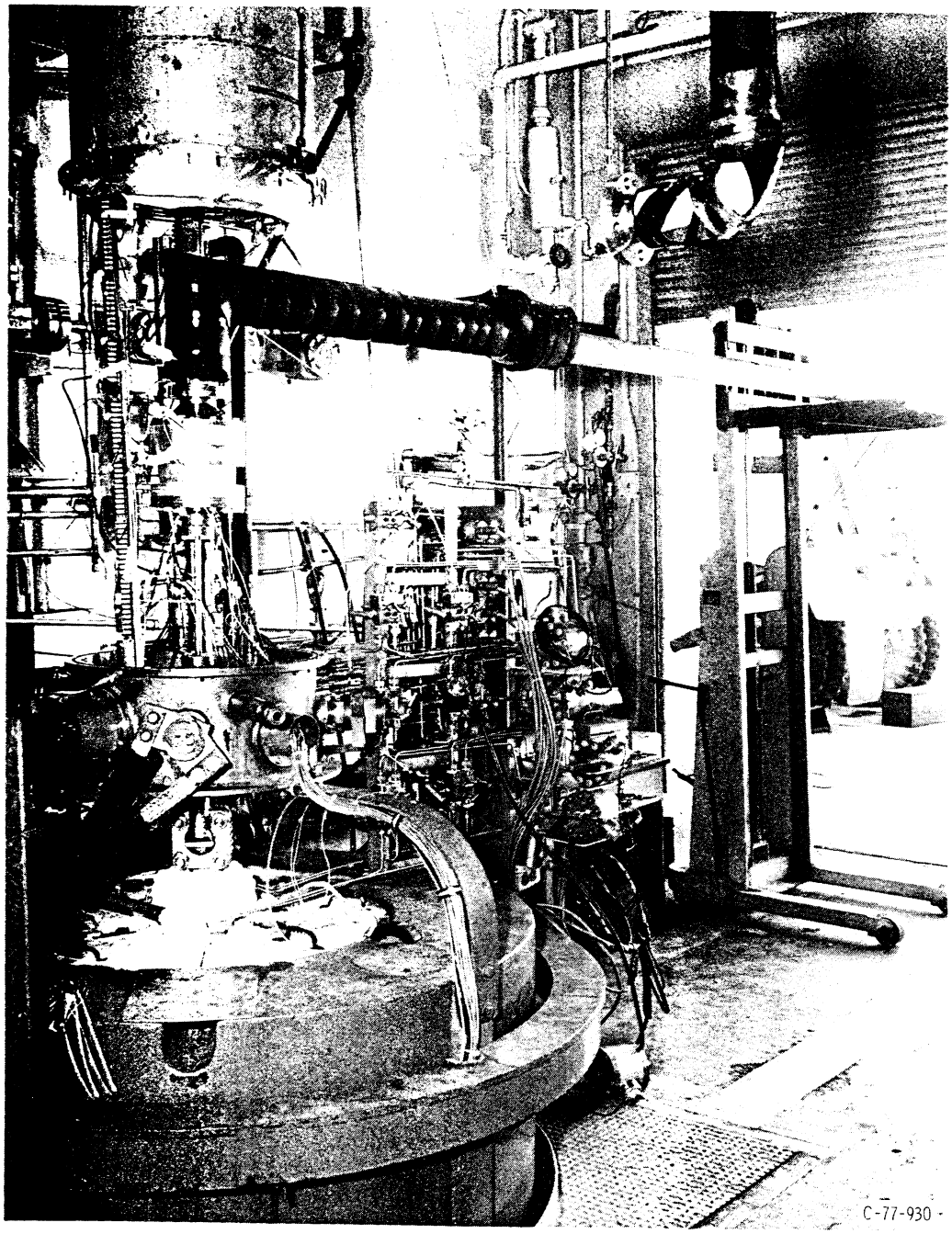

Figure 2.—Seal test installation, 7.62-cm- (3-in.-) diameter exhaust tube. Nitrogen tests only.

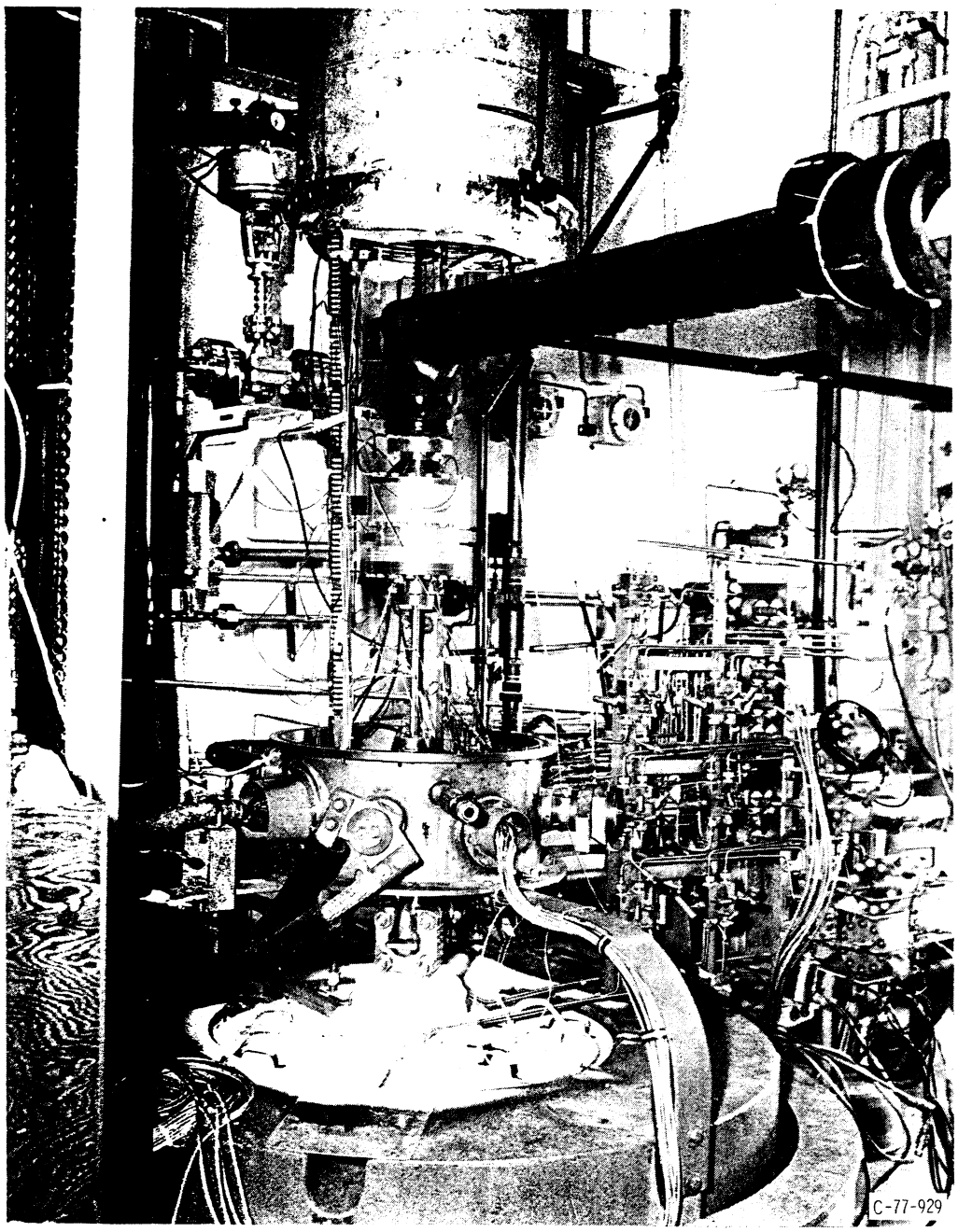

Figure 3.—Seal test installation, 5-cm- (2-in.-) diameter exhaust stacks. Hydrogen tests only.

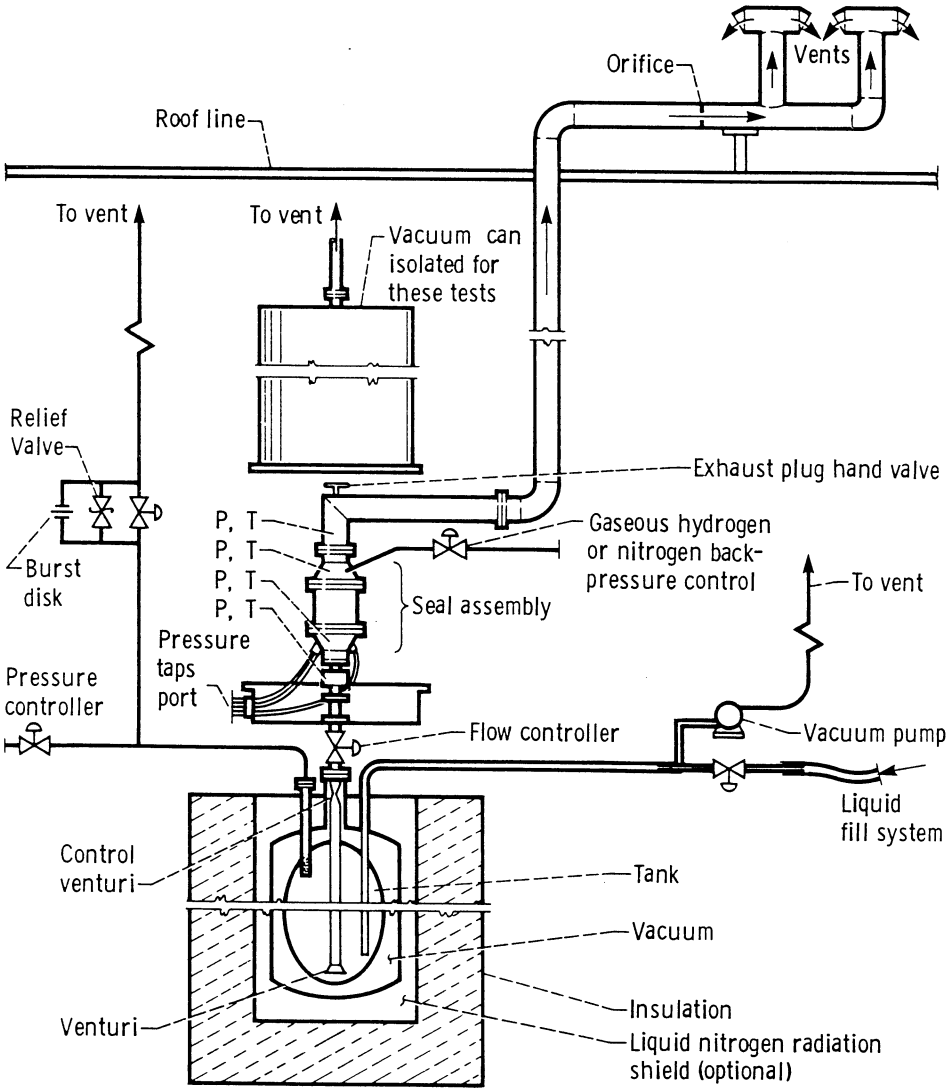

Figure 4.—Schematic of seal test installation.

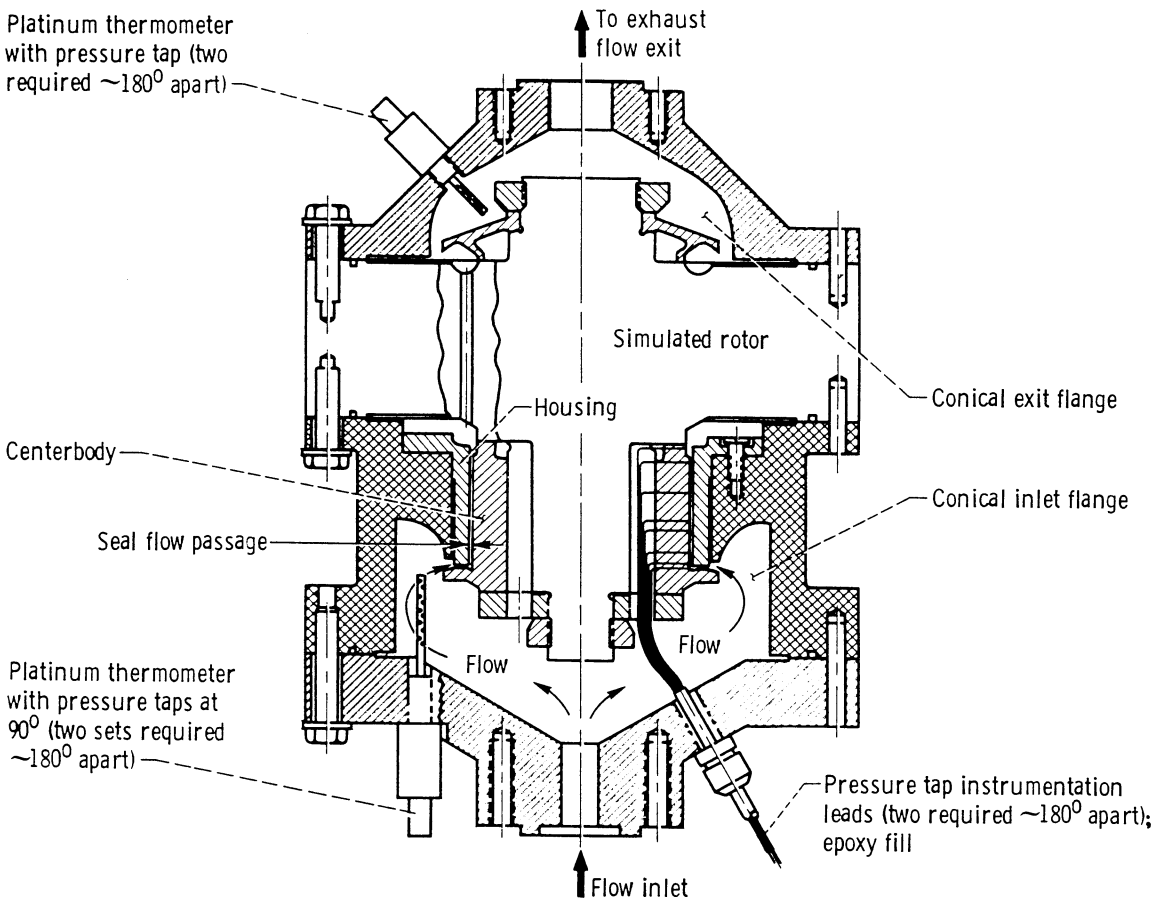

Figure 5.—Cross-sectional view of simulated straight cylindrical seal configuration.

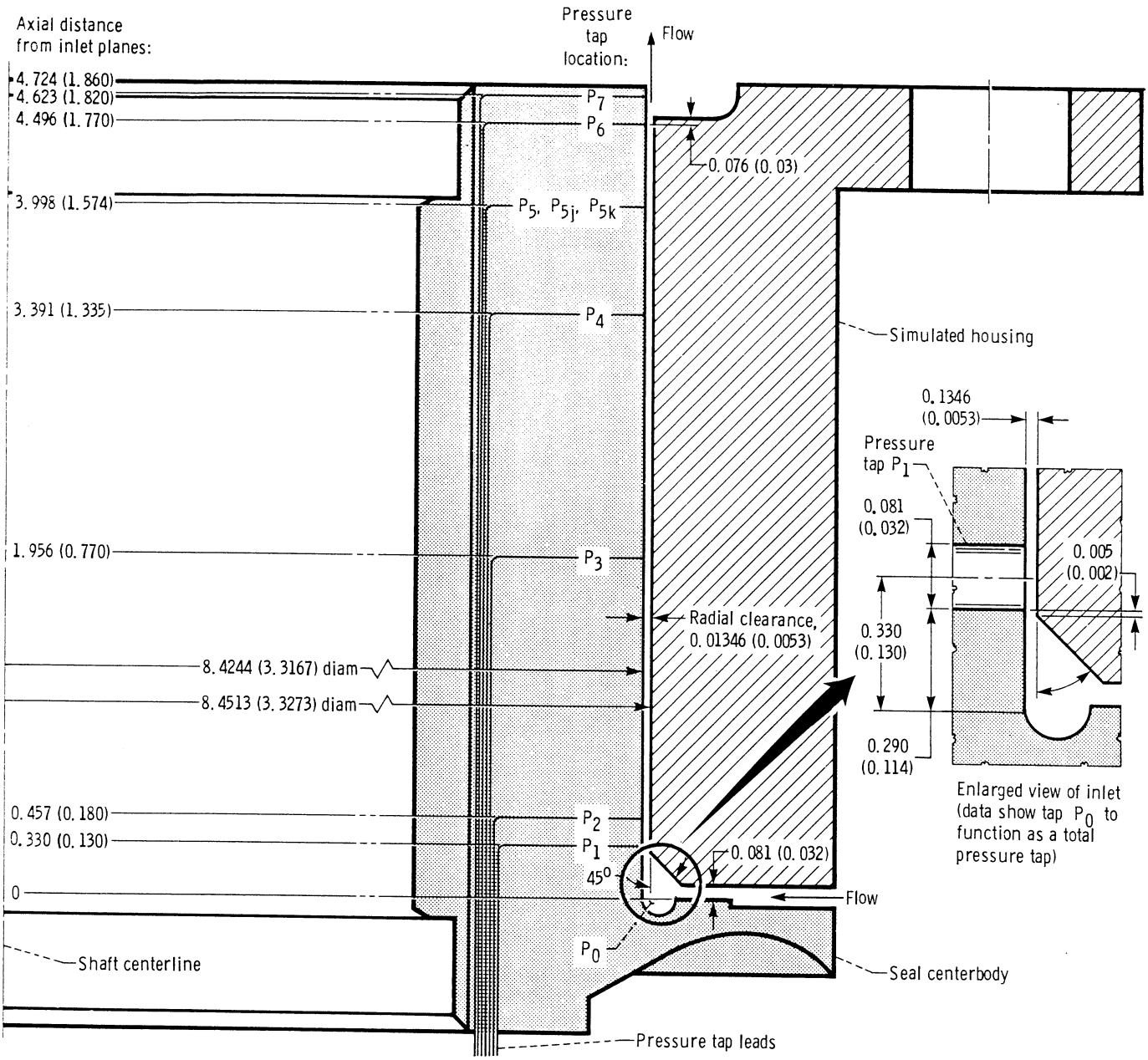

Figure 6.—Overview of pressure taps and geometry for straight cylindrical seal. (Linear dimensions are in centimeters (inches).)

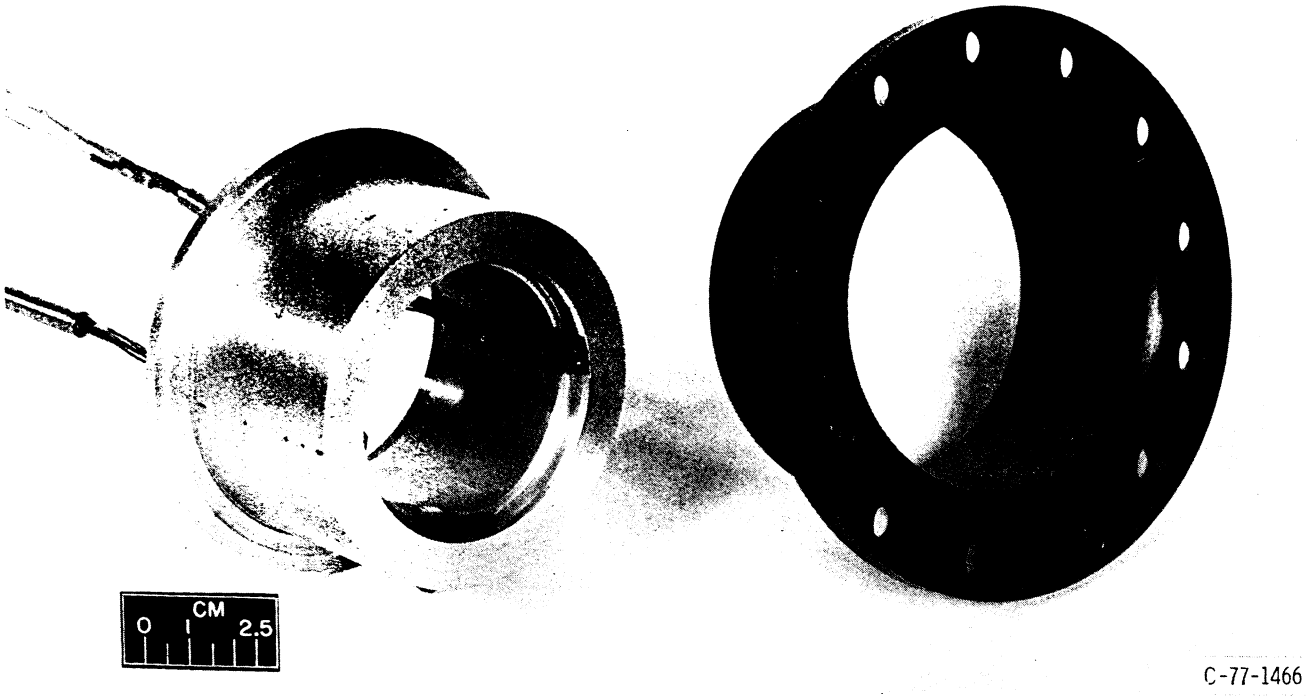

Figure 7.—Straight cylindrical seal and housing.

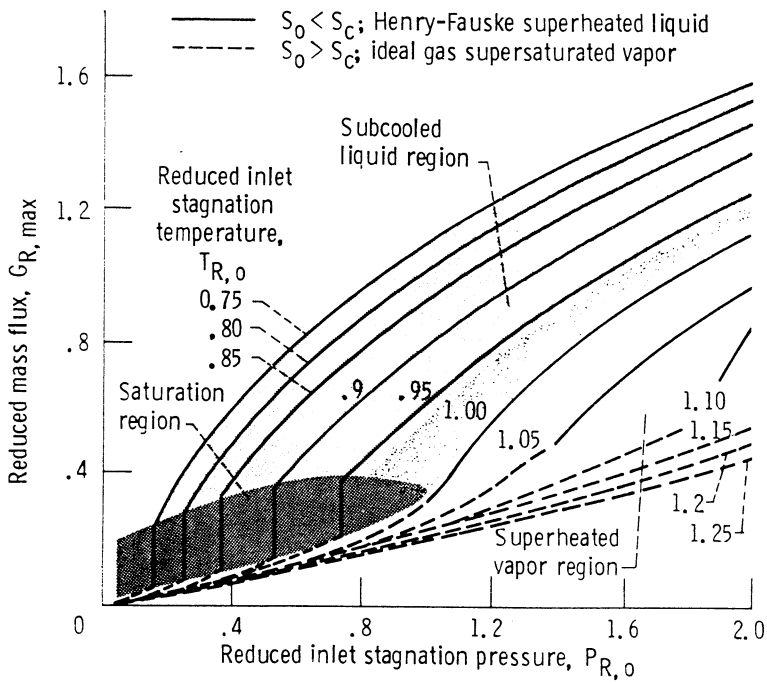

Figure 8.—Reduced choked mass flux based on homogeneous isotropic nonequilibrium models. (From ref. 8.)

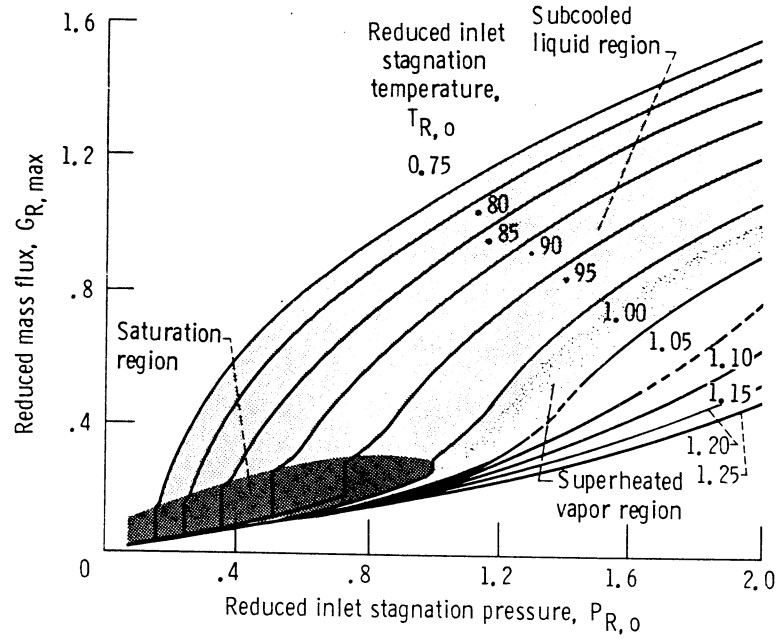

Figure 9.—Reduced choked mass flux based on homogeneous isentropic equilibrium model. (From ref. 8.)

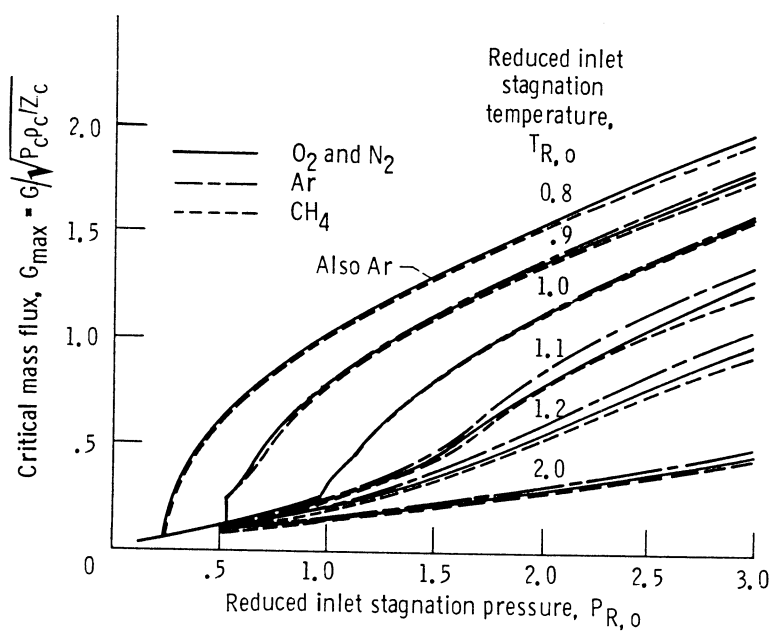

Figure 10.—Critical mass fluxes of oxygen, nitrogen, argon, and methane computed by isentropic equilibrium expansion using corresponding-states principles. (From ref. 7.)

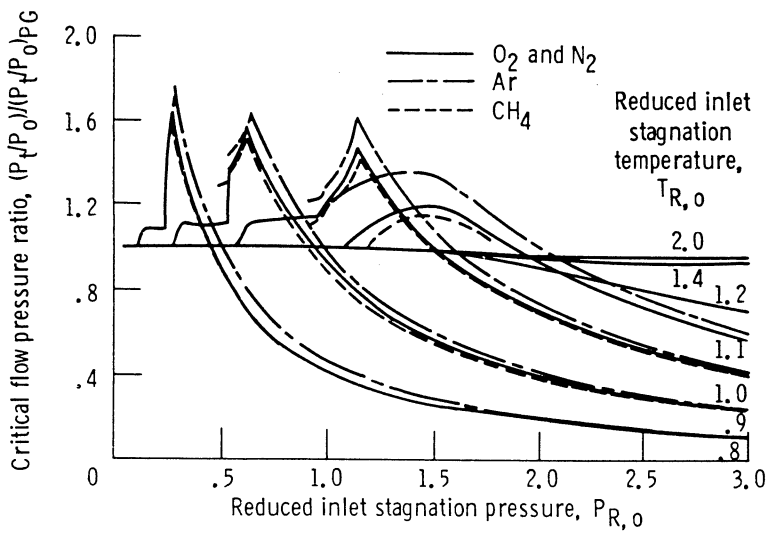

Figure 11.—Critical flow pressure ratios of oxygen, nitrogen, argon, and methane computed by isentropic equilibrium expansion using corresponding-states principles normalized by perfect gas ratio. (From ref. 7.)

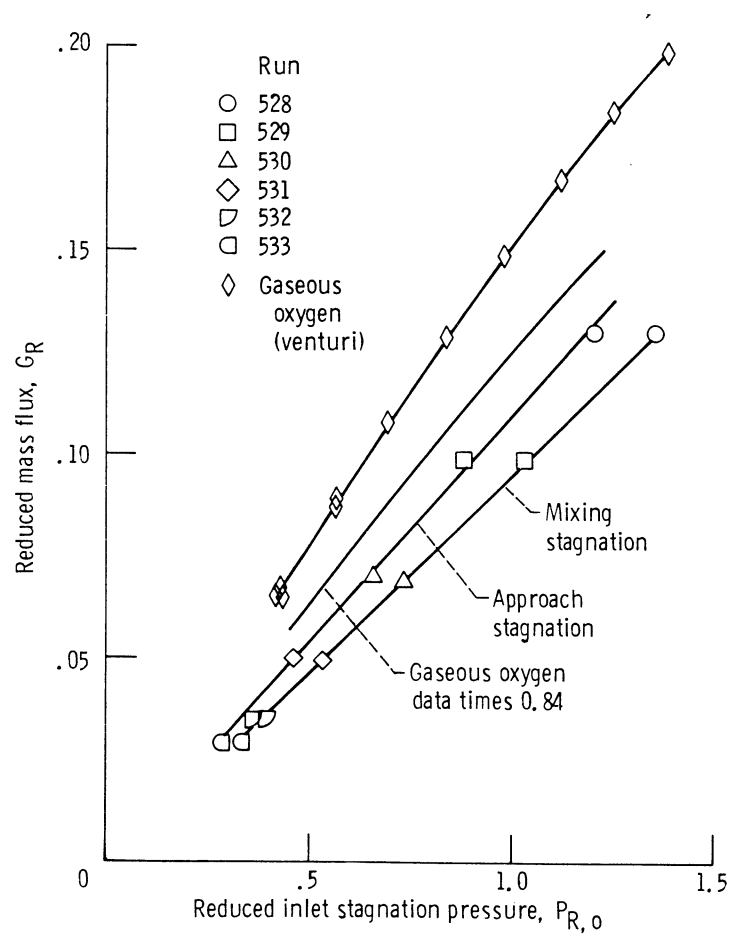

Figure 12.—Reduced mass flux of gaseous nitrogen through straight cylindrical seal in concentric position, as function of reduced pressure. Area, A, 0.3569 cm^2 (0.05532 in.^{2}); flow-normalized parameter, G^*, 6010 g/cm^2 s (85.5 lb/in.^{2} s); normalized flow, G^*A, 2145 g/s (4.730 lbm/s).

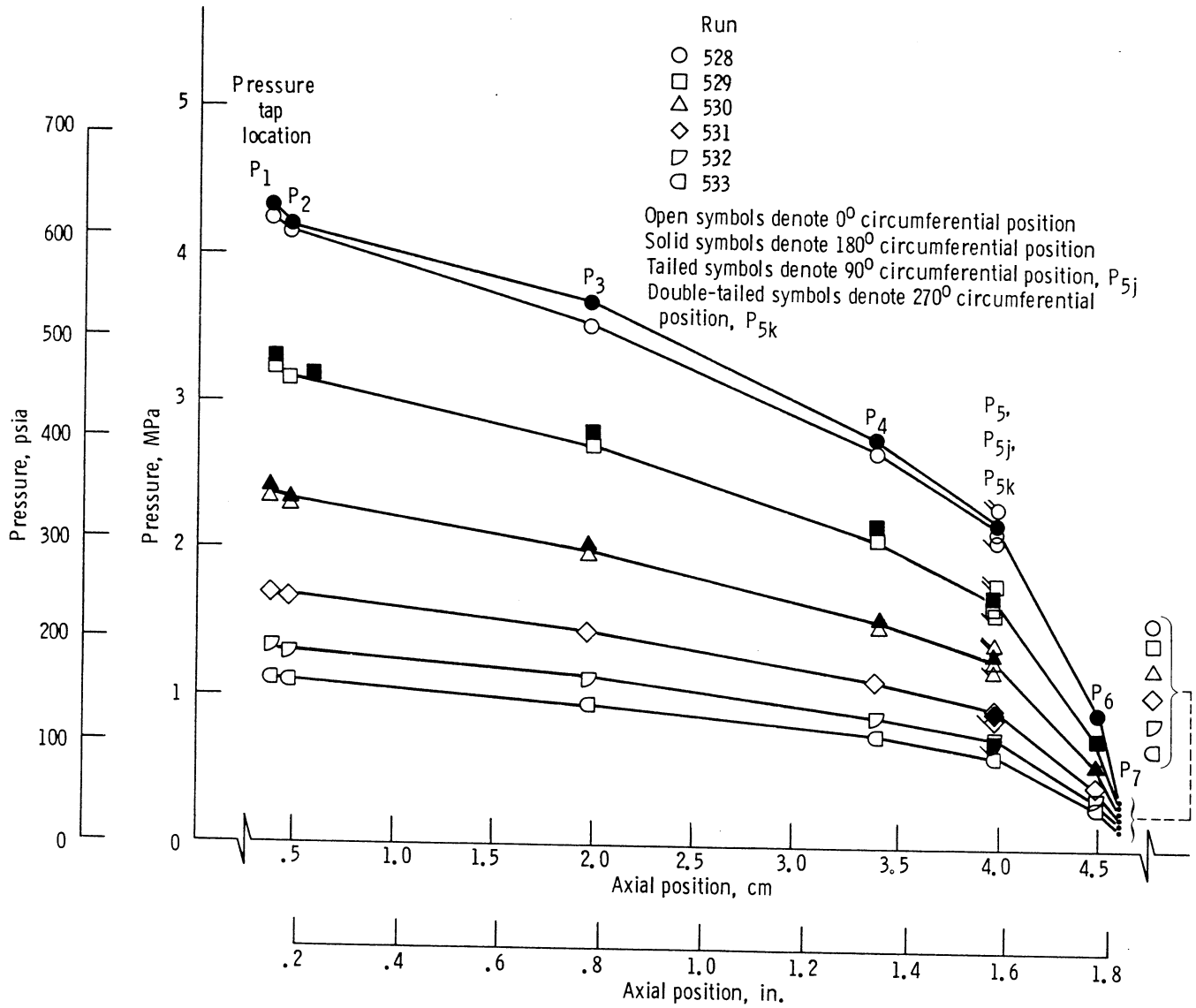

Figure 13.—Axial pressure distribution for gaseous nitrogen flow through straight cylindrical seal in concentric position.

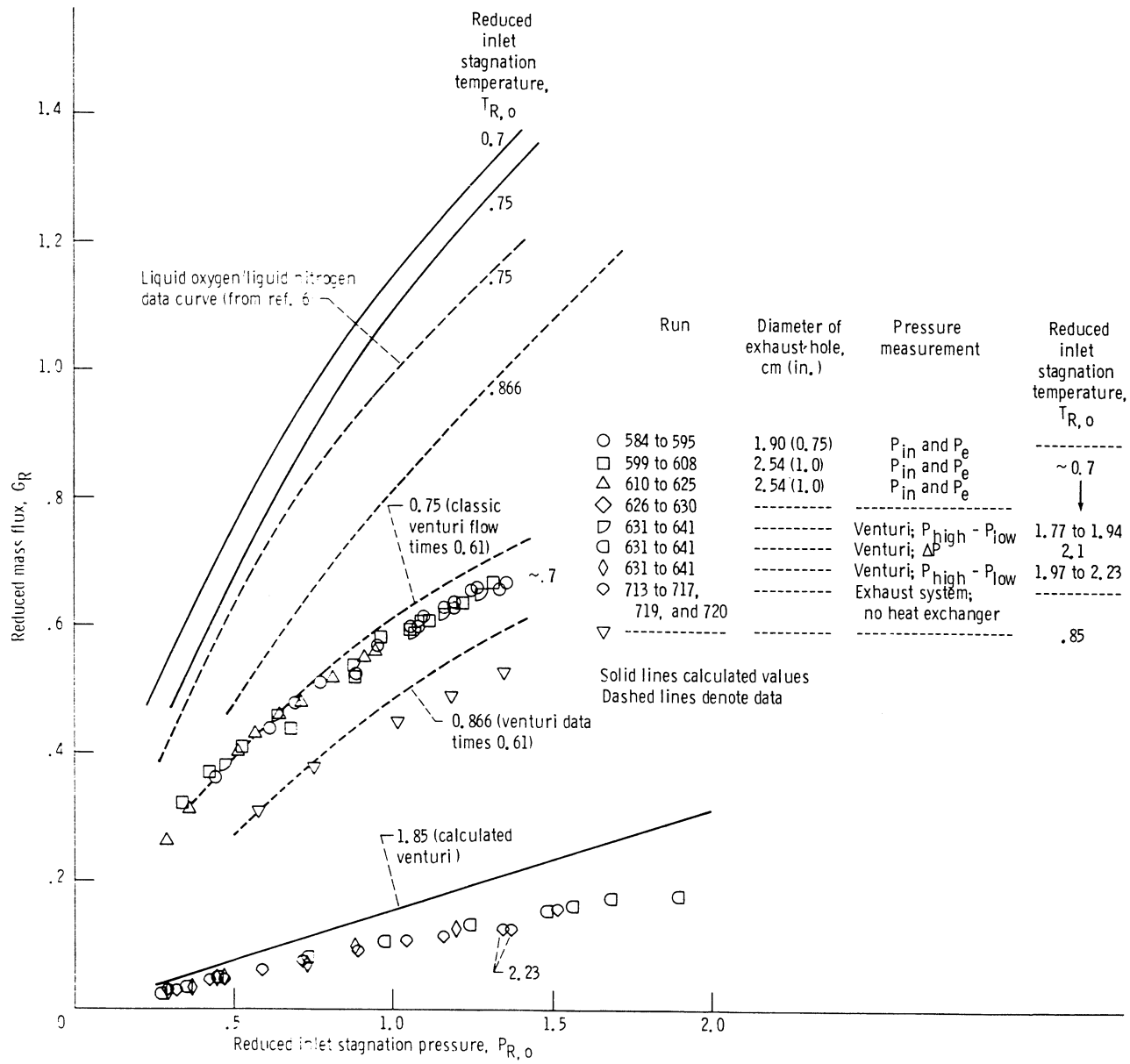

Figure 14.—Reduced mass flux of fluid nitrogen through straight cylindrical seal in concentric position, as function of reduced pressure.

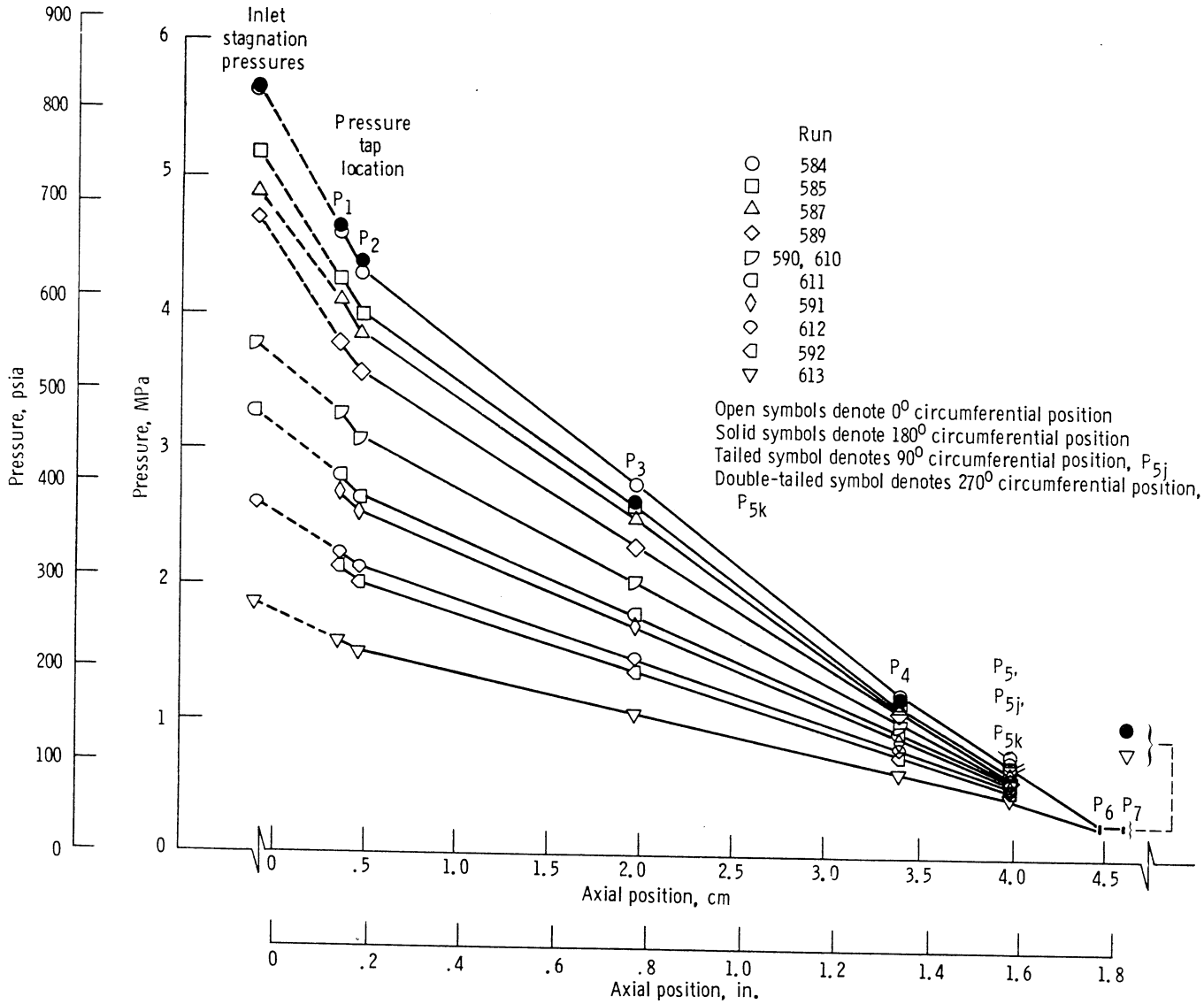

Figure 15.—Axial pressure distribution for fluid nitrogen flow through straight cylindrical seal in concentric position.

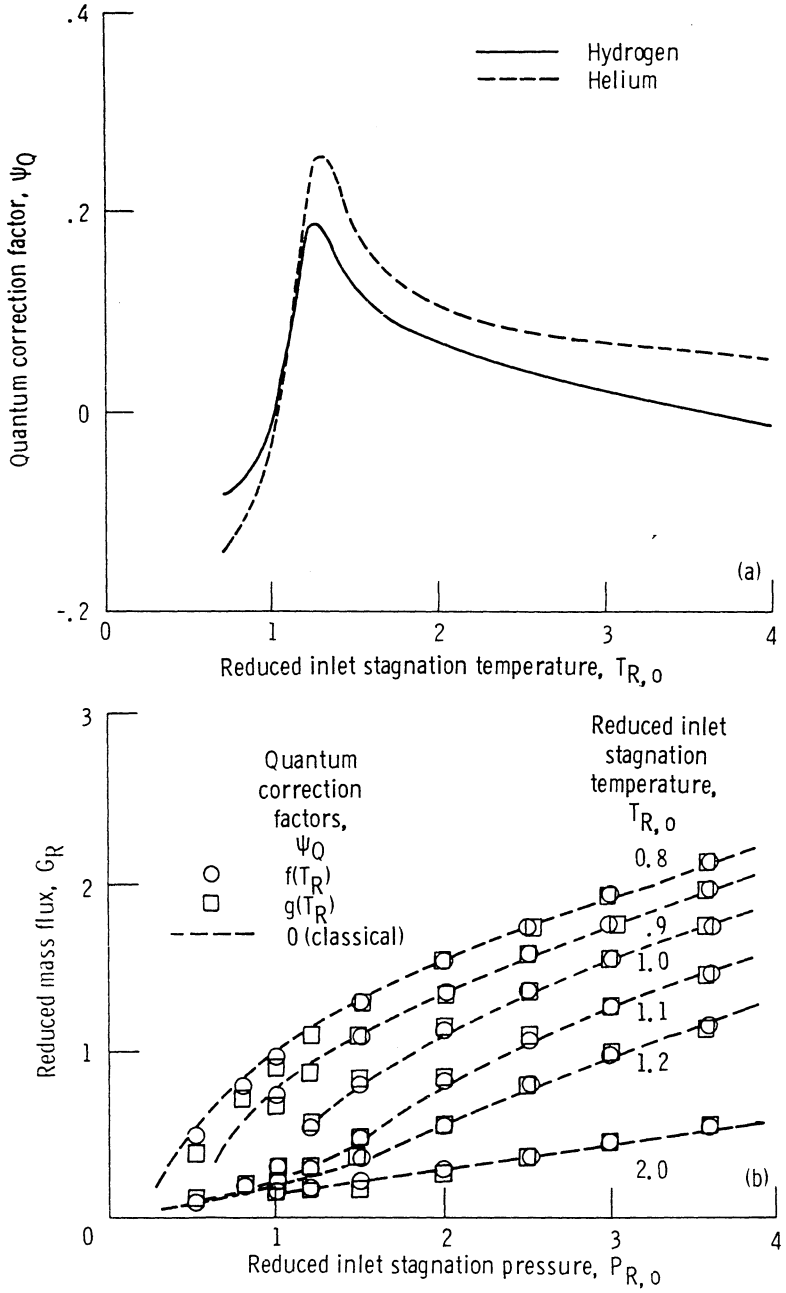

(a) Quantum correction factors for critical flow through nozzle, based on isentropic equilibrium expansion.
(b) Calculated classical (nitrogen-oxygen) reduced mass flux along selected isotherms.

Figure 16.—Normalizing parameters for parahydrogen and helium. (From ref. 10.) (Data for this figure are shown in table VI.)

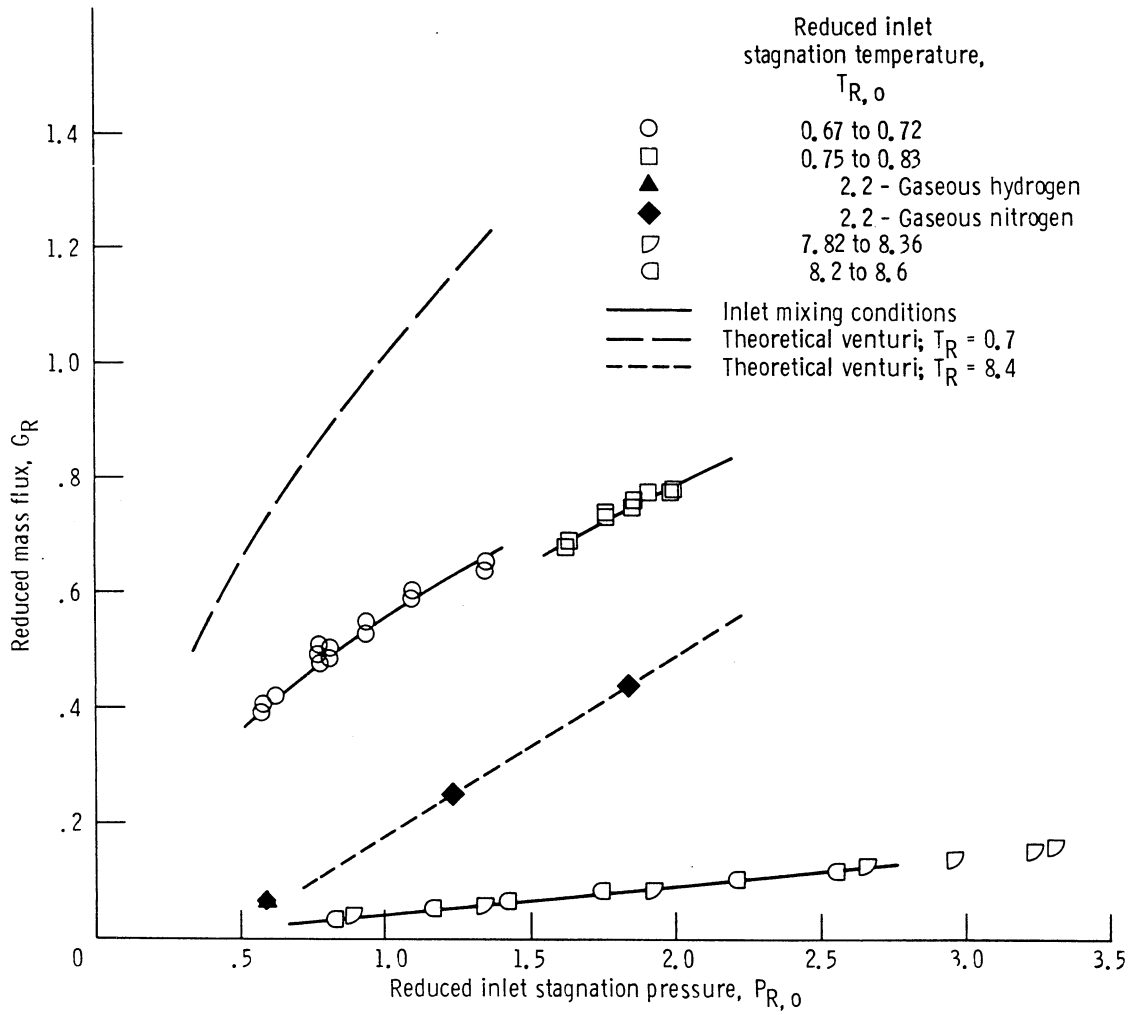

Figure 17.—Reduced mass flux of liquid hydrogen through straight cylindrical seal in concentric position, as function of reduced pressure—first set of data.

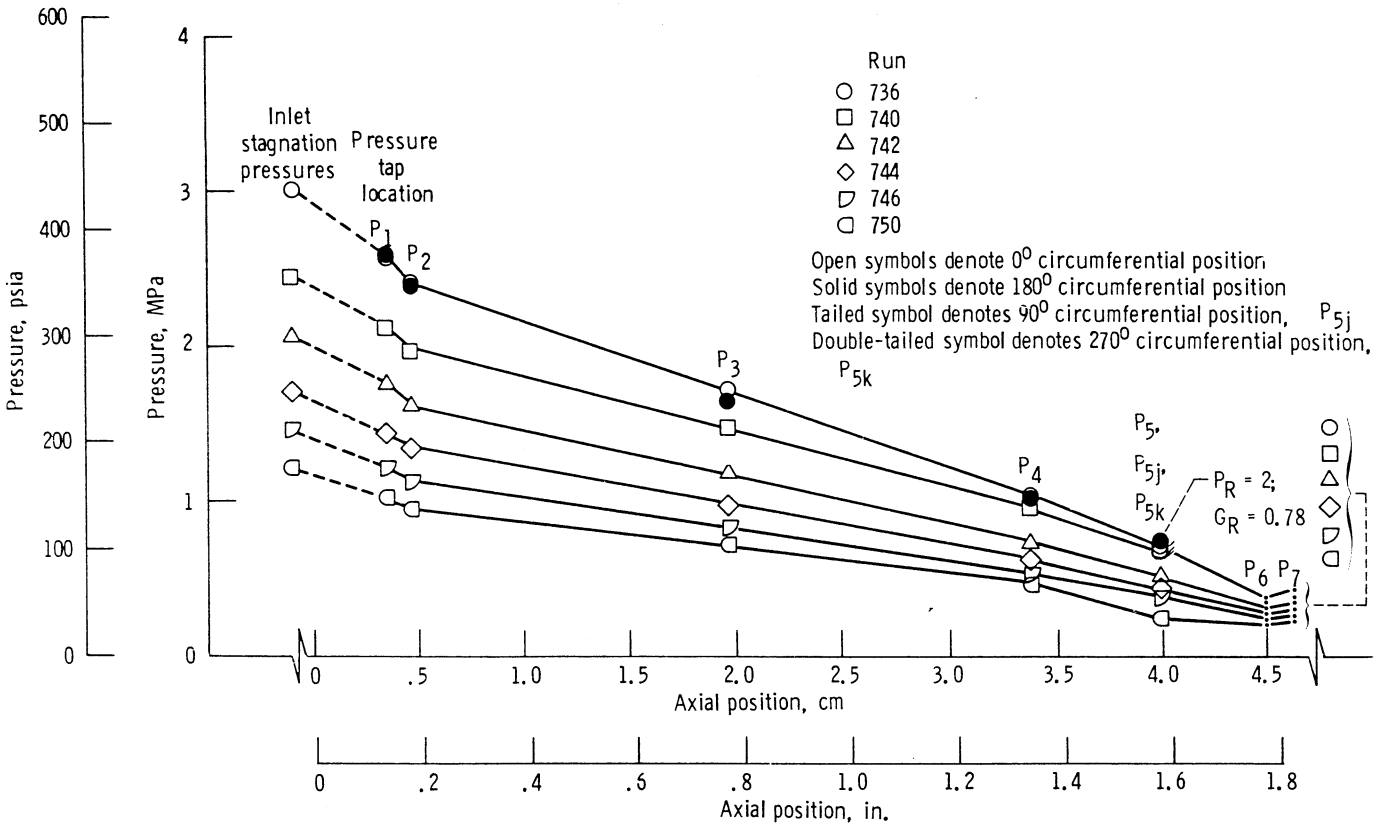

Figure 18.—Axial pressure distribution for liquid hydrogen flow through straight cylindrical seal in concentric position—first set of data.

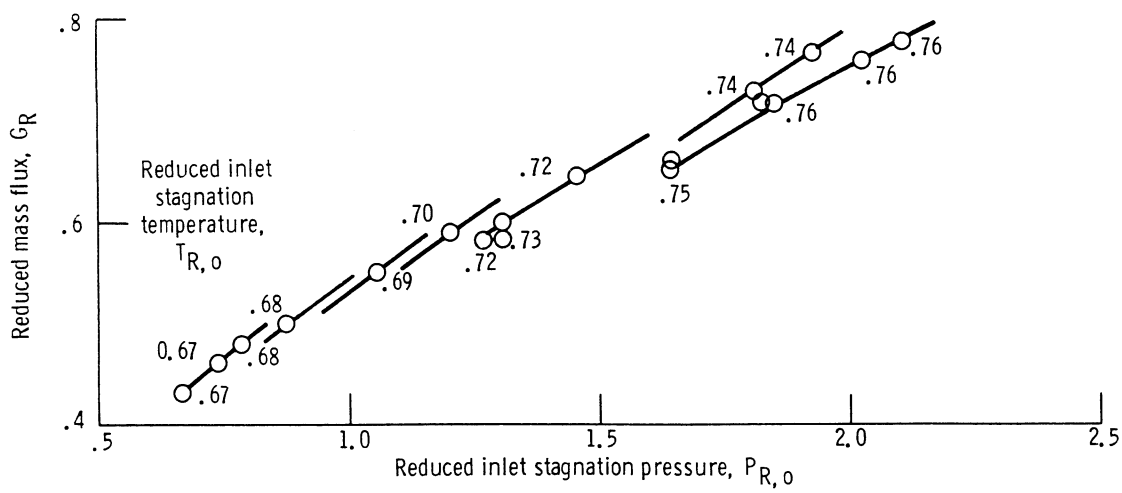

Figure 19.—Reduced mass flux of liquid through straight cylindrical seal in concentric position, as function of reduced pressure—third set of data.

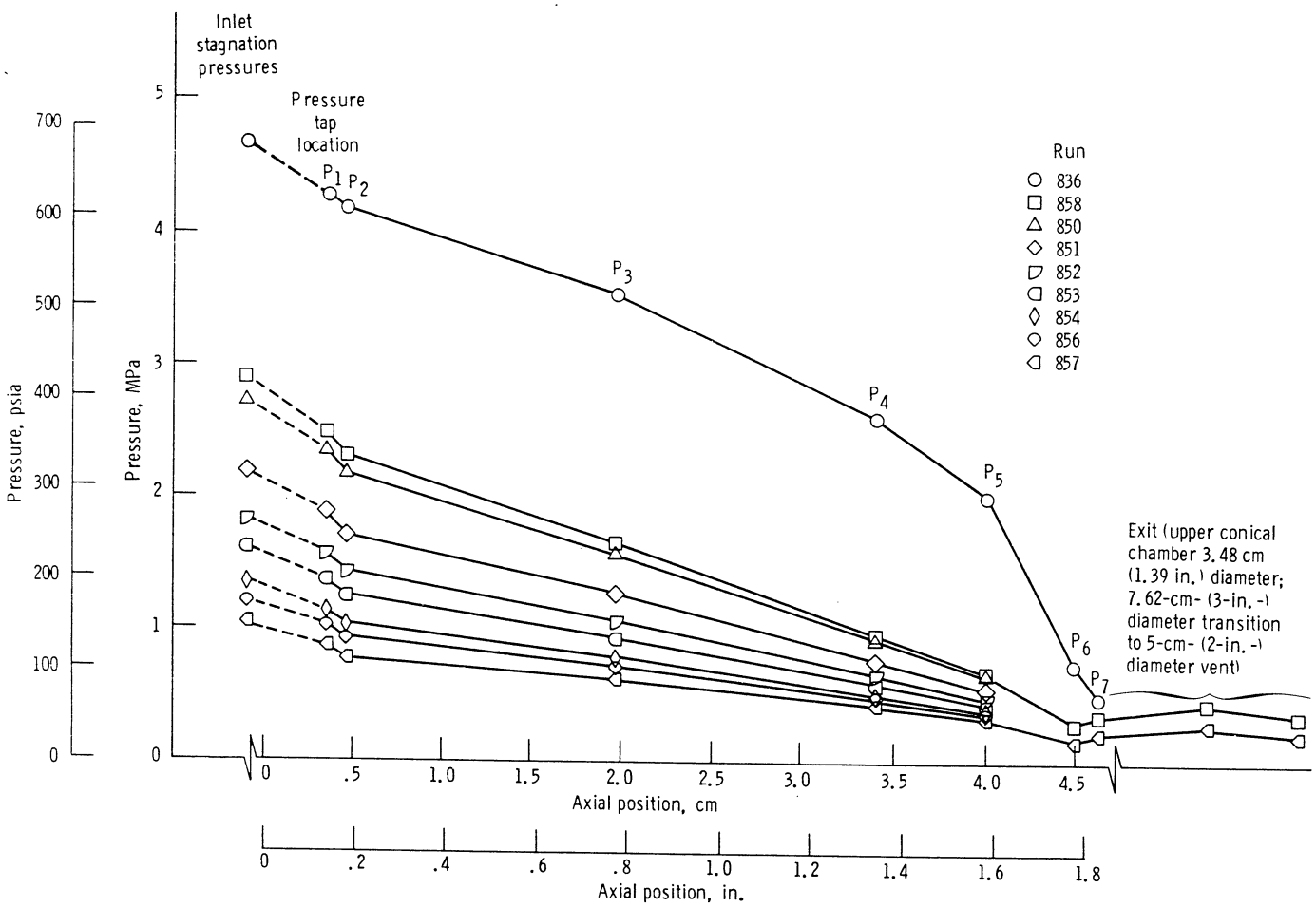

Figure 20.—Axial pressure distribution for liquid hydrogen flow through straight cylindrical seal in concentric position—third set of data.

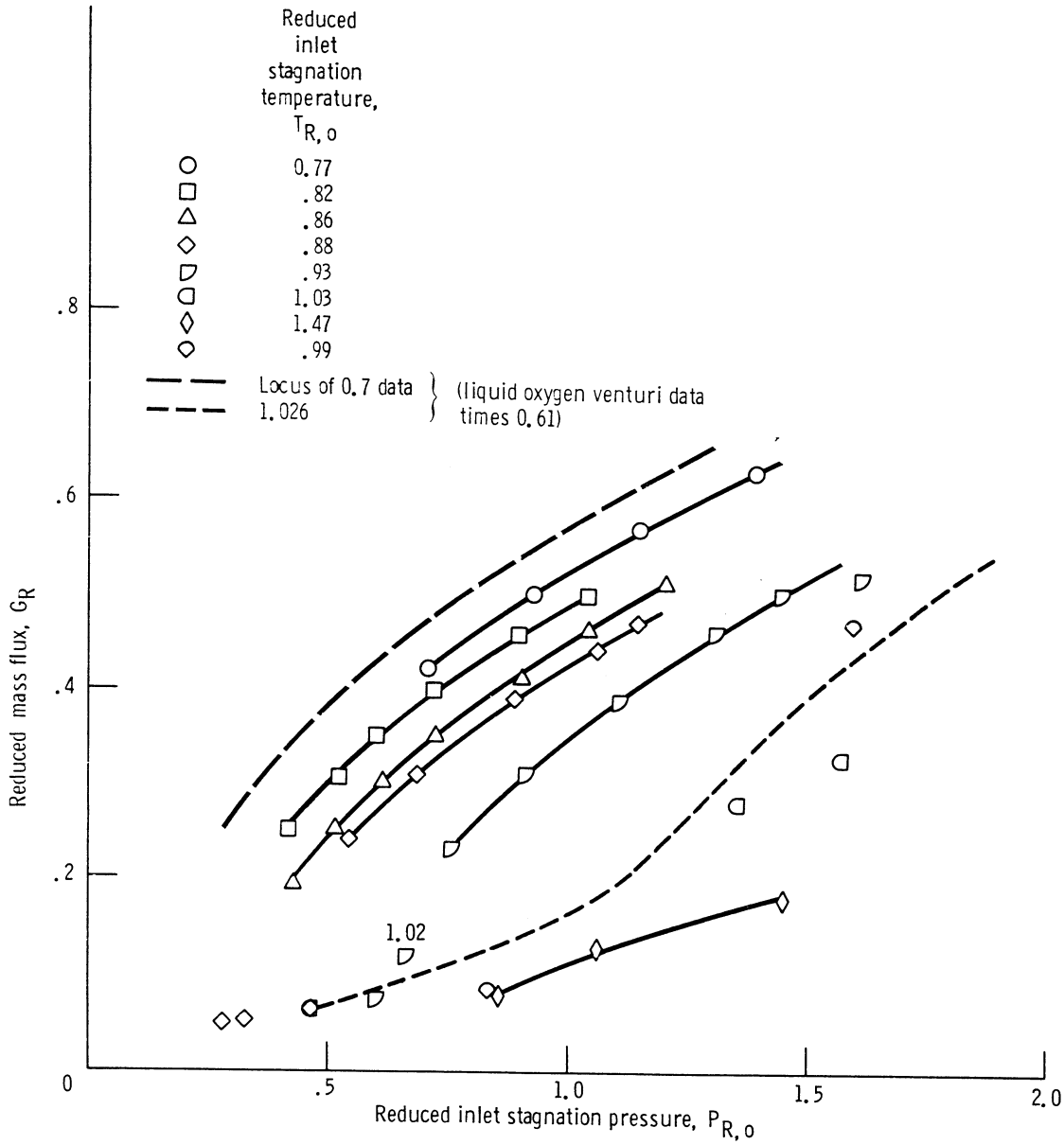

Figure 21.—Reduced mass flux of liquid nitrogen through straight cylindrical seal in concentric position, as function of reduced pressure, for inlet temperatures to and above critical temperature.

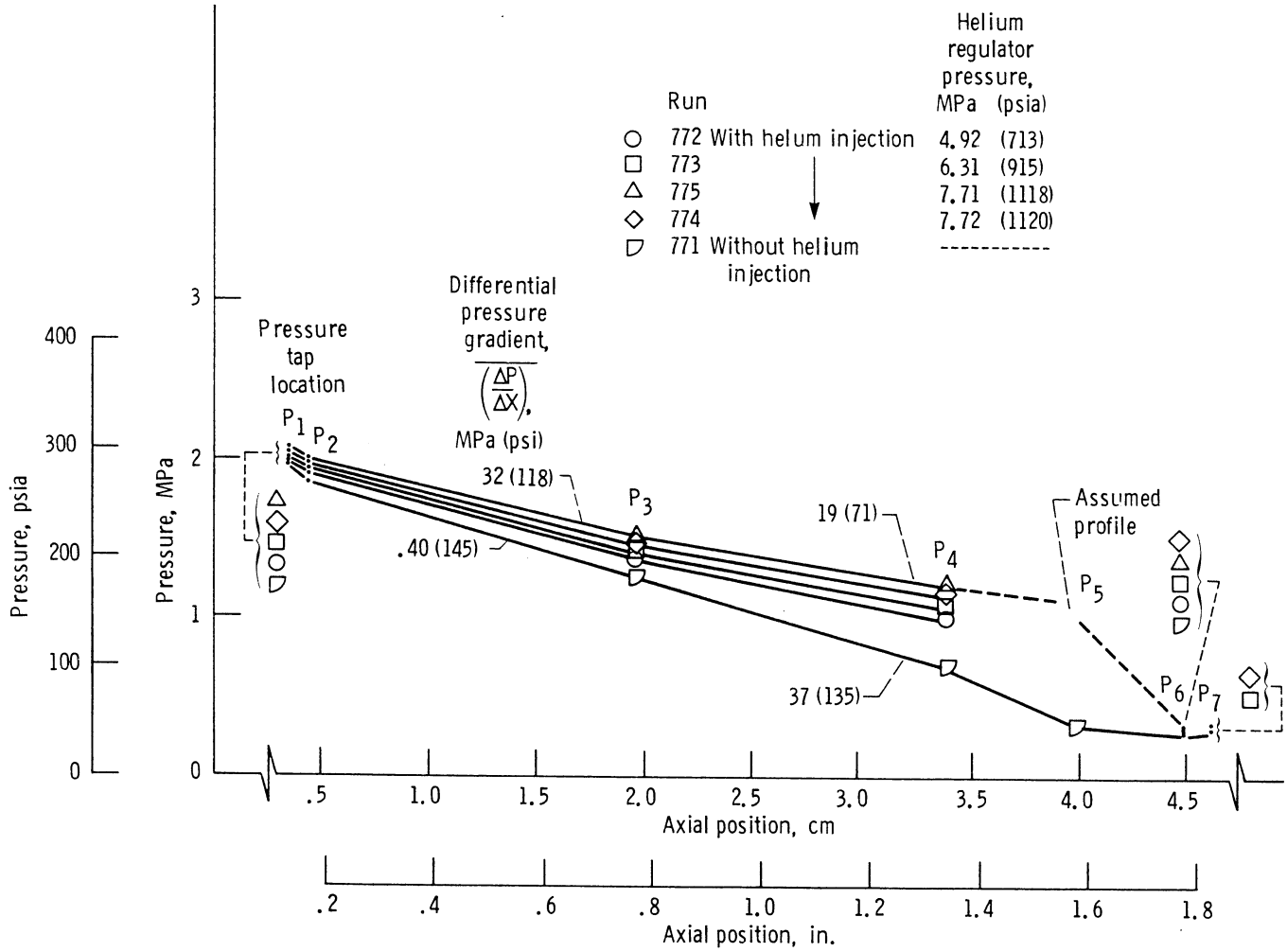

Figure 22.—Axial pressure distribution for helium-augmented gaseous nitrogen flow through straight cylindrical seal in concentric position.

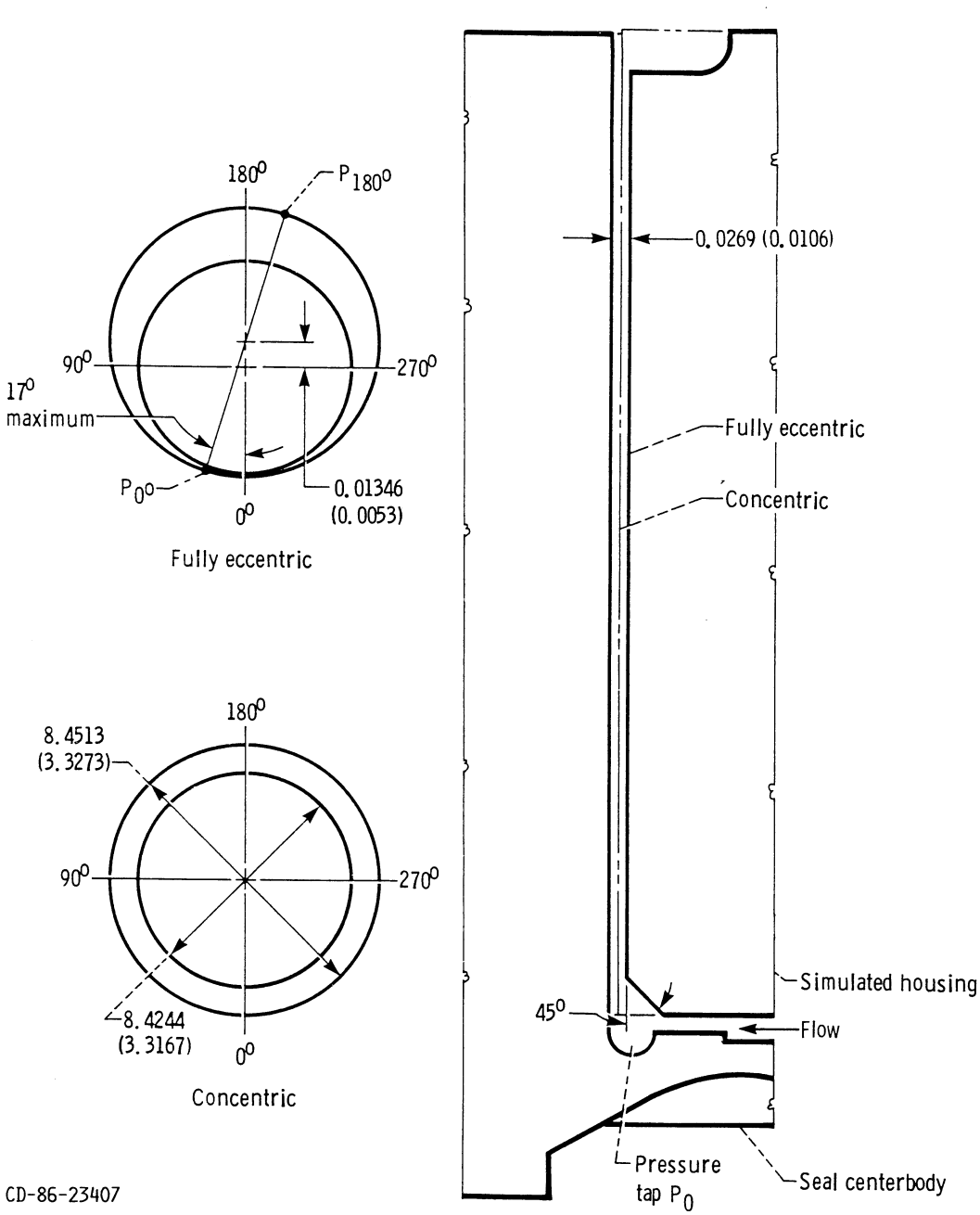

Figure 23.—Schematic of concentric and fully eccentric straight cylindrical seal configurations. (Linear dimensions are in centimeters (inches).)

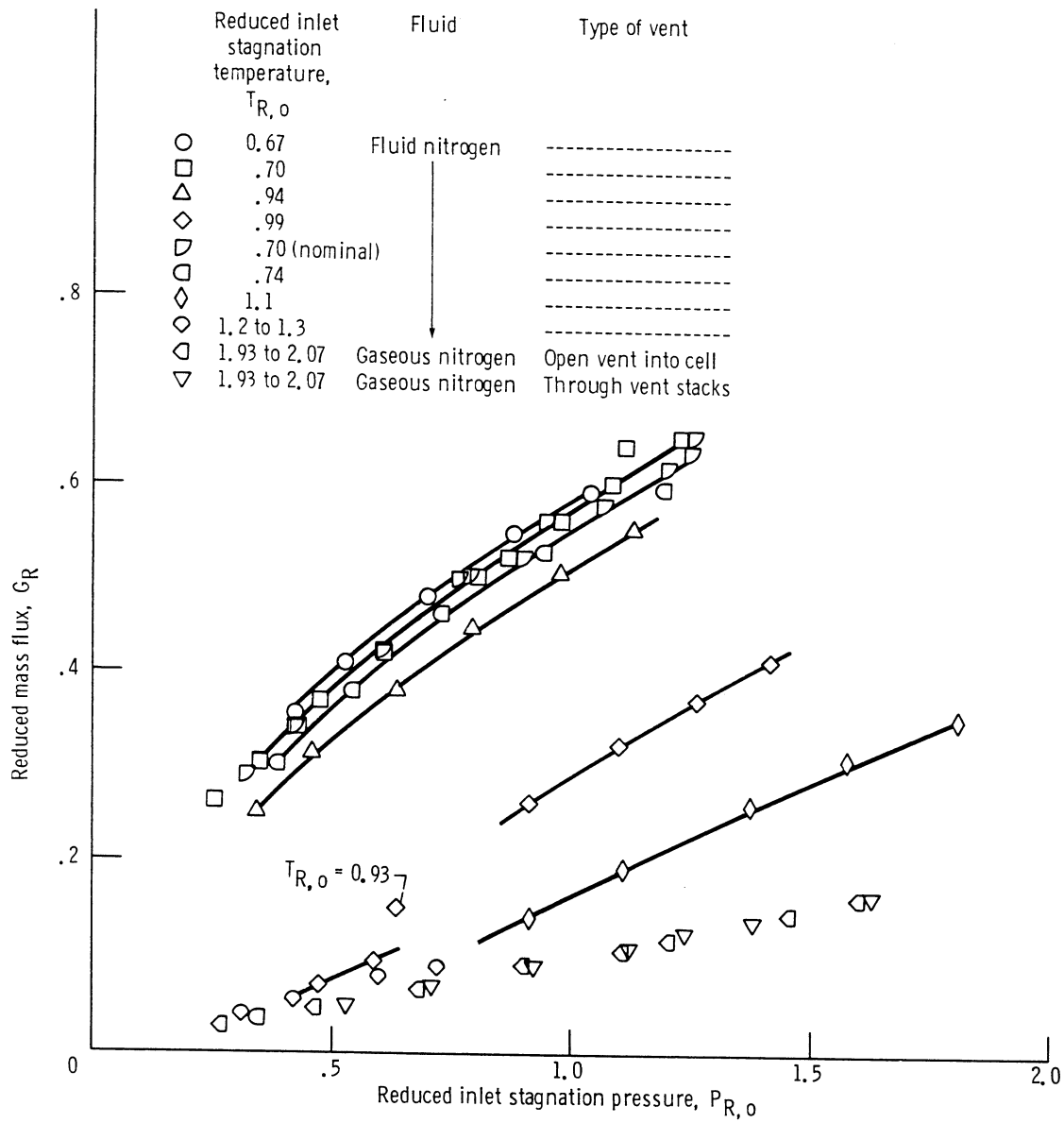

Figure 24.—Reduced mass flux of gaseous and fluid nitrogen through straight cylindrical seal in fully eccentric position, as function of reduced pressure.

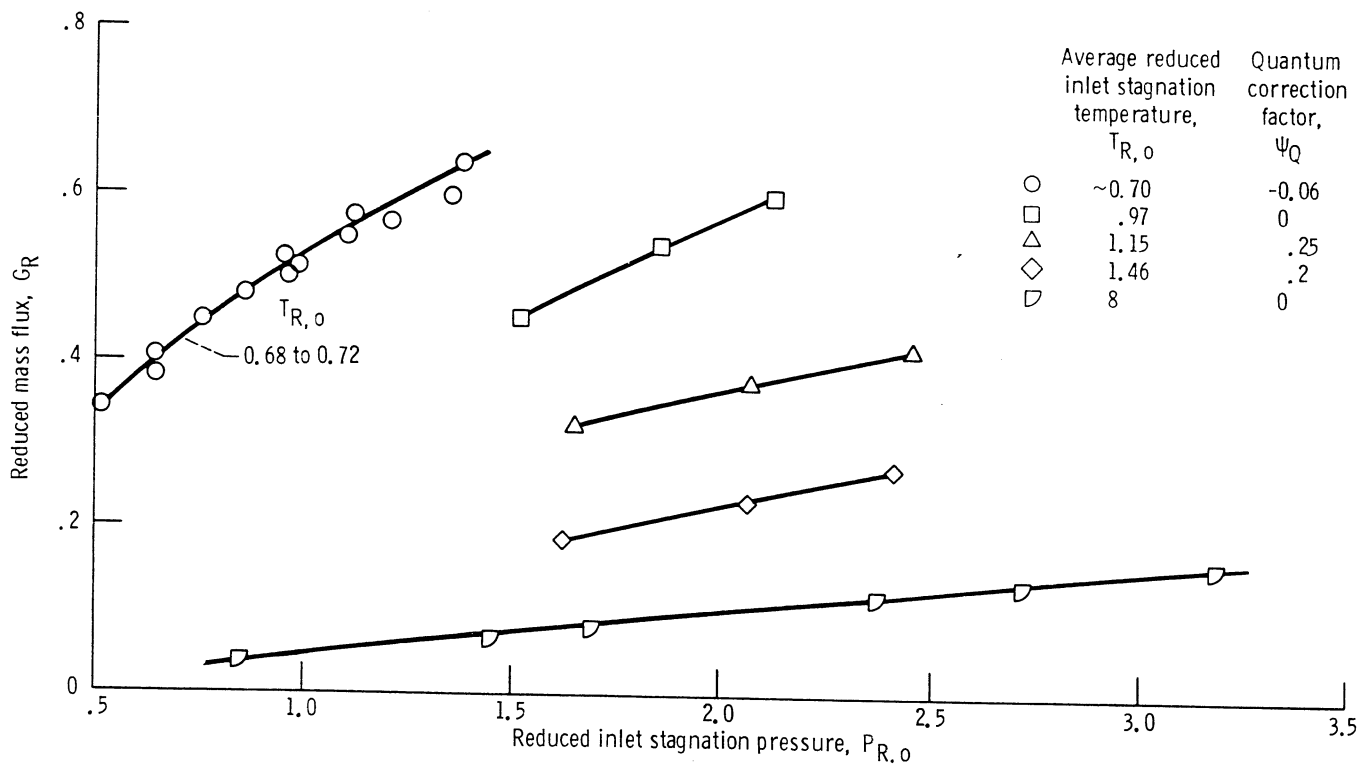

Figure 25.—Reduced mass flux of fluid hydrogen through straight cylindrical seal in fully eccentric position, as function of reduced pressure.

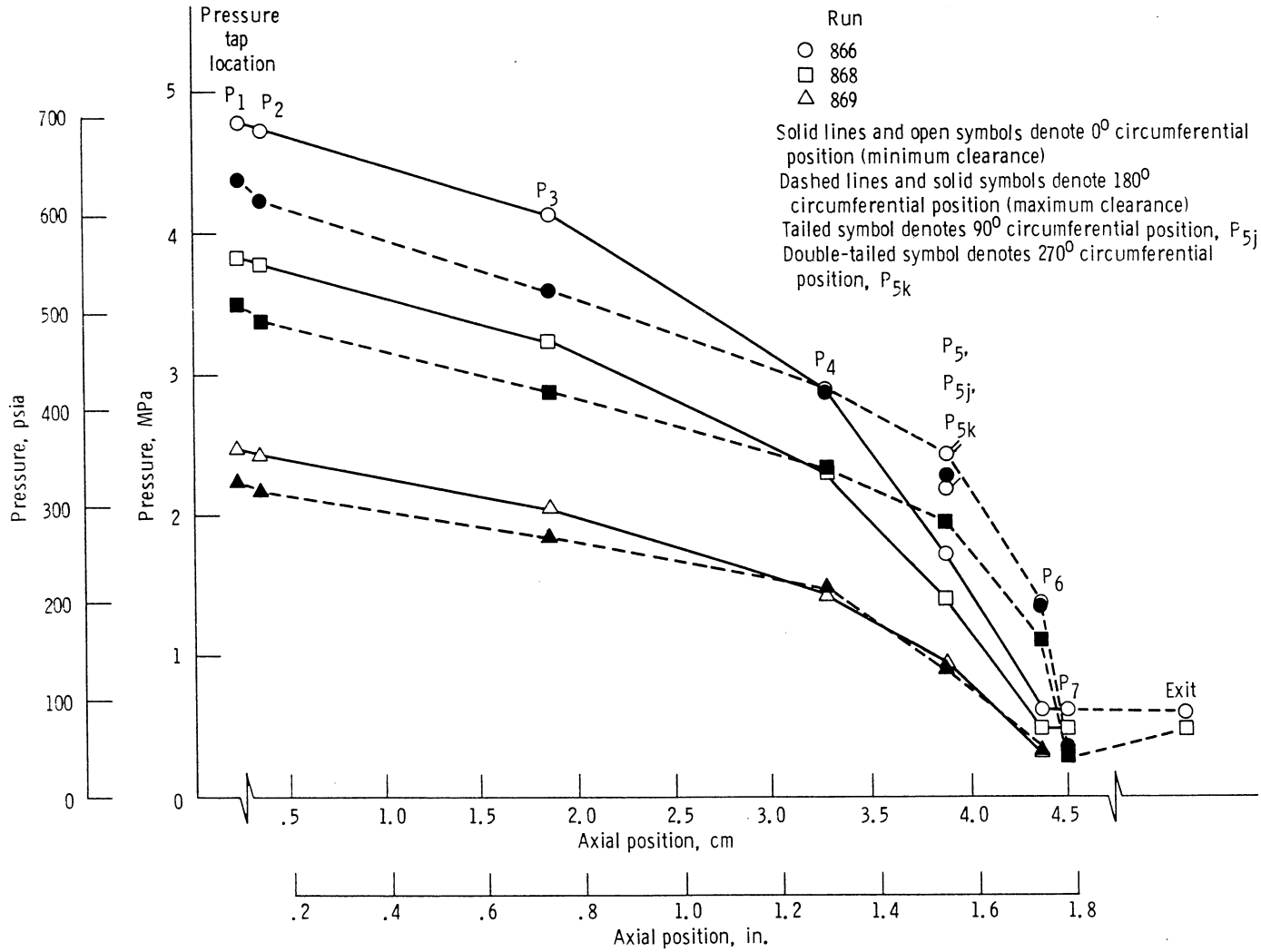

Figure 26.—Axial pressure distribution for gaseous nitrogen flow through straight cylindrical seal in fully eccentric position. (A maximum circumferential position error of 17° off true 0° position was found subsequent to testing and should be realized and considered when interpreting the pressure data.)

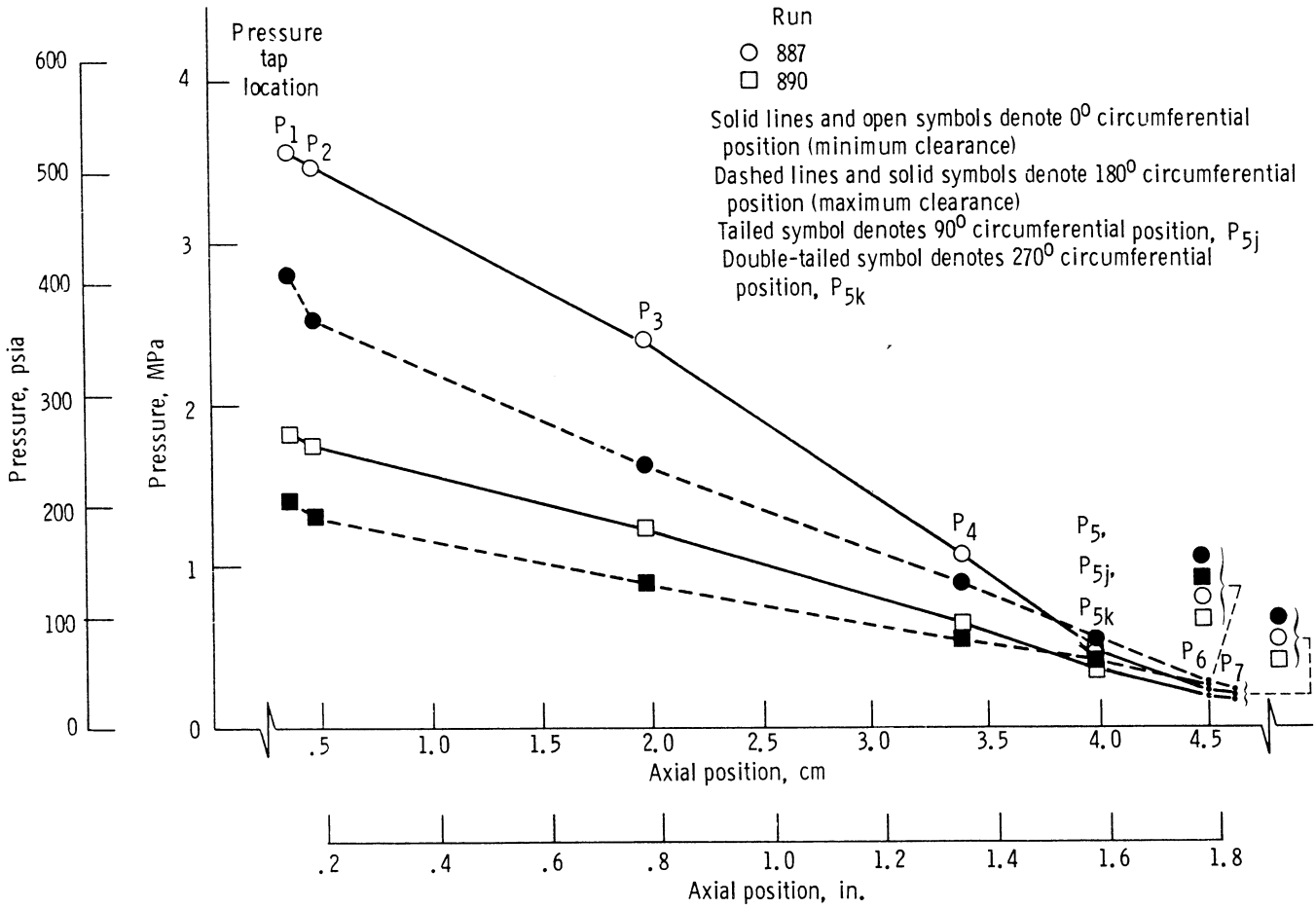

Figure 27.—Axial pressure distribution for liquid nitrogen flow through straight cylindrical seal in fully eccentric position. (A maximum circumferential position error of 17° off true 0° position was found subsequent to testing and should be realized and considered when interpreting the pressure data.)

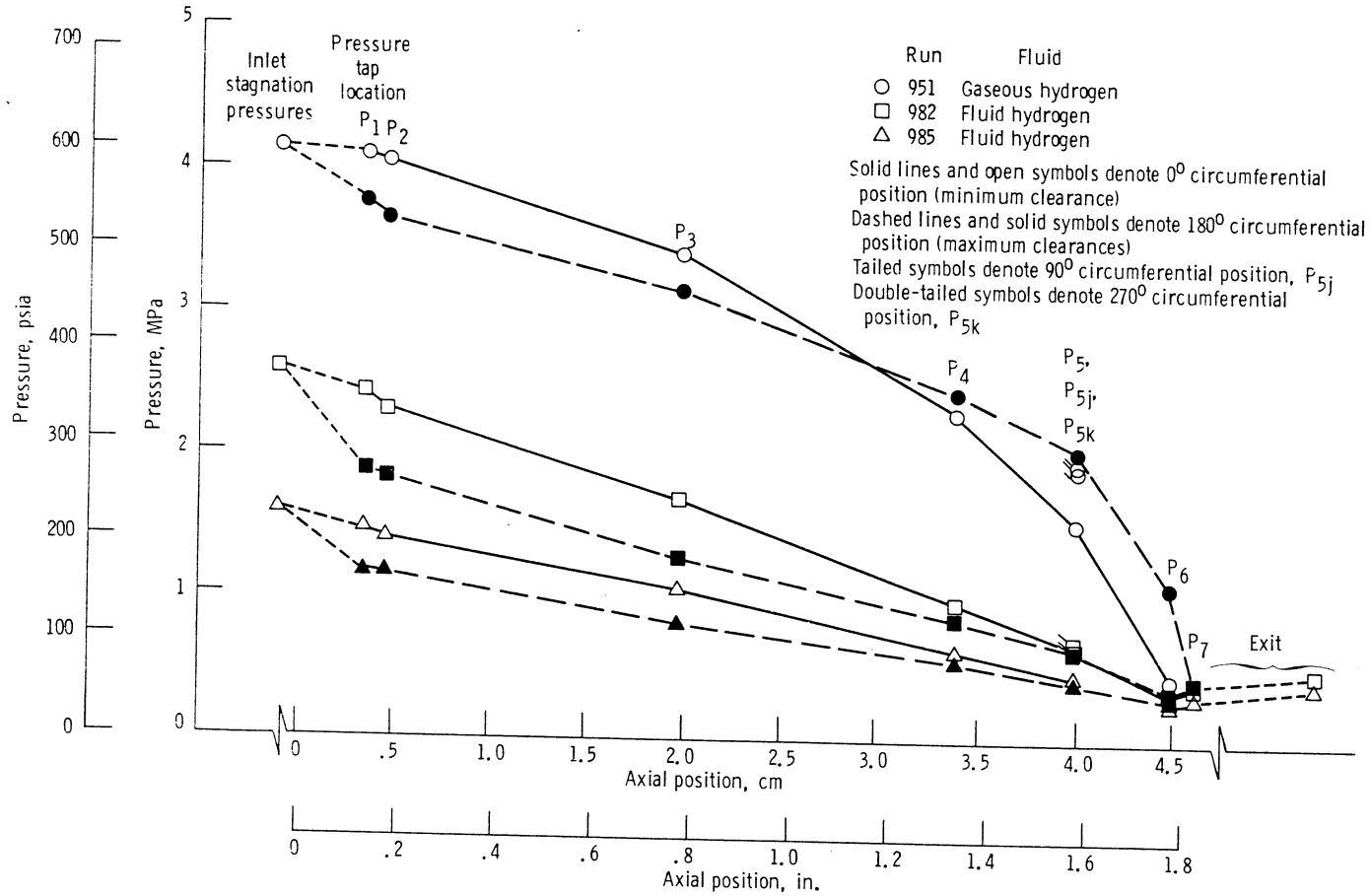

Figure 28.—Axial pressure distribution for gaseous and fluid hydrogen flow through straight cylindrical seal in fully eccentric position.

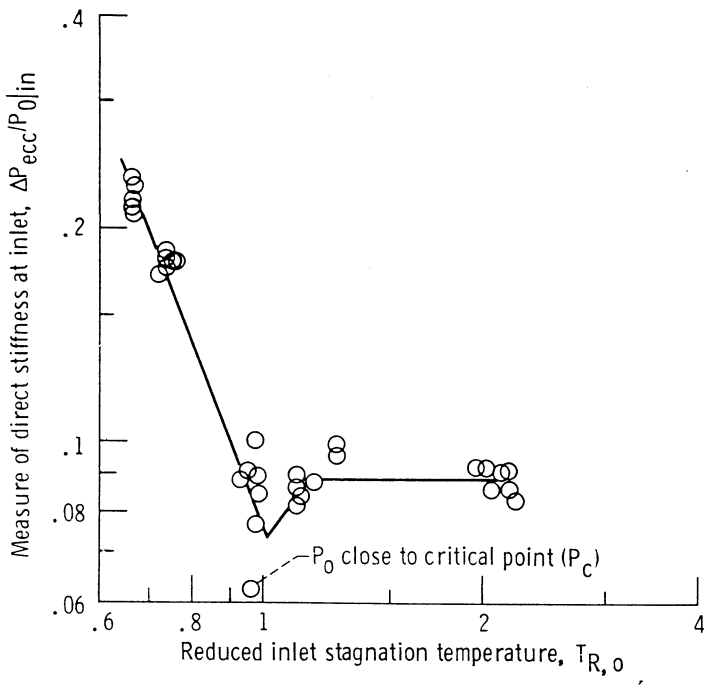

Figure 29.—Eccentric pressure distribution for fluid nitrogen flow through straight cylindrical seal with maximum clearance of 0.0269 cm (0.0106 in.) at 180°; $\Delta P_{ecc}/P_{0\ in} = (P_{0^\circ} - P_{180^\circ})/P_{0^\circ}$.

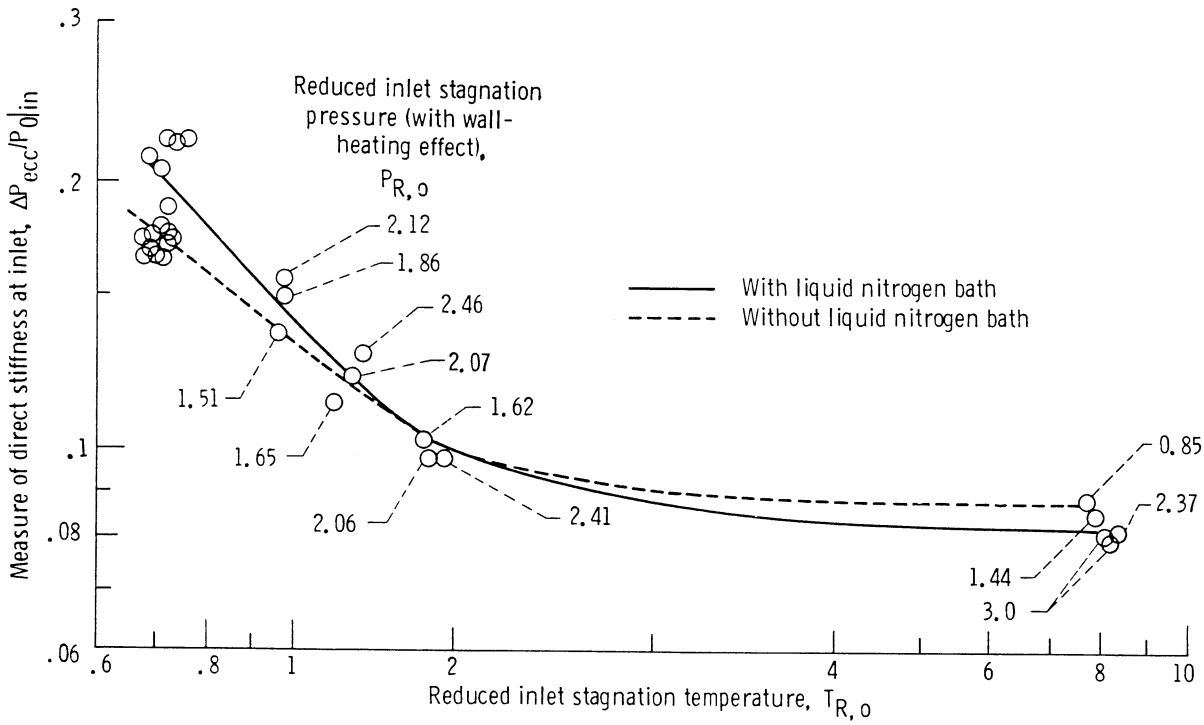

Figure 30.—Eccentric pressure distribution for fluid hydrogen flow through straight cylindrical seal with maximum clearance of 0.0269 cm (0.0106 in.) at 180°; $\Delta P_{ecc}/P_0|_{in} = (P_{0^\circ} - P_{180^\circ})/P_{0^\circ}$. (Wall heating due to operations in ambient environment decreases viscous effects at low $T_{R,o}$ and increases viscous effects near T_c.)

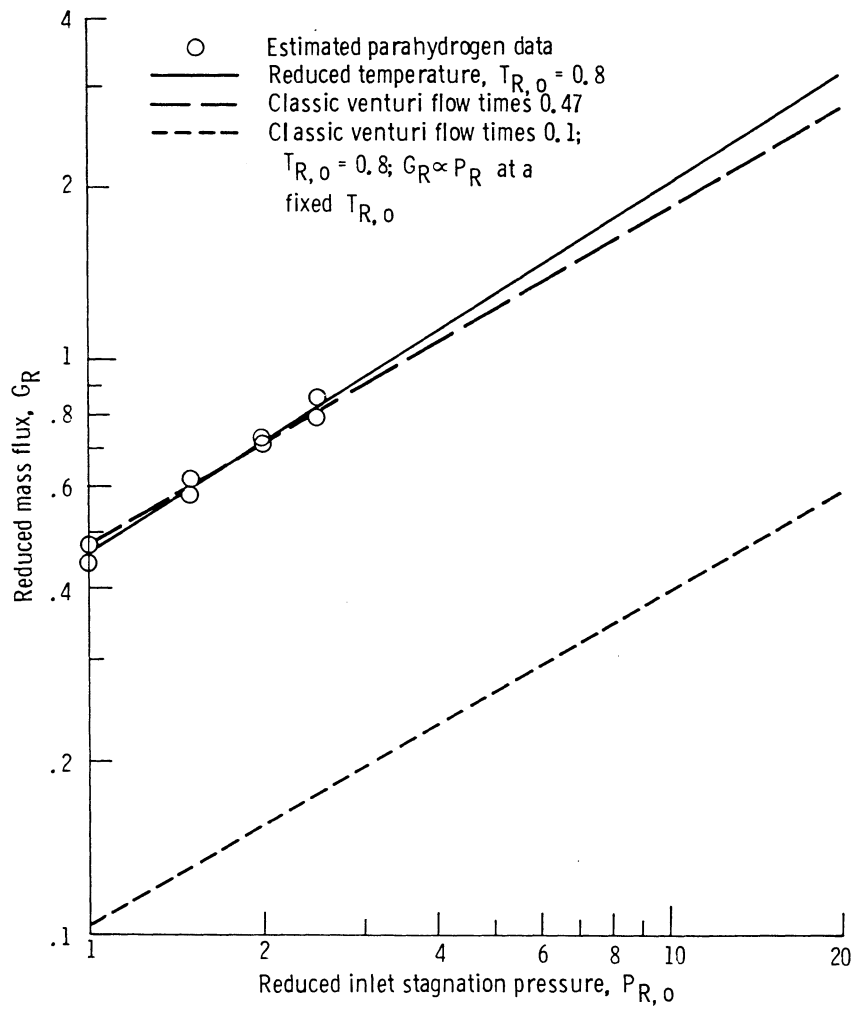

Figure 31.—Extrapolated reduced mass flux of fluid through straight cylindrical seal compared with flow through classical venturi.

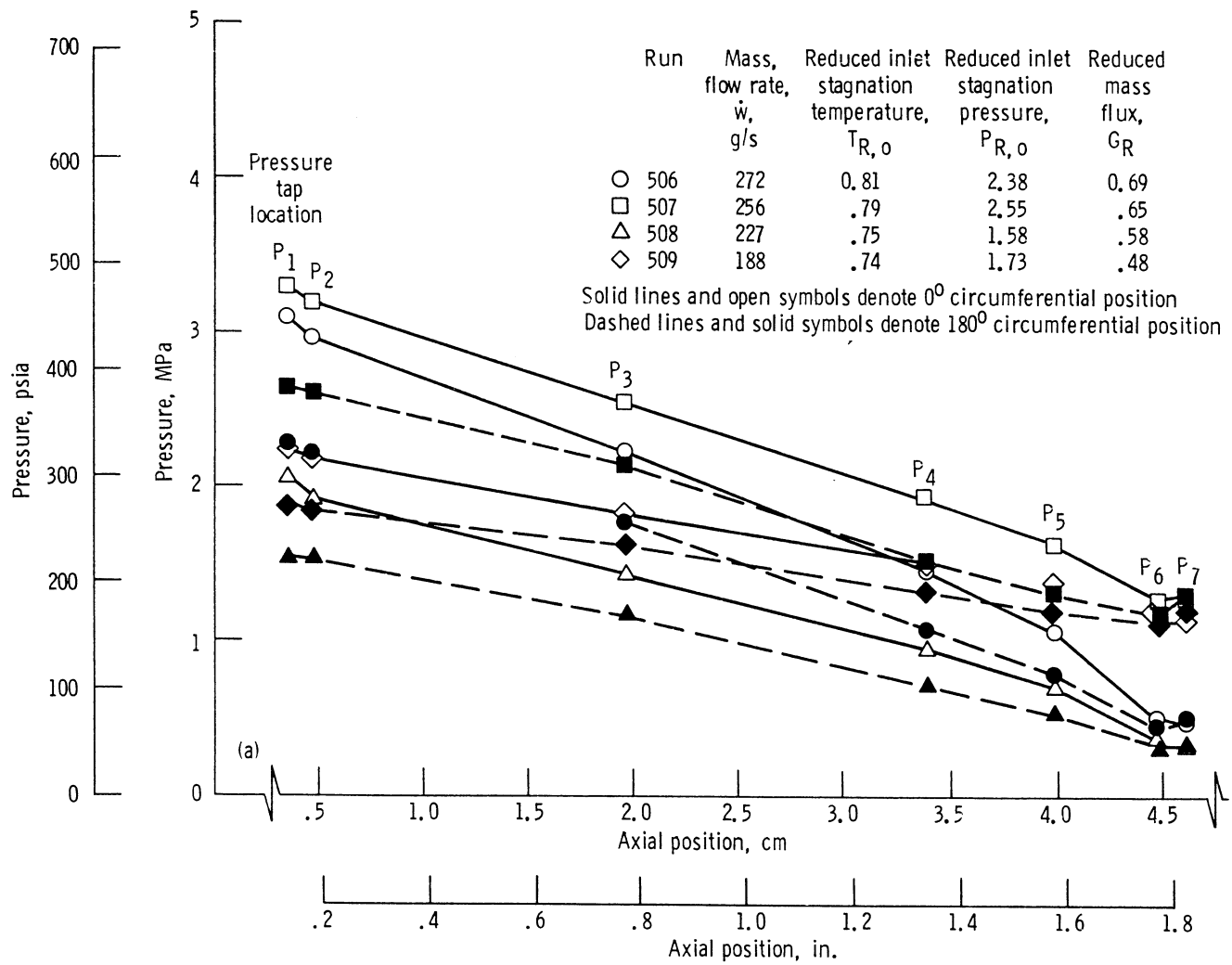

(a) Fluid nitrogen; runs 506 to 509.

Figure 32.—Axial pressure distribution for fluid hydrogen flow through straight cylindrical seal in partially eccentric position, with backpressure control.

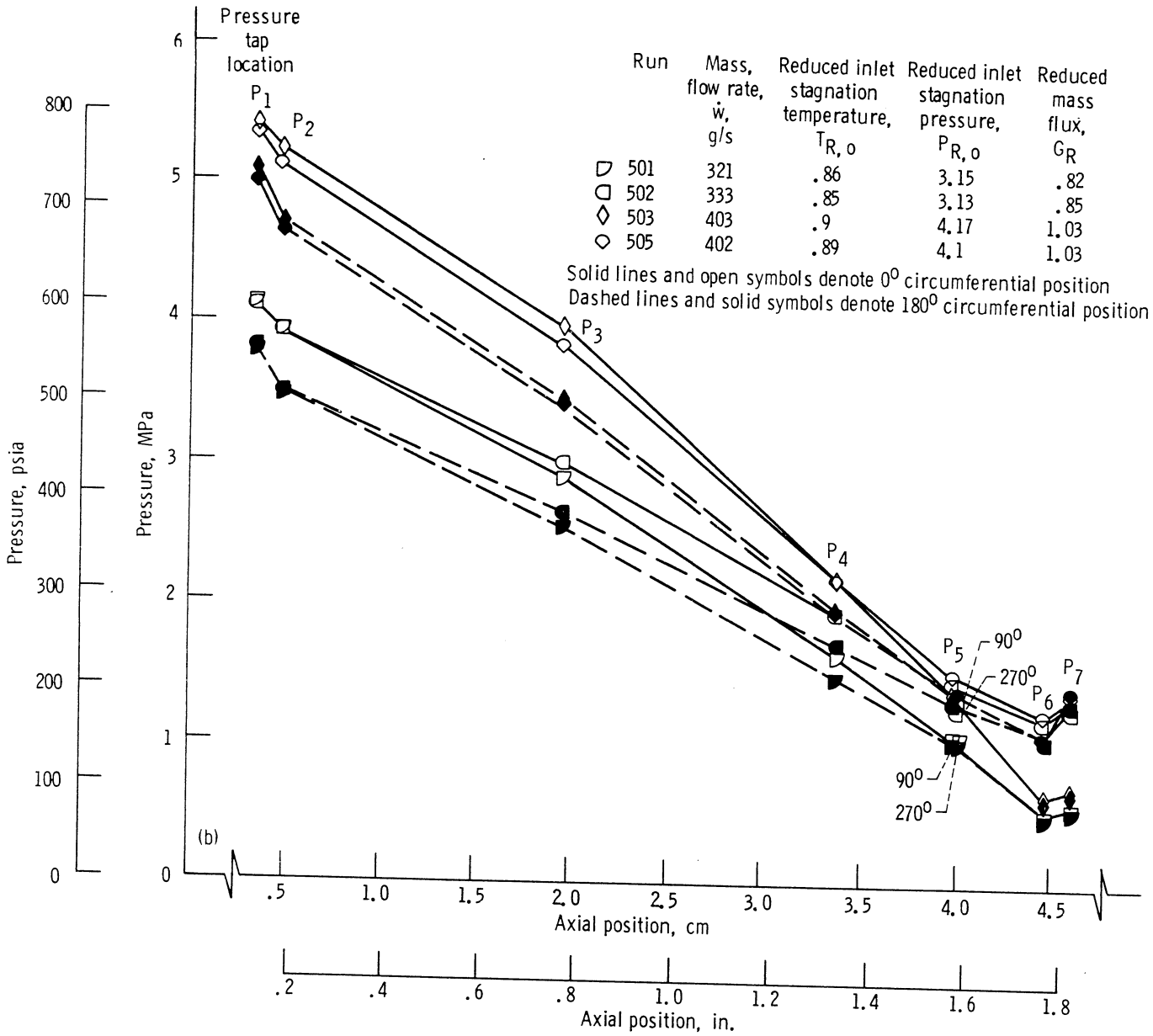

(b) Fluid hydrogen; runs 501 to 505.

Figure 32.—Continued.

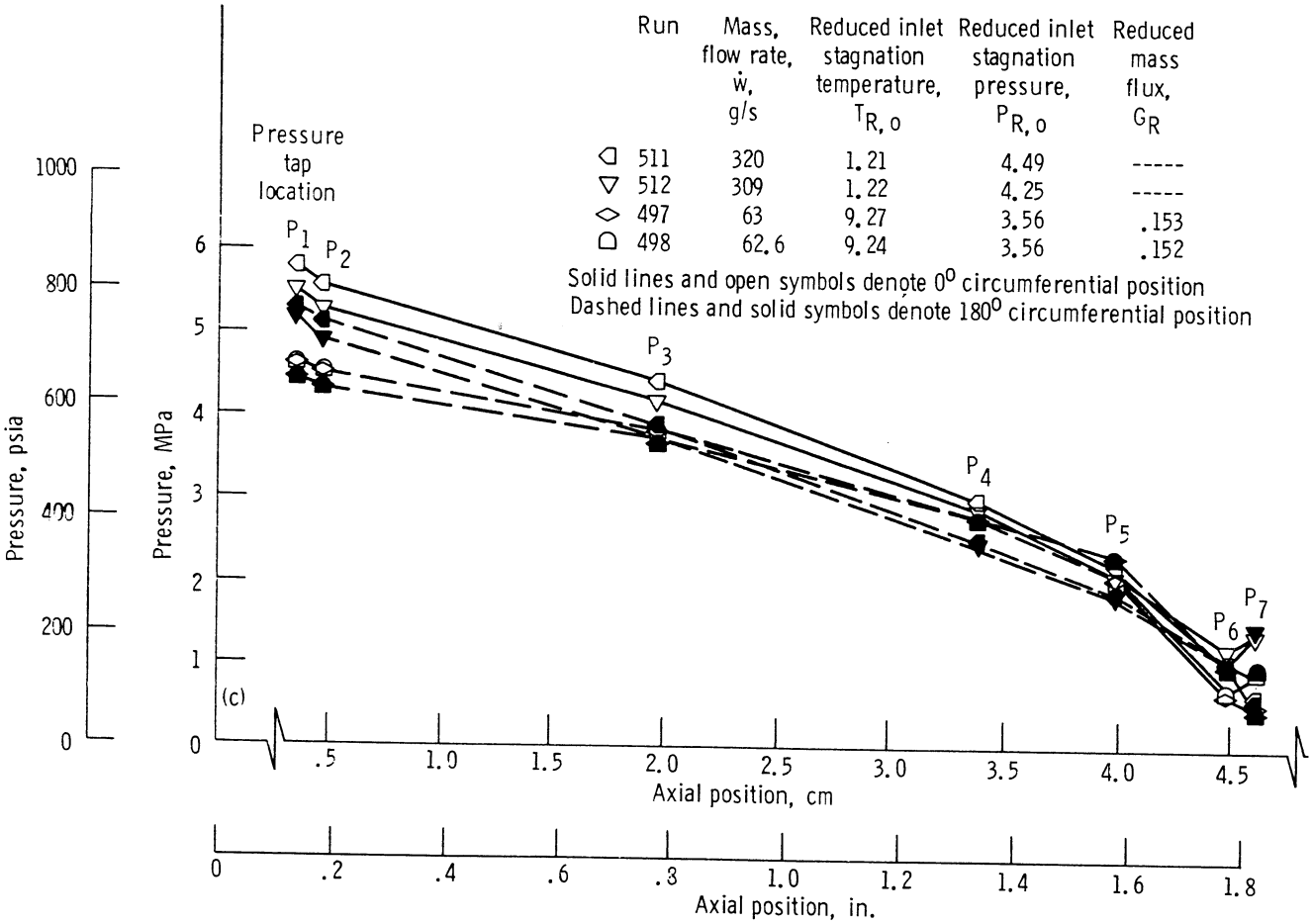

(c) Fluid hydrogen; runs 497, 498, 511, and 512.

Figure 32.—Concluded.

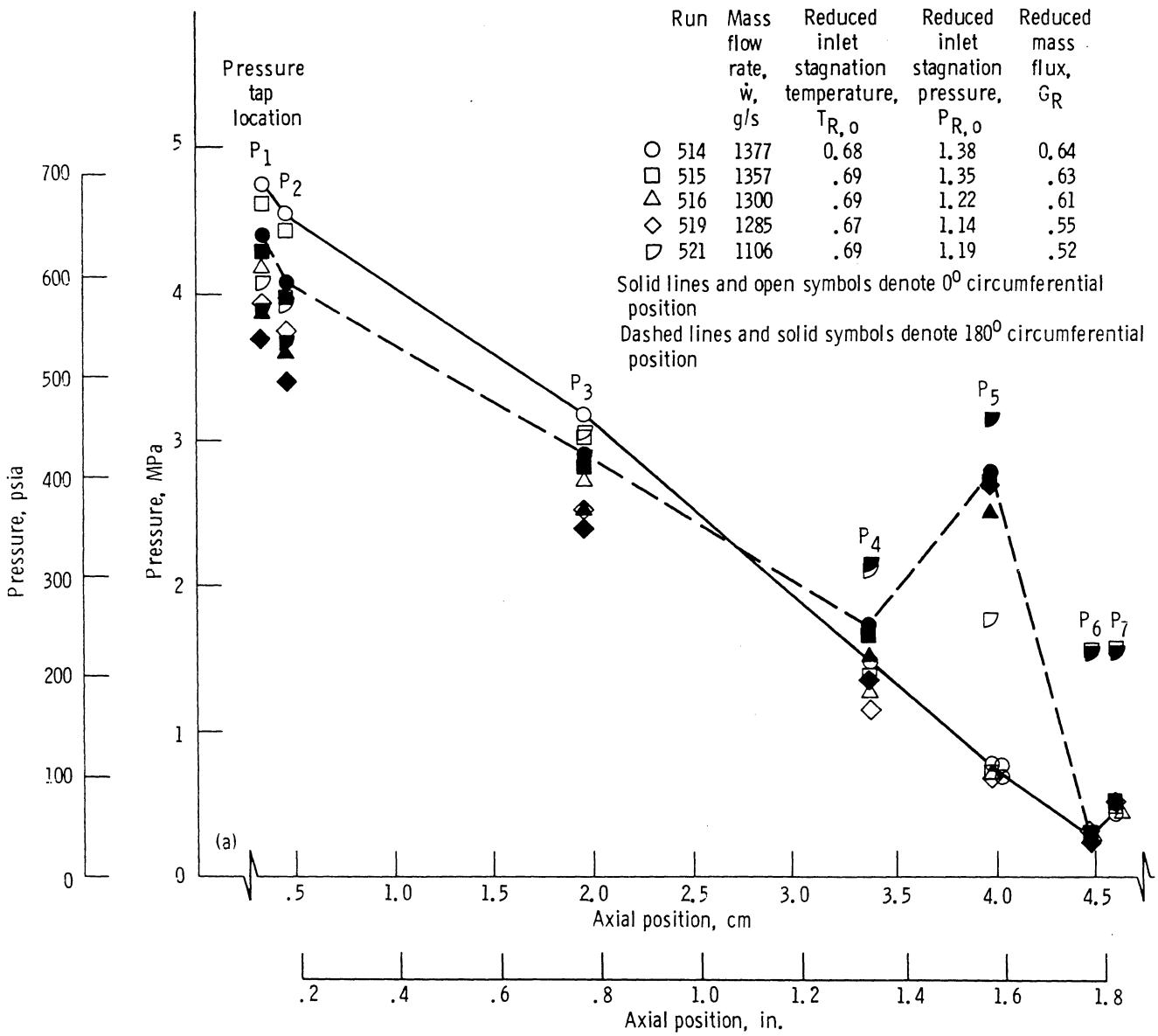

(a) Fluid nitrogen; runs 514 to 516, 519, and 521.

Figure 33.—Axial pressure distribution for nitrogen flow through straight cylindrical seal in partially eccentric position, with backpressure control.

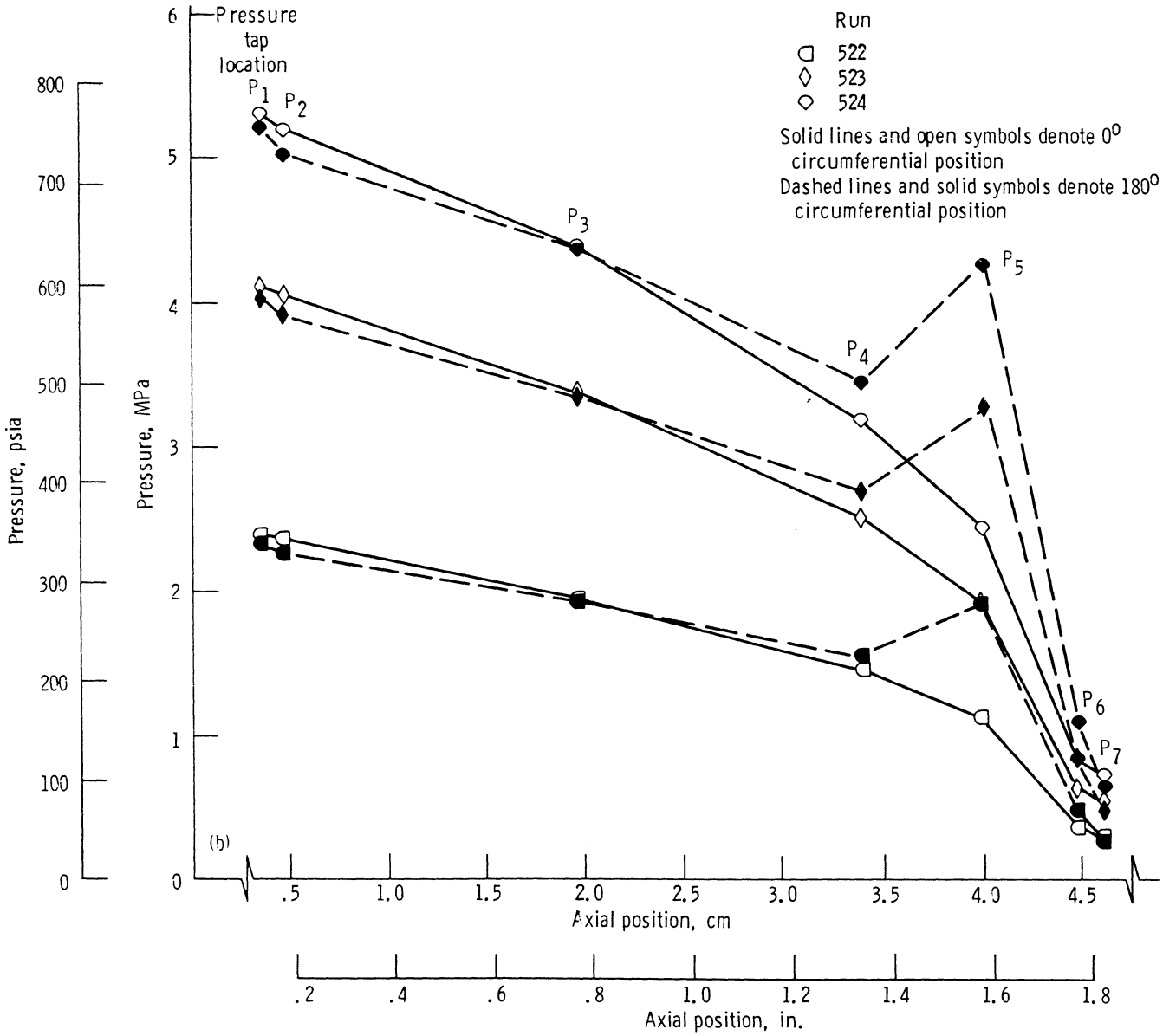

(b) Gaseous nitrogen; runs 522 to 524.

Figure 33.—Continued.

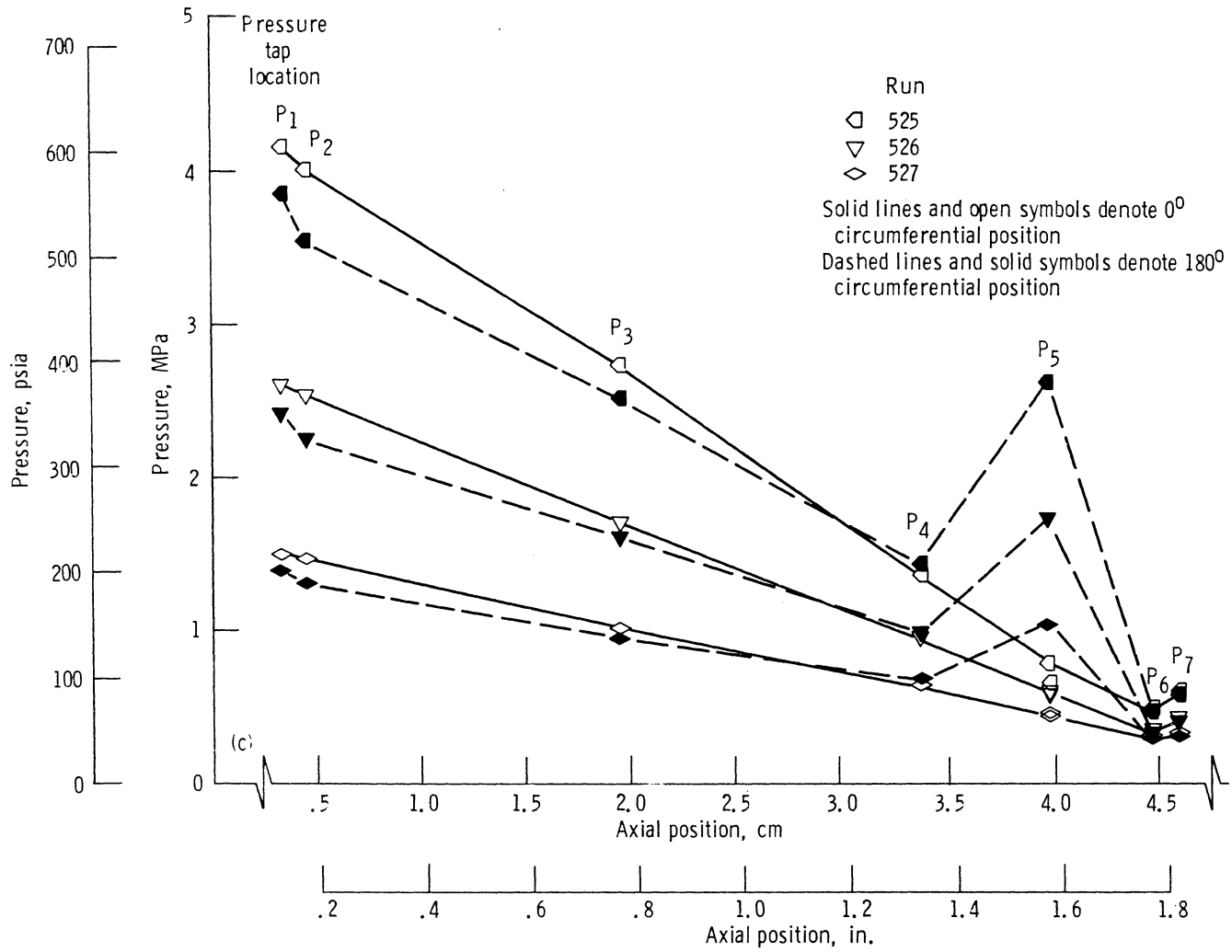

(c) Fluid nitrogen; runs 525 to 527.

Figure 33.—Concluded.

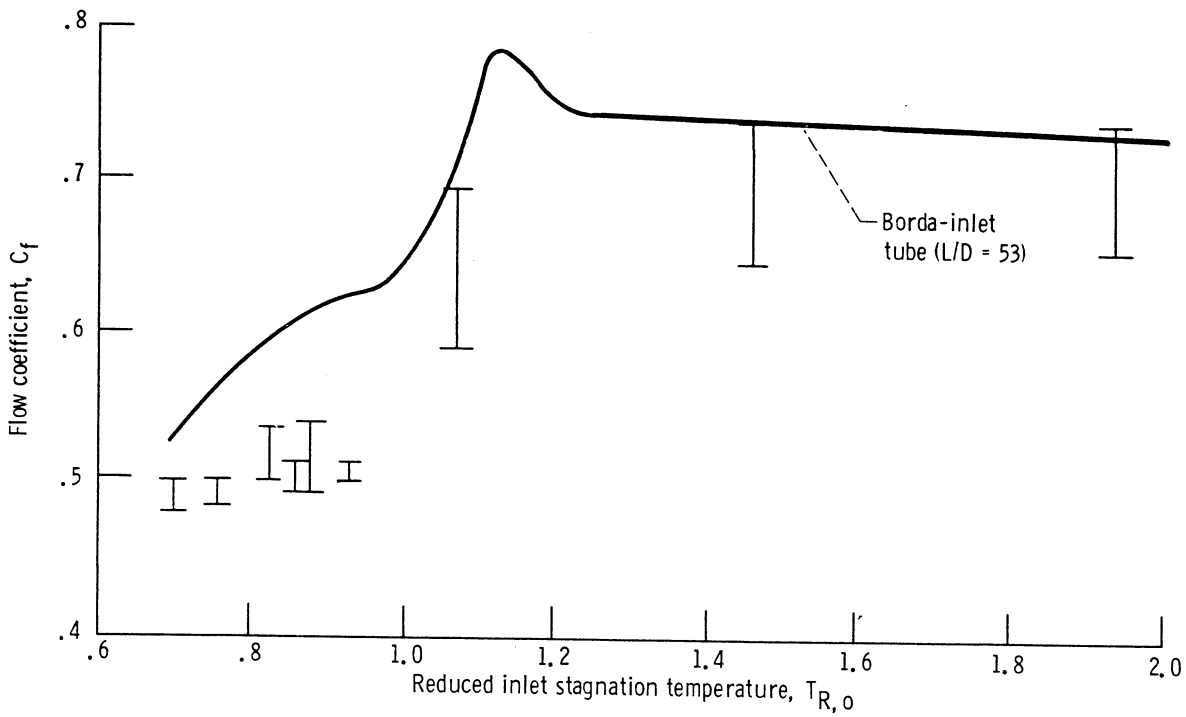

Figure 34.—Flow coefficient as function of reduced inlet stagnation temperature.

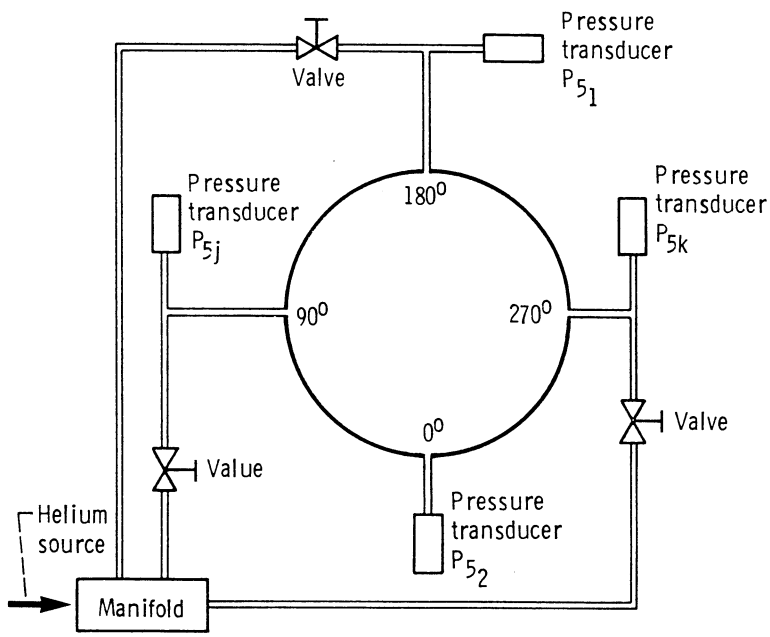

Figure 35.—Helium injection system at axial location 3.998 cm (1.574 in.) from inlet.

TABLE I. – PRESSURE TAP LOCATIONS FOR STRAIGHT CYLINDRICAL SEAL[a]

Pressure tap	Circumferential position, deg	Axial distance from seal inlet	
		cm	in.
1	0,180	0.3302	0.130
2		.4572	.180
3		1.9558	.770
4		3.3909	1.335
5		3.9980	1.574
5j	90	3.9980	1.574
5k	270	3.9980	1.574
6	0,180	4.4958	1.770
7	0,180	4.6228	1.820

[a]See also figure 6.

TABLE II. – CRITICAL CONSTANTS USED IN REDUCING PARAMETERS

Fluid	Critical pressure, P_c		Critical temperature, T_c		Critical density, ρ_c		Compressibility, $Z_c = \frac{P_c}{\rho_c R T_c}$	Flow-normalizing parameter, G^*	
	MPa	psi	K	°R	g/cm³	lbm/in.³		g/cm² s	lbm/in.² s
Nitrogen	3.417	495.5	126.3	227.3	0.3105	0.0112	0.2937	6010.4	85.49
Oxygen	5.083	737.0	154.78	278.6	.4325	.0156	.2922	8073.9	114.8
Methane	4.627	670.9	190.77	343.4	.162	.00585	.2889	5093.7	72.45
Argon	4.865	705.4	150.7	271.3	.531	.0192	.2921	9404.2	133.8
Parahydrogen	1.2925	187.4	32.976	59.36	.03143	.00114	.3023	1158	16.47
Helium	.22746	32.98	5.2014	9.362	.06964	.00252	.3023	724	10.30

TABLE III.—FLOW RATE AND PRESSURE DROP DATA FOR STRAIGHT CYLINDRICAL SEAL, CONCENTRIC POSITION

[Where two values are given, the top value is for the 0° circumferential position and the bottom value is for the 180° circumferential position.]

(a) Nitrogen

Run	$\dot{w}$, g/s	P_o, MPa	T_o, K	P_0, MPa	Pressure at pressure tap locations 1 to 7, MPa								P_e, MPa
					P_1	P_2	P_3	P_4	P_5	(a)	P_6	P_7	
528	279.	4.60	267.0	(b)	4.17	4.03	3.42	2.59	2.07	2.00	0.84	0.27	(b)
					4.24	4.08	3.59	2.67	2.09	2.23	0.84	0.28	
529	213.	3.51	254.9		3.15	3.06	2.60	1.98	1.61	1.56	0.65	0.20	
					3.20	3.08	2.69	2.02	1.60	1.70	0.64	0.21	
530	150.	2.51	245.0		2.28	2.21	1.89	1.46	1.19	1.16	0.48	0.14	
					2.31	2.21	1.93	1.46	1.17	1.24	0.47	0.14	
531	107.	1.80	239.4		1.61	1.56	1.34	1.04	0.86	0.83	0.34	0.10	
					1.63	1.55	1.36	1.03	0.84	0.88	0.33	0.09	
532	77.	1.36	239.8		1.23	1.19	1.03	0.80	0.66	0.65	0.26	0.10	
					1.24	1.18	1.04	0.79	0.64	0.68	0.25	0.10	
533	64.	1.15	239.5		1.01	0.98	0.85	0.66	0.55	0.54	0.21	0.10	
					1.02	0.96	0.85	0.65	0.53	0.56	0.20	0.11	
534	102.	5.51	274.8		5.03	4.88	4.16	3.14	2.50	2.40	1.00	0.30	
					5.12	4.92	4.33	3.22	2.50	2.66	0.98	0.30	
535	152.	2.71	274.7		2.42	2.37	2.01	1.56	1.28	1.23	0.54	0.66	
					2.47	2.39	2.08	1.57	1.25	1.30	0.54	0.67	
536	112.	2.05	271.4		1.82	1.79	1.52	1.18	0.98	0.94	0.40	0.49	
					1.86	1.80	1.56	1.19	0.95	0.99	0.40	0.50	
537	84.	1.57	268.7		1.38	1.36	1.16	0.91	0.75	0.72	0.31	0.33	
					1.41	1.37	1.19	0.91	0.73	0.76	0.31	0.39	
538	192.	3.46	278.7		3.10	3.03	2.57	1.99	1.63	1.57	0.79	0.95	
					3.16	3.06	2.66	2.00	1.59	1.67	0.76	0.96	
540	243.	4.21	273.4		3.79	3.70	3.14	2.41	1.96	1.89	0.98	1.18	
					3.85	3.73	3.25	2.44	1.92	2.03	0.94	1.19	
541	(c)	1.92	87.8		1.58	1.53	1.18	0.85	0.71	0.71	0.63	0.68	
					1.65	1.59	0.88	0.83	0.70	0.71	0.62	0.68	
542		2.40	89.1		1.94	1.86	1.36	0.90	0.72	0.71	0.60	0.67	
					2.04	1.95	0.96	0.89	0.71	0.71	0.60	0.68	
543		1.47	84.5		1.21	1.17	0.92	0.70	0.60	0.59	0.53	0.56	
					1.26	1.22	0.73	0.68	0.58	0.60	0.53	0.58	
546		2.19	89.4		1.75	1.66	1.17	0.71	0.51	0.49	0.28	0.26	
					1.82	1.53	0.98	0.67	0.47	0.52	0.30	0.29	
547		2.51	90.0		2.01	1.91	1.33	0.78	0.56	0.53	0.30	0.27	
					2.09	1.75	1.09	0.74	0.51	0.55	0.31	0.30	
548		2.94	91.6		2.37	2.25	1.55	0.90	0.63	0.61	0.34	0.30	
					2.42	2.17	1.25	0.84	0.58	0.62	0.35	0.33	
549		2.36	85.4		1.82	1.71	1.16	0.63	0.42	0.38	0.19	0.20	
					1.87	1.75	0.96	0.56	0.37	0.42	0.20	0.23	

[a]Top value, P_{5j} (90°); bottom value, P_{5k} (270°).
[b]Pressure unavailable; exhausted to ambient.
[c]Flow rate unavailable; exhausted to ambient.

TABLE III.—Continued.

(a) Continued.

Run	$\dot{w}$, g/s	P_o, MPa	T_o, K	P_0, MPa	Pressure at pressure tap locations 1 to 7, MPa								P_e, MPa
					P_1	P_2	P_3	P_4	P_5	(a)	P_6	P_7	
550	(c)	2.71	85.8	(b)	2.11	1.98	1.32	0.71	0.46	0.42	0.20	0.22	(b)
					2.16	2.03	1.09	0.63	0.41	0.45	0.21	0.24	
551		3.06	86.3		2.37	2.22	1.47	0.75	0.48	0.46	0.22	0.23	
					2.42	2.28	1.22	0.70	0.44	0.49	0.23	0.25	
552		3.63	87.0		2.82	2.65	1.74	0.87	0.55	0.52	0.24	0.25	
					2.88	2.71	1.42	0.82	0.50	0.55	0.25	0.27	
554		4.29	88.9		3.12	3.11	2.08	1.04	0.65	0.61	0.28	0.29	
					3.47	3.26	1.71	0.99	0.60	0.66	0.30	0.32	
555		4.98	93.4		4.07	3.74	2.46	1.24	0.80	0.81	0.40	0.38	
					4.13	3.89	2.13	1.24	0.78	0.87	0.42	0.41	
556		4.50	88.6		3.61	3.36	2.16	1.05	0.62	0.64	0.29	0.29	
					3.68	3.46	1.86	1.04	0.62	0.69	0.30	0.32	
557		4.84	89.2		3.93	3.64	2.33	1.10	0.67	0.68	0.30	0.31	
					4.00	3.76	2.04	1.12	0.66	0.73	0.32	0.33	
558		5.37	90.0		4.43	4.12	2.63	1.22	0.73	0.74	0.33	0.34	
					4.47	4.21	2.37	1.24	0.72	0.82	0.34	0.36	
559		2.99	89.8		2.43	2.30	1.58	0.88	0.61	0.58	0.34	0.36	
					2.46	2.33	1.44	0.85	0.57	0.60	0.35	0.37	
560		3.37	88.5		2.70	2.53	1.67	0.86	0.57	0.56	0.27	0.28	
					2.74	2.58	1.53	0.85	0.54	0.57	0.28	0.29	
562		4.04	88.5		3.25	3.05	1.97	0.97	0.62	0.63	0.28	0.29	
					3.30	3.11	1.82	0.97	0.59	0.65	0.30	0.31	
563		4.35	89.0		3.53	3.30	2.12	1.03	0.65	0.67	0.29	0.30	
					3.58	3.35	1.96	1.04	0.63	0.69	0.31	0.32	
564		4.69	87.9		3.82	3.57	2.25	1.03	0.63	0.67	0.27	0.29	
					3.87	3.64	2.09	1.06	0.62	0.70	0.29	0.30	
565		5.29	87.8		4.39	4.11	2.58	1.14	0.67	0.71	0.27	0.30	
					4.42	4.16	2.40	1.19	0.67	0.77	0.29	0.31	
566		4.68	87.8		3.81	3.58	2.30	1.07	0.65	0.66	0.26	0.29	
					3.86	3.64	2.11	1.08	0.63	0.71	0.28	0.29	
567		3.28	91.7		2.74	2.63	1.96	1.20	0.85	0.81	0.49	0.50	
					2.60	2.45	1.61	1.02	0.74	0.77	0.49	0.52	
568		3.53	89.6		2.87	2.73	1.86	1.00	0.66	0.63	0.35	0.38	
					2.87	2.71	1.65	0.93	0.60	0.65	0.35	0.39	
569		4.00	90.2		3.28	3.07	2.06	1.05	0.68	0.65	0.34	0.33	
					3.32	3.12	1.85	1.00	0.63	0.68	0.34	0.35	
570		3.45	89.9		2.78	2.62	1.76	0.93	0.62	0.60	0.31	0.30	
					2.83	2.68	1.61	0.90	0.58	0.63	0.32	0.33	
571		3.09	90.4		2.47	2.34	1.59	0.86	0.60	0.58	0.32	0.30	
					2.53	2.38	1.46	0.84	0.56	0.60	0.32	0.32	

[a]Top value, P_{5j} (90°); bottom value, P_{5k} (270°).
[b]Pressure unavailable; exhausted to ambient.
[c]Flow rate unavailable; exhausted to ambient.

TABLE III.—Continued.

(a) Continued.

Run	$\dot{w}$, g/s	P_o, MPa	T_o, K	P_0, MPa	Pressure at pressure tap locations 1 to 7, MPa								P_e, MPa
					P_1	P_2	P_3	P_4	P_5	(a)	P_6	P_7	
572	1217.	3.99	89.8	(b)	3.29	3.15	2.29	1.29	0.83	0.76	0.42	0.50	(b)
					3.15	2.94	1.82	1.07	0.71	0.71	0.42	0.51	
573	1288.	4.61	88.9		3.76	3.55	2.38	1.17	0.70	0.70	0.32	0.38	
					3.79	3.57	2.00	1.06	0.63	0.68	0.33	0.39	
574	1315.	4.82	89.0		4.00	3.75	2.46	1.16	0.70	0.70	0.31	0.32	
					4.09	3.86	2.21	1.14	0.66	0.74	0.32	0.34	
575	1397.	5.41	89.7		4.58	4.29	2.78	1.25	0.74	0.75	0.33	0.34	
					4.67	4.42	2.58	1.29	0.72	0.84	0.34	0.36	
576	1366.	5.18	89.6		4.25	3.97	2.58	1.16	0.69	0.70	0.31	0.33	
					4.34	4.10	2.34	1.19	0.68	0.79	0.32	0.35	
577	1315.	4.73	88.5		3.89	3.65	2.38	1.08	0.64	0.65	0.28	0.29	
					3.98	3.76	2.12	1.09	0.62	0.72	0.29	0.32	
579	1295.	4.67	88.7		3.86	3.61	2.33	1.06	0.64	0.66	0.30	0.30	
					3.96	3.74	2.14	1.10	0.63	0.73	0.30	0.33	
580	(d)	2.35	190.6		2.29	2.29	2.28	2.29	2.29	2.29	2.28	2.28	
					2.29	2.29	2.29	2.29	2.28	2.30	2.28	2.32	
581	(d)	1.76	197.6		1.71	1.70	1.70	1.70	1.71	1.70	1.69	1.70	
					1.70	1.70	1.70	1.71	1.70	1.72	1.70	1.73	
582	1459.	11.10	86.9		3.10	10.18	3.56	1.68	0.84	0.85	0.32	0.37	
					8.51	8.25	4.51	1.29	0.82	0.66	0.41	0.45	
583	1600.	9.67	207.5		7.67	7.43	5.52	0.94	1.03	0.58	0.28	0.39	
					7.96	5.12	3.31	0.87	0.53	0.86	0.38	0.30	
584	1455.	5.56	87.5		4.59	4.30	2.75	1.20	0.68	0.67	0.27	0.27	
					4.68	4.40	2.62	1.23	0.66	0.78	0.28	0.29	
585	1414.	5.08	86.4		4.26	4.01	2.58	1.14	0.65	0.64	0.24	0.24	
					4.36	4.11	2.40	1.13	0.61	0.73	0.26	0.27	
586	1378.	4.91	86.7		4.11	3.85	2.49	1.12	0.65	0.63	0.25	0.25	
					4.20	3.95	2.31	1.10	0.60	0.71	0.27	0.29	
587	1354.	4.80	86.9		3.99	3.75	2.42	1.10	0.64	0.63	0.25	0.25	
					4.09	3.84	2.25	1.08	0.60	0.71	0.27	0.29	
588	1357.	5.00	88.2		4.08	3.83	2.44	1.10	0.65	0.65	0.28	0.27	
					4.17	3.93	2.34	1.14	0.64	0.73	0.29	0.30	
589	1317.	4.58	87.9		3.79	3.55	2.28	1.06	0.64	0.63	0.27	0.26	
					3.89	3.66	2.17	1.08	0.61	0.70	0.29	0.29	
590	1215.	3.99	88.0		3.27	3.08	2.02	0.99	0.61	0.59	0.27	0.26	
					3.35	3.16	1.89	0.98	0.57	0.63	0.28	0.29	
591	1083.	3.33	88.3		2.68	2.54	1.70	0.88	0.57	0.54	0.26	0.25	
					2.75	2.59	1.57	0.86	0.53	0.57	0.28	0.28	
592	943.	2.68	89.0		2.12	2.00	1.38	0.76	0.52	0.50	0.27	0.24	
					2.18	2.06	1.28	0.74	0.49	0.52	0.28	0.29	

[a]Top value, P_{5j} (90°); bottom value, P_{5k} (270°).
[b]Pressure unavailable; exhausted to ambient.
[d]Static test of transducer efficiency.

TABLE III.—Continued.

(a) Continued.

Run	$\dot{w}$, g/s	P_o, MPa	T_o, K	P_0, MPa	Pressure at pressure tap locations 1 to 7, MPa								P_e, MPa
					P_1	P_2	P_3	P_4	P_5	(a)	P_6	P_7	
593	1472.	5.65	87.3	(b)	4.65	4.36	2.80	1.20	0.68	0.68	0.26	0.28	(b)
					4.73	4.45	2.62	1.22	0.65	0.79	0.28	0.29	
594	1415.	5.14	86.0		4.26	4.01	2.57	1.12	0.63	0.63	0.23	0.23	
					4.35	4.09	2.36	1.11	0.59	0.72	0.25	0.26	
595	1300.	4.37	85.8		3.62	3.41	2.20	1.00	0.58	0.57	0.22	0.22	
					3.71	3.48	2.00	0.97	0.54	0.64	0.24	0.26	
599	1451.	5.40	87.6		4.52	4.28	2.82	1.30	0.74	0.75	0.30	0.29	
					4.43	4.16	2.47	1.21	0.69	0.79	0.32	0.29	
600	1380.	4.94	87.7		4.21	3.98	2.62	1.21	0.70	0.70	0.28	0.24	
					4.15	3.90	2.29	1.12	0.64	0.73	0.30	0.26	
601	1300.	4.52	88.2		3.84	3.64	2.42	1.16	0.69	0.67	0.28	0.24	
					3.79	3.55	2.12	1.07	0.62	0.68	0.31	0.25	
602	1206.	3.97	88.3		3.33	3.16	2.12	1.05	0.64	0.61	0.28	0.23	
					3.29	3.08	1.86	0.97	0.59	0.63	0.30	0.25	
603	1277.	4.44	86.2		3.59	3.39	2.16	0.99	0.58	0.57	0.23	0.21	
					3.57	3.34	1.97	0.98	0.55	0.62	0.25	0.24	
604	1175.	3.73	85.4		3.03	2.88	1.88	0.90	0.54	0.52	0.21	0.19	
					3.03	2.83	1.69	0.86	0.50	0.54	0.23	0.20	
605	1017.	2.90	85.4		2.37	2.24	1.50	0.77	0.48	0.45	0.21	0.18	
					2.36	2.22	1.34	0.72	0.44	0.47	0.22	0.19	
606	877.	2.28	85.6		1.82	1.73	1.18	0.64	0.42	0.40	0.20	0.17	
					1.39	1.70	1.06	0.60	0.39	0.41	0.21	0.17	
607	784.	1.87	85.2		1.47	1.40	0.97	0.54	0.37	0.35	0.19	0.15	
					1.47	1.38	0.88	0.51	0.34	0.36	0.19	0.16	
608	681.	1.51	85.9		1.18	1.13	0.79	0.46	0.34	0.32	0.19	0.15	
					1.18	1.11	0.73	0.45	0.32	0.33	0.19	0.16	
609	857.	5.36	78.0		5.02	4.89	4.21	3.04	2.33	2.43	0.87	0.19	
					5.07	4.94	4.17	3.11	2.40	2.53	1.00	0.25	
610	1200.	4.06	88.4	3.74	3.25	3.07	2.05	1.02	0.63	0.60	0.27	0.22	0.23
					3.21	3.01	1.86	0.97	0.59	0.65	0.29	0.26	
611	1101.	3.51	88.5	3.25	2.80	2.63	1.79	0.92	0.59	0.56	0.26	0.20	0.21
					2.77	2.60	1.62	0.87	0.54	0.59	0.28	0.24	
612	964.	2.81	88.8	2.60	2.23	2.11	1.46	0.80	0.53	0.50	0.25	0.19	0.19
					2.21	2.08	1.32	0.76	0.49	0.53	0.27	0.23	
613	784.	1.98	88.9	1.84	1.57	1.49	1.06	0.63	0.45	0.43	0.23	0.17	0.16
					1.55	1.46	0.96	0.60	0.42	0.45	0.25	0.20	
614	648.	1.52	91.1	1.41	1.22	1.16	0.86	0.56	0.44	0.42	0.25	0.16	0.15
					1.20	1.14	0.79	0.54	0.41	0.44	0.25	0.19	
615	547.	1.22	92.3	1.14	0.98	0.94	0.72	0.51	0.42	0.41	0.25	0.14	0.14
					0.97	0.93	0.68	0.50	0.40	0.43	0.25	0.20	

[a]Top value, P_{5j} (90°); bottom value, P_{5k} (270°).
[b]Pressure unavailable; exhausted to ambient.

TABLE III.—Continued.

(a) Continued.

Run	$\dot{w}$, g/s	P_c, MPa	T_o, K	P_0, MPa	Pressure at pressure tap locations 1 to 7, MPa								P_e, MPa
					P_1	P_2	P_3	P_4	P_5	(a)	P_6	P_7	
616	1365.	5.04	85.9	4.65	4.16	3.91	2.51	1.10	0.62	0.60	0.22	0.21	0.22
					4.08	3.81	2.36	1.10	0.59	0.70	0.24	0.24	
617	1304.	4.64	85.5	4.28	3.75	3.53	2.29	1.04	0.59	0.56	0.21	0.19	0.21
					3.68	3.45	2.12	1.01	0.55	0.65	0.23	0.23	
618	1186.	3.93	85.5	3.63	3.13	2.96	1.95	0.93	0.55	0.52	0.20	0.18	0.20
					3.08	2.88	1.78	0.89	0.50	0.58	0.22	0.22	
619	1031.	3.10	85.7	2.86	2.46	2.32	1.56	0.79	0.49	0.46	0.19	0.17	0.18
					2.42	2.26	1.41	0.75	0.44	0.50	0.21	0.21	
620	864.	2.27	85.9	2.10	1.79	1.69	1.16	0.63	0.42	0.40	0.19	0.16	0.16
					1.76	1.64	1.05	0.60	0.38	0.43	0.20	0.22	
621	1439.	5.58	85.5	5.14	4.60	4.30	2.75	1.17	0.63	0.60	0.22	0.21	0.23
					4.54	4.17	2.54	1.16	0.61	0.72	0.24	0.26	
622	1346.	4.96	84.9	4.58	4.01	3.77	2.41	1.06	0.59	0.55	0.19	0.19	0.21
					3.98	3.65	2.20	1.03	0.54	0.64	0.22	0.24	
623	1230.	4.24	84.9	3.92	3.38	3.18	2.06	0.95	0.55	0.52	0.19	0.18	0.19
					3.35	3.07	1.84	0.90	0.49	0.57	0.21	0.22	
624	1129.	3.66	85.2	3.38	2.89	2.72	1.79	0.87	0.51	0.48	0.19	0.18	0.18
					2.88	2.63	1.59	0.81	0.46	0.52	0.21	0.21	
625	994.	2.93	85.7	2.71	2.29	2.16	1.45	0.74	0.47	0.44	0.19	0.17	0.17
					2.28	2.09	1.29	0.69	0.42	0.47	0.21	0.22	
626	1149.	5.12	106.4	4.77	4.28	4.01	2.87	1.73	1.31	1.32	0.78	0.37	0.35
					4.31	4.00	2.76	1.75	1.31	1.39	0.82	0.38	
627	1064.	4.55	106.5	4.24	3.78	3.55	2.60	1.65	1.29	1.30	0.77	0.35	0.33
					3.81	3.54	2.49	1.66	1.28	1.34	0.81	0.36	
628	956.	3.86	106.4	3.61	3.23	3.04	2.29	1.54	1.24	1.24	0.73	0.32	0.29
					3.21	3.02	2.13	1.52	1.22	1.24	0.77	0.33	
629	807.	3.05	106.4	2.86	2.56	2.43	1.90	1.37	1.16	1.15	0.68	0.27	0.25
					2.54	2.41	1.77	1.35	1.13	1.17	0.72	0.30	
630	645.	2.33	106.7	2.19	1.99	1.90	1.56	1.22	1.08	1.09	0.63	0.22	0.21
					1.97	1.89	1.48	1.21	1.06	1.09	0.68	0.26	
631	403.	6.98	245.0	6.66	6.46	6.26	5.35	3.85	2.92	3.01	1.06	0.27	0.35
					6.41	6.20	5.19	3.94	3.08	3.23	1.40	0.32	
632	376.	6.19	242.2	5.90	5.68	5.50	4.72	3.47	2.67	2.69	0.99	0.25	0.32
					5.65	5.45	4.57	3.50	2.76	2.90	1.25	0.29	
633	360.	5.82	240.6	5.55	5.32	5.15	4.41	3.25	2.52	2.54	0.93	0.23	0.30
					5.30	5.11	4.30	3.31	2.62	2.75	1.19	0.28	
634	340.	5.55	240.6	5.29	5.05	4.89	4.19	3.10	2.41	2.43	0.89	0.22	0.29
					5.03	4.85	4.08	3.14	2.49	2.61	1.13	0.26	
635	285.	4.68	238.3	4.46	4.24	4.10	3.51	2.62	2.06	2.08	0.76	0.17	0.24
					4.22	4.07	3.41	2.64	2.10	2.20	0.95	0.23	

[a]Top value, P_{5j} (90°); bottom value, P_{5k} (270°).

TABLE III.—Continued.

(a) Continued.

Run	$\dot{w}$, g/s	P_o, MPa	T_o, K	P_0, MPa	Pressure at pressure tap locations 1 to 7, MPa								P_e, MPa
					P_1	P_2	P_3	P_4	P_5	(a)	P_6	P_7	
636	226.	3.68	230.7	3.50	3.34	3.23	2.76	2.08	1.65	1.67	0.60	0.13	0.19
					3.31	3.20	2.67	2.08	1.67	1.75	0.75	0.20	
637	170.	2.76	224.1	2.63	2.48	2.41	2.06	1.56	1.25	1.27	0.45	0.09	0.14
					2.46	2.38	1.98	1.55	1.26	1.31	0.56	0.15	
638	106.	1.82	225.9	1.73	1.61	1.56	1.33	1.02	0.82	0.84	0.29	0.07	0.11
					1.60	1.54	1.29	1.01	0.82	0.86	0.36	0.13	
639	104.	1.85	234.7	1.76	1.63	1.59	1.36	1.04	0.84	0.85	0.29	0.07	0.11
					1.62	1.57	1.32	1.03	0.84	0.87	0.36	0.12	
640	76.	1.37	235.7	1.31	1.21	1.17	1.00	0.76	0.62	0.63	0.21	0.07	0.10
					1.20	1.15	0.97	0.76	0.62	0.65	0.27	0.08	
641	54.	1.03	234.0	0.98	0.91	0.88	0.75	0.57	0.46	0.47	0.15	0.08	0.10
					0.90	0.86	0.73	0.57	0.47	0.49	0.20	0.09	
642	328.	5.58	272.1	5.31	5.09	4.95	4.23	3.11	2.41	2.40	0.89	0.26	0.31
					5.05	4.89	4.12	3.16	2.51	2.63	1.16	0.27	
643	278.	4.70	262.9	4.47	4.25	4.14	3.53	2.63	2.06	2.06	0.76	0.20	0.26
					4.22	4.09	3.43	2.64	2.11	2.21	0.96	0.24	
644	225.	3.84	257.5	3.67	3.47	3.38	2.88	2.16	1.71	1.72	0.63	0.16	0.21
					3.44	3.34	2.80	2.16	1.74	1.81	0.79	0.19	
645	158.	2.75	250.7	2.62	2.47	2.41	2.05	1.55	1.24	1.26	0.45	0.10	0.15
					2.45	2.39	1.99	1.54	1.25	1.30	0.56	0.15	
646	100.	1.82	250.0	1.74	1.62	1.58	1.34	1.03	0.83	0.84	0.29	0.08	0.11
					1.61	1.56	1.31	1.01	0.83	0.86	0.36	0.12	
647	62.	1.21	253.0	1.15	1.06	1.04	0.88	0.68	0.55	0.55	0.18	0.08	0.10
					1.06	1.03	0.86	0.67	0.55	0.58	0.23	0.05	
648	275.	5.12	281.8	4.89	4.68	4.56	3.87	2.87	2.24	2.28	0.83	0.20	0.27
					4.65	4.52	3.79	2.90	2.30	2.38	1.03	0.23	
649	244.	4.37	271.1	4.17	3.95	3.85	3.26	2.42	1.91	1.95	0.71	0.17	0.23
					3.93	3.82	3.20	2.46	1.97	2.05	0.89	0.23	
650	194.	3.38	258.9	3.22	3.04	2.97	2.51	1.88	1.50	1.52	0.55	0.13	0.18
					3.03	2.94	2.46	1.90	1.53	1.58	0.69	0.16	
651	131.	2.29	249.5	2.18	2.05	2.00	1.70	1.29	1.04	1.05	0.37	0.09	0.13
					2.04	1.98	1.66	1.28	1.05	1.08	0.46	0.12	
652	89.	1.63	254.3	1.55	1.44	1.42	1.20	0.92	0.75	0.75	0.26	0.08	0.11
					1.44	1.40	1.17	0.91	0.75	0.77	0.32	0.06	
653	63.	1.22	257.1	1.17	1.08	1.06	0.90	0.69	0.56	0.56	0.19	0.08	0.10
					1.08	1.04	0.88	0.69	0.57	0.58	0.24	0.08	
654	1081.	4.23	103.1	3.94	3.55	3.35	2.39	1.46	1.11	1.12	0.65	0.34	0.31
					3.51	3.25	2.30	1.44	1.09	1.15	0.69	0.34	
655	997.	3.73	103.3	3.48	3.11	2.95	2.16	1.38	1.08	1.08	0.64	0.32	0.29
					3.08	2.87	2.06	1.35	1.05	1.09	0.68	0.32	

[a]Top value, P_{5j} (90°); bottom value, P_{5k} (270°).

TABLE III.—Continued.

(a) Continued.

Run	$\dot{w}$, g/s	P_o, MPa	T_o, K	P_0, MPa	Pressure at pressure tap locations 1 to 7, MPa								P_e, MPa
					P_1	P_2	P_3	P_4	P_5	(a)	P_6	P_7	
656	860.	2.99	103.2	2.80	2.51	2.39	1.81	1.24	1.00	1.00	0.59	0.28	0.25
					2.46	2.33	1.72	1.20	0.98	1.01	0.64	0.28	
657	745.	2.45	103.2	2.30	2.07	1.98	1.55	1.12	0.94	0.93	0.56	0.25	0.22
					2.04	1.93	1.48	1.09	0.92	0.94	0.60	0.27	
658	668.	2.12	102.8	1.99	1.78	1.71	1.37	1.02	0.88	0.87	0.52	0.23	0.20
					1.76	1.67	1.31	1.00	0.86	0.88	0.57	0.24	
659	552.	1.70	103.1	1.60	1.45	1.41	1.17	0.93	0.83	0.84	0.48	0.19	0.17
					1.44	1.38	1.13	0.92	0.82	0.84	0.53	0.23	
660	1089.	4.91	109.4	4.59	4.15	3.95	2.93	1.92	1.52	1.54	0.92	0.40	0.36
					4.08	3.89	2.84	1.86	1.50	1.55	0.96	0.38	
661	980.	4.20	109.1	3.94	3.56	3.39	2.58	1.75	1.43	1.44	0.87	0.36	0.32
					3.50	3.35	2.49	1.71	1.40	1.44	0.91	0.34	
662	891.	3.65	108.8	3.43	3.11	2.97	2.30	1.63	1.37	1.37	0.83	0.32	0.29
					3.07	2.94	2.23	1.60	1.34	1.37	0.88	0.33	
663	751.	2.91	108.6	2.74	2.50	2.40	1.92	1.45	1.26	1.26	0.76	0.28	0.25
					2.48	2.36	1.88	1.43	1.24	1.26	0.81	0.28	
664	646.	2.41	108.0	2.28	2.08	2.01	1.65	1.31	1.17	1.18	0.69	0.24	0.21
					2.08	2.00	1.63	1.30	1.16	1.17	0.76	0.27	
665	547.	2.03	107.9	1.93	1.78	1.73	1.46	1.21	1.11	1.12	0.65	0.21	0.18
					1.77	1.72	1.45	1.21	1.10	1.11	0.71	0.21	
666	421.	1.64	107.8	1.56	1.47	1.43	1.27	1.11	1.01	1.03	0.56	0.17	0.15
					1.46	1.43	1.27	1.12	1.01	1.04	0.61	0.20	
667	1028.	4.73	111.4	4.44	3.98	3.79	2.85	1.92	1.57	1.57	0.95	0.38	0.35
					4.00	3.75	2.80	1.89	1.55	1.61	1.01	0.38	
668	956.	4.30	111.7	4.03	3.65	3.49	2.68	1.87	1.57	1.56	0.94	0.36	0.33
					3.67	3.45	2.63	1.84	1.54	1.59	1.00	0.37	
669	832.	3.55	111.3	3.35	3.05	2.93	2.32	1.72	1.48	1.49	0.89	0.31	0.28
					3.06	2.89	2.26	1.68	1.46	1.49	0.95	0.32	
670	660.	2.69	110.8	2.54	2.34	2.26	1.88	1.51	1.36	1.37	0.80	0.25	0.22
					2.33	2.24	1.84	1.48	1.33	1.36	0.86	0.26	
671	522.	2.12	110.2	2.01	1.87	1.82	1.58	1.34	1.24	1.24	0.69	0.20	0.18
					1.87	1.81	1.56	1.33	1.22	1.24	0.77	0.21	
673	611.	5.09	135.2	4.85	4.60	4.48	3.87	3.02	2.43	2.49	1.06	0.32	0.31
					4.60	4.47	3.85	3.06	2.49	2.59	1.24	0.32	
674	509.	4.22	131.3	4.03	3.82	3.73	3.21	2.49	2.06	2.08	0.91	0.26	0.26
					3.82	3.72	3.17	2.47	2.06	2.13	1.03	0.27	
676	219.	2.43	129.4	2.32	2.18	2.12	1.82	1.42	1.16	1.16	0.47	0.12	0.13
					2.18	2.11	1.79	1.40	1.15	1.19	0.55	0.13	
677	138.	1.74	137.0	1.66	1.55	1.50	1.28	1.00	0.82	0.82	0.31	0.08	0.11
					1.55	1.49	1.27	0.99	0.82	0.84	0.35	0.12	

[a]Top value, P_{5j} (90°); bottom value, P_{5k} (270°).

TABLE III.—Continued.

(a) Continued.

Run	$\dot{w}$, g/s	P_o, MPa	T_o, K	P_0, MPa	Pressure at pressure tap locations 1 to 7, MPa								P_e, MPa
					P_1	P_2	P_3	P_4	P_5	(a)	P_6	P_7	
678	1165.	6.40	118.7	6.00	5.54	5.28	4.00	2.64	2.13	2.17	1.29	0.47	0.44
					5.53	5.23	3.95	2.67	2.16	2.25	1.42	0.49	
679	1069.	5.77	118.9	5.42	4.97	4.74	3.68	2.57	2.13	2.17	1.25	0.44	0.41
					4.97	4.71	3.62	2.57	2.14	2.22	1.40	0.46	
680	983.	5.22	118.8	4.91	4.49	4.31	3.41	2.48	2.10	2.13	1.21	0.41	0.38
					4.50	4.27	3.34	2.46	2.10	2.17	1.36	0.42	
681	843.	4.36	118.5	4.12	3.79	3.66	3.00	2.32	2.03	2.06	1.12	0.35	0.33
					3.78	3.61	2.92	2.29	2.02	2.07	1.29	0.36	
682	663.	3.51	119.0	3.35	3.12	3.02	2.61	2.19	1.94	2.01	0.96	0.28	0.27
					3.11	3.00	2.56	2.17	1.96	2.01	1.12	0.29	
683	1368.	5.72	96.5	5.30	4.77	4.48	3.00	1.48	0.81	0.94	0.50	0.35	0.34
					4.75	4.38	2.91	1.47	0.92	1.05	0.52	0.36	
684	1230.	4.78	96.9	4.43	3.94	3.69	2.53	1.35	0.82	0.90	0.49	0.32	0.31
					3.89	3.62	2.41	1.30	0.86	0.97	0.51	0.34	
685	1083.	3.90	97.3	3.62	3.19	3.01	2.12	1.22	0.80	0.85	0.48	0.29	0.28
					3.15	2.95	1.99	1.15	0.80	0.88	0.50	0.31	
686	901.	2.96	98.5	2.76	2.43	2.30	1.69	1.07	0.78	0.80	0.48	0.26	0.24
					2.40	2.25	1.59	1.02	0.77	0.82	0.49	0.27	
687	1034.	6.24	124.4	5.88	5.45	5.24	4.15	2.99	2.56	2.60	1.35	0.44	0.43
					5.43	5.19	4.07	3.00	2.58	2.66	1.62	0.46	
688	906.	5.40	123.6	5.10	4.73	4.57	3.72	2.83	2.47	2.51	1.25	0.39	0.38
					4.72	4.53	3.63	2.81	2.48	2.54	1.51	0.41	
689	793.	4.65	122.7	4.42	4.12	3.98	3.33	2.65	2.34	2.40	1.13	0.34	0.33
					4.10	3.95	3.25	2.64	2.37	2.42	1.36	0.36	
690	649.	3.80	121.6	3.61	3.40	3.30	2.86	2.40	2.02	2.10	0.95	0.28	0.27
					3.39	3.28	2.81	2.40	2.10	2.18	1.11	0.29	
691	495.	2.93	120.4	2.80	2.66	2.60	2.34	1.87	1.50	1.57	0.72	0.21	0.21
					2.65	2.59	2.31	1.87	1.57	1.61	0.82	0.22	
692	377.	2.28	117.9	2.17	2.07	2.00	1.74	1.41	1.14	1.18	0.54	0.17	0.17
					2.06	2.00	1.70	1.38	1.17	1.21	0.61	0.21	
693	128.	1.76	112.9	1.67	1.56	1.48	1.28	1.05	0.87	0.88	0.40	0.14	0.14
					1.55	1.48	1.24	1.02	0.87	0.92	0.46	0.15	
694	114.	1.26	111.2	1.20	1.12	1.08	0.94	0.74	0.60	0.61	0.23	0.07	0.11
					1.11	1.07	0.91	0.72	0.59	0.63	0.28	0.09	
695	96.	1.09	113.3	1.04	0.95	0.91	0.79	0.62	0.50	0.51	0.18	0.08	0.11
					0.94	0.91	0.76	0.60	0.50	0.53	0.22	0.07	
696	441.	5.92	176.2	5.65	5.40	5.25	4.50	3.35	2.56	2.65	0.94	0.23	0.31
					5.39	5.23	4.38	3.35	2.66	2.83	1.10	0.29	
697	384.	5.47	185.7	5.22	4.97	4.83	4.14	3.09	2.37	2.45	0.87	0.21	0.28
					4.95	4.81	4.01	3.07	2.45	2.59	1.02	0.26	

[a]Top value, P_{5j} (90°); bottom value, P_{5k} (270°).

TABLE III.—Continued.

(a) Continued.

Run	$\dot{w}$, g/s	P_o, MPa	T_o, K	P_0, MPa	Pressure at pressure tap locations 1 to 7, MPa								P_e, MPa
					P_1	P_2	P_3	P_4	P_5	(a)	P_6	P_7	
698	275.	4.02	184.8	3.83	3.63	3.51	3.01	2.29	1.78	1.84	0.66	0.14	0.21
					3.61	3.49	2.90	2.24	1.80	1.90	0.79	0.19	
699	184.	2.74	183.0	2.61	2.45	2.37	2.03	1.56	1.23	1.27	0.46	0.10	0.15
					2.43	2.35	1.94	1.52	1.23	1.30	0.55	0.16	
[e]700	354.	6.16	281.1	5.86	5.67	5.50	4.72	3.49	2.61	2.65	0.95	0.72	0.77
					5.62	5.46	4.61	3.51	2.78	2.88	1.31	0.66	
701	324.	5.53	273.1	5.27	5.04	4.90	4.20	3.13	2.37	2.41	0.86	0.64	0.70
					5.01	4.86	4.10	3.13	2.49	2.58	1.17	0.59	
702	275.	4.65	263.7	4.43	4.21	4.09	3.50	2.63	2.02	2.06	0.73	0.54	0.60
					4.18	4.06	3.41	2.62	2.10	2.17	0.97	0.49	
703	219.	3.70	255.7	3.52	3.32	3.23	2.77	2.10	1.63	1.66	0.59	0.43	0.48
					3.30	3.21	2.69	2.07	1.67	1.72	0.77	0.38	
704	150.	2.62	252.3	2.50	2.34	2.29	1.95	1.50	1.18	1.20	0.43	0.31	0.35
					2.34	2.27	1.90	1.47	1.20	1.22	0.54	0.27	
705	101.	1.91	268.7	1.83	1.70	1.66	1.42	1.09	0.87	0.88	0.31	0.23	0.27
					1.70	1.66	1.38	1.07	0.88	0.90	0.39	0.23	
706	610.	4.91	84.0	4.54	4.01	3.80	2.57	1.34	0.84	0.79	0.68	0.76	0.79
					3.98	3.73	2.44	1.29	0.83	0.83	0.62	0.76	
707	570.	4.70	85.0	4.36	3.81	3.60	2.43	1.29	0.83	0.77	0.66	0.75	0.77
					3.80	3.56	2.33	1.25	0.81	0.81	0.61	0.74	
708	1345.	5.22	89.6	4.84	4.30	4.06	2.78	1.51	0.99	0.96	0.83	0.92	0.93
					4.27	4.01	2.67	1.47	0.98	0.98	0.76	0.91	
709	1231.	4.41	89.3	4.09	3.57	3.37	2.32	1.26	0.82	0.78	0.66	0.74	0.78
					3.55	3.33	2.19	1.21	0.80	0.81	0.61	0.74	
710	1212.	4.33	89.4	4.01	3.51	3.31	2.28	1.24	0.81	0.77	0.65	0.73	0.77
					3.49	3.26	2.16	1.19	0.80	0.80	0.61	0.73	
711	1077.	3.55	89.5	3.29	2.86	2.71	1.91	1.10	0.75	0.72	0.61	0.68	0.71
					2.84	2.67	1.80	1.05	0.73	0.74	0.58	0.68	
712	918.	2.75	90.0	2.55	2.22	2.11	1.53	0.93	0.67	0.66	0.56	0.62	0.65
					2.21	2.09	1.44	0.90	0.66	0.67	0.54	0.61	
713	1358.	4.95	85.3	4.57	4.00	3.75	2.44	1.15	0.54	0.58	0.42	0.51	0.54
					3.98	3.72	2.34	1.10	0.61	0.66	0.34	0.52	
714	1320.	4.69	85.4	4.33	3.74	3.51	2.28	1.08	0.47	0.55	0.31	0.40	0.44
					3.74	3.49	2.19	1.03	0.57	0.63	0.25	0.42	
715	1161.	3.74	85.5	3.45	2.96	2.78	1.86	0.93	0.47	0.49	0.27	0.34	0.38
					2.95	2.76	1.74	0.87	0.50	0.54	0.24	0.36	
716	986.	2.80	85.7	2.59	2.20	2.08	1.42	0.75	0.43	0.43	0.25	0.30	0.35
					2.20	2.05	1.32	0.70	0.43	0.46	0.24	0.31	
717	811.	2.02	87.0	1.87	1.59	1.51	1.06	0.61	0.39	0.38	0.26	0.29	0.32
					1.59	1.49	0.99	0.57	0.39	0.41	0.25	0.29	

[a]Top value, P_{5j} (90°); bottom value, P_{5k} (270°).
[e]Runs above 700 are connected to vent system.

TABLE III.—Continued.

(a) Concluded.

Run	$\dot{w}$, g/s	P_o, MPa	T_o, K	P_0, MPa	Pressure at pressure tap locations 1 to 7, MPa								P_e, MPa
					P_1	P_2	P_3	P_4	P_5	(a)	P_6	P_7	
718	290.	3.70	153.3	3.53	3.32	3.23	2.74	2.10	1.64	1.68	0.62	0.37	0.45
					3.33	3.23	2.70	2.09	1.69	1.71	0.71	0.33	
719	1400.	5.42	89.5	5.01	4.38	4.14	2.76	1.33	0.72	0.76	0.38	0.45	0.50
					4.40	4.10	2.59	1.25	0.71	0.80	0.36	0.47	
720	1265.	4.60	90.3	4.25	3.68	3.49	2.35	1.20	0.69	0.71	0.36	0.42	0.46
					3.70	3.45	2.21	1.12	0.67	0.73	0.36	0.42	
721	1050.	3.41	92.5	3.16	2.72	2.59	1.81	1.03	0.68	0.67	0.39	0.40	0.44
					2.74	2.56	1.71	0.97	0.65	0.68	0.39	0.39	
722	782.	2.27	96.2	2.12	1.83	1.75	1.31	0.86	0.66	0.65	0.41	0.37	0.40
					1.85	1.75	1.26	0.85	0.66	0.67	0.43	0.36	

(b) Hydrogen

Run	$\dot{w}$, g/s	P_o, MPa	T_o, K	P_0, MPa	Pressure at pressure tap locations 1 to 7, MPa								P_e, MPa
					P_1	P_2	P_3	P_4	P_5	(a)	P_6	P_7	
724	51.	3.63	281.6	3.54	3.30	3.23	2.73	2.04	1.57	1.63	0.60	0.38	0.45
					3.31	3.22	2.71	2.05	1.62	1.68	0.69	0.36	
725	45.	3.15	277.8	3.07	2.85	2.79	2.36	1.78	1.38	1.42	0.52	0.33	0.40
					2.86	2.78	2.34	1.77	1.41	1.46	0.60	0.32	
726	35.	2.49	270.9	2.43	2.25	2.20	1.87	1.41	1.10	1.13	0.40	0.28	0.33
					2.25	2.19	1.84	1.40	1.12	1.16	0.47	0.27	
727	28.	2.03	272.5	1.98	1.83	1.79	1.52	1.16	0.91	0.93	0.32	0.23	0.28
					1.83	1.78	1.50	1.15	0.91	0.94	0.37	0.22	
728	22.	1.66	274.7	1.62	1.50	1.46	1.25	0.95	0.75	0.77	0.26	0.20	0.24
					1.50	1.46	1.23	0.94	0.75	0.77	0.30	0.21	
729	15.	1.20	273.6	1.17	1.07	1.04	0.89	0.68	0.54	0.55	0.19	0.15	0.18
					1.07	1.04	0.88	0.68	0.54	0.56	0.22	0.17	
730	211.	1.68	23.7	1.60	1.37	1.29	0.97	0.65	0.49	0.48	0.31	0.33	0.36
					1.38	1.28	0.93	0.63	0.48	0.51	0.31	0.33	
731	193.	1.47	23.5	1.40	1.20	1.13	0.86	0.59	0.46	0.45	0.28	0.30	0.33
					1.20	1.12	0.82	0.58	0.44	0.47	0.29	0.30	
732	47.	1.47	74.5	1.43	1.30	1.26	1.08	0.83	0.66	0.66	0.23	0.20	0.23
					1.29	1.26	1.05	0.83	0.65	0.67	0.26	0.20	
734	287.	2.81	24.8	2.65	2.26	2.11	1.53	0.94	0.64	0.65	0.35	0.39	0.43
					2.28	2.10	1.45	0.91	0.64	0.68	0.37	0.39	
[f]735	306.	3.19	25.3	3.01	2.58	2.41	1.74	1.05	0.72	0.72	0.40	0.45	0.49
					2.60	2.40	1.65	1.02	0.72	0.76	0.41	0.44	

[a]Top value, P_{5j} (90°); bottom value, P_{5k} (270°).
[f]Duplicated runs; flow stopped and restarted.

TABLE III.—Continued.

(b) Continued.

Run	$\dot{w}$, g/s	P_o, MPa	T_o, K	P_0, MPa	Pressure at pressure tap locations 1 to 7, MPa								P_e, MPa
					P_1	P_2	P_3	P_4	P_5	(a)	P_6	P_7	
[f]736	305.	3.18	25.4	3.00	2.57	2.40	1.73	1.06	0.72	0.73	0.39	0.41	0.46
					2.60	2.39	1.65	1.02	0.72	0.76	0.40	0.41	
[f]737	296.	2.97	25.1	2.81	2.39	2.23	1.61	0.98	0.67	0.68	0.37	0.40	0.45
					2.41	2.22	1.53	0.95	0.67	0.72	0.38	0.40	
[f]738	292.	2.99	25.6	2.84	2.39	2.23	1.62	1.00	0.69	0.69	0.37	0.39	0.45
					2.41	2.22	1.54	0.97	0.69	0.73	0.39	0.39	
[f]739	265.	2.60	26.8	2.46	2.11	1.96	1.47	0.96	0.72	0.72	0.40	0.38	0.44
					2.12	1.96	1.40	0.95	0.72	0.75	0.42	0.39	
[f]740	264.	2.61	27.1	2.47	2.11	1.97	1.48	0.97	0.73	0.73	0.40	0.36	0.43
					2.13	1.96	1.41	0.96	0.73	0.76	0.42	0.37	
[f]741	253.	2.19	23.9	2.07	1.75	1.61	1.19	0.75	0.53	0.54	0.32	0.36	0.40
					1.76	1.61	1.12	0.74	0.53	0.57	0.33	0.36	
[f]742	252.	2.18	24.0	2.06	1.74	1.61	1.19	0.75	0.53	0.54	0.31	0.33	0.38
					1.75	1.60	1.12	0.74	0.54	0.57	0.32	0.33	
[f]743	231.	1.81	23.2	1.71	1.44	1.32	0.98	0.63	0.45	0.46	0.28	0.32	0.37
					1.45	1.32	0.92	0.62	0.45	0.48	0.29	0.33	
[f]744	230.	1.81	23.3	1.71	1.44	1.33	0.99	0.64	0.46	0.47	0.27	0.31	0.35
					1.45	1.33	0.93	0.63	0.46	0.49	0.28	0.31	
[f]745	213.	1.54	22.6	1.45	1.21	1.12	0.85	0.55	0.40	0.41	0.26	0.30	0.34
					1.22	1.12	0.79	0.54	0.14	0.43	0.27	0.31	
[f]746	213.	1.54	22.7	1.46	1.22	1.13	0.85	0.56	0.41	0.41	0.26	0.29	0.34
					1.23	1.12	0.80	0.55	0.16	0.44	0.27	0.30	
[f]747	191.	1.32	22.4	1.25	1.05	0.97	0.73	0.49	0.37	0.37	0.25	0.29	0.34
					1.04	0.96	0.69	0.49	0.36	0.40	0.26	0.31	
[f]748	195.	1.33	22.6	1.25	1.05	0.97	0.74	0.50	0.37	0.37	0.25	0.28	0.32
					1.05	0.97	0.69	0.49	0.37	0.40	0.26	0.29	
749	194.	1.29	22.2	1.21	1.01	0.93	0.71	0.48	0.23	0.11	0.25	0.29	0.33
					1.01	0.94	0.66	0.21	0.35	0.29	0.21	0.15	
750	193.	1.28	22.2	1.21	1.02	0.93	0.71	0.48	0.27	0.11	0.24	0.28	0.32
					1.01	0.93	0.66	0.22	0.35	0.30	0.24	0.17	
751	178.	1.15	22.3	1.08	0.91	0.83	0.64	0.45	0.33	0.12	0.22	0.25	0.29
					0.89	0.83	0.60	0.23	0.33	0.30	0.24	0.17	
752	107.	1.27	30.4	1.22	1.00	0.94	0.77	0.57	0.36	0.12	0.23	0.26	0.30
					0.99	0.94	0.73	0.23	0.44	0.30	0.25	0.17	
754	191.	1.25	22.2	1.18	0.99	0.91	0.70	0.47	0.35	0.36	0.09	0.12	0.33
					0.98	0.91	0.65	0.47	0.35	0.12	0.26	0.19	
755	159.	0.96	21.9	0.91	0.76	0.70	0.55	0.40	0.32	0.32	0.10	0.12	0.28
					0.74	0.70	0.52	0.40	0.31	0.13	0.23	0.22	
756	30.	0.87	53.0	0.84	0.75	0.72	0.62	0.48	0.39	0.39	0.13	0.15	0.20
					0.74	0.72	0.59	0.48	0.38	0.33	0.16	0.24	

[a]Top value, P_{5j} (90°); bottom value, P_{5k} (270°).
[f]Duplicated runs; flow stopped and restarted.

TABLE III.—Continued.

(b) Continued.

Run	$\dot{w}$, g/s	P_o, MPa	T_o, K	P_0, MPa	Pressure at pressure tap locations 1 to 7, MPa								P_e, MPa
					P_1	P_2	P_3	P_4	P_5	(a)	P_6	P_7	
757	28.	0.88	72.9	0.84	0.75	0.72	0.62	0.48	0.38	0.38	0.13	0.17	0.20
					0.74	0.72	0.59	0.48	0.37	0.41	0.15	0.21	
759	167.	1.02	22.2	0.96	0.81	0.74	0.58	0.42	0.33	0.33	0.22	0.25	0.28
					0.79	0.74	0.55	0.41	0.32	0.36	0.23	0.26	
760	154.	0.92	22.5	0.87	0.73	0.68	0.54	0.40	0.32	0.32	0.21	0.24	0.27
					0.71	0.68	0.51	0.39	0.31	0.35	0.22	0.26	
761	30.	0.91	55.7	0.88	0.79	0.75	0.65	0.50	0.40	0.40	0.13	0.16	0.17
					0.77	0.75	0.62	0.50	0.39	0.43	0.16	0.15	
763	303.	3.11	27.3	2.95	2.49	2.31	1.70	1.08	0.77	0.79	0.43	0.37	0.44
					2.52	2.31	1.61	1.05	0.79	0.83	0.45	0.38	
764	254.	3.25	30.3	3.10	2.54	2.36	1.76	1.15	0.86	0.89	0.48	0.37	0.47
					2.58	2.39	1.72	1.17	0.92	0.98	0.53	0.39	
830	17.	1.26	258.4	1.24	1.16	1.11	0.97	0.73	0.59	0.59	0.19	0.17	0.20
					1.14	1.11	0.94	0.73	0.59	0.60	0.24	0.17	
831	25.	1.88	270.0	1.84	1.73	1.68	1.45	1.10	0.88	0.89	0.29	0.22	0.26
					1.71	1.67	1.42	1.09	0.88	0.88	0.36	0.24	
832	37.	2.69	274.5	2.64	2.48	2.42	2.07	1.56	1.24	1.27	0.43	0.28	0.35
					2.47	2.41	2.03	1.55	1.25	1.24	0.53	0.29	
833	53.	3.71	273.3	3.64	3.44	3.36	2.84	2.12	1.66	1.72	0.60	0.39	0.47
					3.42	3.35	2.81	2.13	1.70	1.71	0.74	0.38	
834	60.	4.11	271.4	4.03	3.83	3.74	3.17	2.35	1.83	1.90	0.66	0.43	0.52
					3.81	3.73	3.12	2.36	1.87	1.90	0.82	0.42	
835	66.	4.51	275.6	4.43	4.20	4.10	3.47	2.56	1.98	2.07	0.72	0.48	0.57
					4.15	4.06	3.42	2.58	2.04	2.10	0.90	0.47	
836	69.	4.58	266.5	4.49	4.28	4.17	3.54	2.61	2.02	2.09	0.73	0.50	0.59
					4.22	4.13	3.48	2.62	2.08	2.16	0.92	0.50	
837	231.	2.07	24.0	1.96	1.70	1.58	1.18	0.75	0.56	0.5[illegible]	0.30	0.37	0.[illegible]3
					1.64	1.53	1.11	0.73	0.53	0.59	0.32	0.40	
838	232.	2.05	24.1	1.95	1.69	1.57	1.18	0.75	0.56	0.54	0.29	0.35	0.42
					1.63	1.52	1.10	0.73	0.53	0.59	0.32	0.38	
841	228.	2.00	23.9	1.89	1.64	1.52	1.15	0.73	0.55	0.53	0.29	0.37	0.44
					1.58	1.47	1.06	0.71	0.51	0.58	0.32	0.40	
842	229.	1.99	23.7	1.89	1.63	1.51	1.14	0.72	0.54	0.52	0.27	0.34	0.41
					1.57	1.47	1.05	0.70	0.51	0.58	0.30	0.37	
843	259.	2.55	24.8	2.42	2.10	1.96	1.46	0.90	0.66	0.64	0.33	0.41	0.49
					2.04	1.90	1.35	0.87	0.62	0.70	0.37	0.45	
844	261.	2.54	24.7	2.41	2.09	1.94	1.45	0.89	0.65	0.62	0.32	0.38	0.46
					2.03	1.89	1.34	0.85	0.61	0.69	0.35	0.41	
845	282.	2.88	24.7	2.73	2.37	2.21	1.61	0.96	0.69	0.67	0.33	0.40	0.48
					2.31	2.16	1.51	0.93	0.65	0.73	0.36	0.44	

[a]Top value, P_{5j} (90°); bottom value, P_{5k} (270°).

TABLE III.—Continued.

(b) Concluded.

Run	$\dot{w}$, g/s	P_o, MPa	T_o, K	P_0, MPa	Pressure at pressure tap locations 1 to 7, MPa								P_e, MPa
					P_1	P_2	P_3	P_4	P_5	(a)	P_6	P_7	
846	281.	2.89	25.1	2.74	2.38	2.21	1.61	0.96	0.69	0.67	0.33	0.37	0.46
					2.32	2.15	1.52	0.94	0.66	0.74	0.36	0.41	
847	297.	3.17	25.1	3.00	2.61	2.44	1.76	1.03	0.73	0.71	0.35	0.41	0.49
					2.56	2.38	1.67	1.00	0.69	0.78	0.38	0.45	
848	297.	3.17	25.3	3.00	2.61	2.43	1.76	1.04	0.74	0.72	0.34	0.38	0.47
					2.55	2.38	1.67	1.01	0.70	0.78	0.38	0.42	
849	306.	3.29	25.0	3.12	2.71	2.53	1.82	1.06	0.74	0.72	0.34	0.39	0.48
					2.66	2.47	1.73	1.03	0.71	0.79	0.38	0.43	
850	284.	2.85	24.5	2.70	2.33	2.17	1.57	0.93	0.66	0.64	0.30	0.35	0.44
					2.28	2.11	1.49	0.91	0.63	0.70	0.34	0.39	
851	256.	2.32	23.6	2.19	1.87	1.73	1.27	0.77	0.56	0.54	0.25	0.30	0.38
					1.82	1.69	1.19	0.75	0.52	0.59	0.29	0.35	
852	233.	1.93	23.1	1.82	1.55	1.43	1.06	0.66	0.49	0.47	0.22	0.28	0.36
					1.50	1.39	0.99	0.64	0.45	0.52	0.26	0.32	
853	216.	1.71	22.7	1.61	1.36	1.25	0.94	0.59	0.44	0.43	0.22	0.28	0.35
					1.31	1.21	0.86	0.57	0.41	0.48	0.25	0.32	
854	197.	1.42	22.5	1.33	1.12	1.02	0.79	0.51	0.39	0.38	0.19	0.25	0.32
					1.08	1.00	0.72	0.50	0.36	0.43	0.22	0.29	
855	178.	1.21	22.4	1.14	0.96	0.87	0.69	0.46	0.36	0.35	0.18	0.23	0.30
					0.92	0.85	0.62	0.45	0.33	0.41	0.21	0.28	
856	184.	1.28	22.0	1.21	1.02	0.93	0.72	0.47	0.37	0.36	0.18	0.23	0.30
					0.98	0.90	0.65	0.46	0.33	0.41	0.21	0.28	
857	166.	1.09	22.1	1.02	0.86	0.78	0.62	0.42	0.34	0.33	0.17	0.22	0.29
					0.82	0.76	0.56	0.41	0.31	0.38	0.20	0.26	
858	297.	3.01	24.3	2.84	2.47	2.30	1.65	0.97	0.68	0.65	0.30	0.35	0.44
					2.41	2.23	1.57	0.94	0.64	0.72	0.33	0.39	

(c) Nitrogen with helium gas injection[g]

[h]765	150.	2.65	259.5	2.57	2.38	2.33	1.98	1.52	1.20	1.22	0.48	0.30	0.36
					2.38	2.32	1.96	1.51	1.22	1.25	0.54	0.15	
766	147.	2.69	263.6	2.61	2.43	2.38	2.05	1.65	5.02	5.02	0.42	0.31	0.36
					2.43	2.36	2.00	1.56	5.01	1.26	0.50	5.00	
767	147.	2.70	263.2	2.63	2.44	2.39	2.06	1.69	6.29	6.29	0.40	0.32	0.37
					2.44	2.38	2.03	1.68	6.26	1.27	0.44	6.26	
768	147.	2.71	263.1	2.64	2.45	2.40	2.08	1.73	7.84	7.84	0.39	0.32	0.37
					2.45	2.39	2.05	1.71	7.81	1.27	0.43	7.80	
[h]771	275.	2.47	201.3	2.33	1.95	1.85	1.26	0.71	0.34	0.41	0.28	0.32	0.34
					1.96	1.84	1.21	0.72	0.31	0.41	0.08	0.32	
772	266.	2.49	202.0	2.36	2.01	1.91	1.39	1.03	4.92	4.92	0.30	0.32	0.34
					2.01	1.90	1.33	1.00	4.89	0.42	0.08	4.88	

[a]Top value, P_{5j} (90°); bottom value, P_{5k} (270°).
[g]See figure 35.
[h]Without helium injection.

TABLE III.—Continued.

(c) Concluded.

Run	$\dot{w}$, g/s	P_o, MPa	T_o, K	P_0, MPa	Pressure at pressure tap locations 1 to 7, MPa								P_e, MPa
					P_1	P_2	P_3	P_4	P_5	(a)	P_6	P_7	
773	261.	2.48	202.7	2.35	2.01	1.92	1.42	1.09	6.31	6.31	0.31	0.32	0.34
					2.02	1.90	1.36	1.05	6.28	0.44	0.08	6.25	
774	258.	2.50	204.2	2.37	2.04	1.95	1.47	1.18	7.72	7.72	0.32	0.34	0.35
					2.04	1.93	1.41	1.13	7.69	0.47	0.08	7.65	
775	257.	2.54	206.7	2.42	2.08	1.99	1.51	1.22	7.71	7.71	0.34	0.35	0.37
					2.08	1.97	1.46	1.20	7.68	0.52	0.08	7.64	

(d) Hydrogen with helium gas injection[g]

[i]783	33.	2.56	298.7	2.51	2.36	2.31	1.97	1.49	1.17	1.20	0.44	0.25	0.33
					2.37	2.31	1.95	1.48	1.20	1.20	0.49	0.26	
[i]784	58.	4.19	297.1	4.11	3.90	3.81	3.22	2.39	1.85	1.90	0.72	0.43	0.51
					3.91	3.80	3.22	2.42	1.93	1.98	0.82	0.44	
[i]785	74.	5.02	284.9	4.91	4.76	4.65	3.95	2.91	2.22	2.25	0.86	0.57	0.63
					4.75	4.62	3.92	2.94	2.33	2.42	1.03	0.58	
[i]786	56.	3.76	274.5	3.68	3.46	3.39	2.88	2.15	1.67	1.70	0.63	0.41	0.48
					3.47	3.38	2.85	2.15	1.72	1.77	0.73	0.42	
[i]787	41.	2.83	272.5	2.78	2.60	2.55	2.17	1.64	1.28	1.31	0.48	0.31	0.37
					2.61	2.54	2.14	1.62	1.31	1.32	0.54	0.31	
[i]788	27.	1.92	269.6	1.88	1.76	1.72	1.46	1.11	0.88	0.89	0.31	0.22	0.27
					1.76	1.71	1.44	1.10	0.89	0.90	0.36	0.23	
[i]789	17.	1.30	272.4	1.27	1.18	1.15	0.98	0.75	0.60	0.60	0.21	0.15	0.19
					1.18	1.15	0.97	0.75	0.60	0.61	0.24	0.16	
[i]790	239.	2.18	24.2	2.08	1.81	1.71	1.26	0.81	0.58	0.56	0.36	0.40	0.42
					1.83	1.70	1.25	0.82	0.58	0.60	0.37	0.40	
[i]791	238.	2.17	24.5	2.07	1.80	1.70	1.25	0.80	0.58	0.56	0.34	0.36	0.39
					1.82	1.69	1.24	0.81	0.57	0.59	0.35	0.36	
792	240.	2.34	24.9	2.24	1.99	1.88	1.47	1.12	5.80	5.80	0.38	0.40	0.43
					1.99	1.87	1.44	1.10	5.78	0.67	0.39	5.76	
793	240.	2.33	24.9	2.24	1.98	1.87	1.46	1.11	5.81	5.82	0.35	0.37	0.40
					1.98	1.85	1.42	1.09	5.79	0.66	0.36	5.77	
794	285.	3.28	26.6	3.15	2.84	2.70	2.11	1.55	5.79	5.79	0.41	0.47	0.49
					2.82	2.66	2.03	1.40	5.77	0.88	0.40	5.74	
795	285.	3.27	26.7	3.14	2.82	2.68	2.09	1.54	5.79	5.79	0.38	0.43	0.46
					2.80	2.63	2.01	1.39	5.77	0.87	0.38	5.75	
[i]796	268.	2.89	26.4	2.76	2.47	2.34	1.79	1.22	0.73	0.66	0.42	0.41	0.45
					2.46	2.31	1.73	1.12	0.73	0.80	0.44	0.42	
[i]797	269.	2.87	26.2	2.75	2.45	2.32	1.77	1.20	0.73	0.66	0.41	0.39	0.43
					2.44	2.29	1.71	1.11	0.72	0.79	0.43	0.39	

[a]Top value, P_{5j} (90°); bottom value, P_{5k} (270°).
[g]See figure 35.
[i]Without helium injection; mass flow $\dot{w}$ data seem 12 percent low.

TABLE III.—Continued.

(d) Continued.

Run	$\dot{w}$, g/s	P_o, MPa	T_o, K	P_0, MPa	Pressure at pressure tap locations 1 to 7, MPa								P_c, MPa
					P_1	P_2	P_3	P_4	P_5	(a)	P_6	P_7	
[i]798	289.	3.27	26.3	3.13	2.79	2.65	1.99	1.32	0.77	0.69	0.43	0.42	0.47
					2.78	2.61	1.94	1.23	0.77	0.84	0.46	0.43	
[i]799	290.	3.26	26.4	3.12	2.78	2.63	1.98	1.31	0.77	0.69	0.42	0.40	0.45
					2.77	2.60	1.93	1.22	0.77	0.84	0.45	0.41	
800	273.	2.94	25.1	2.81	2.52	2.40	1.88	1.41	5.80	5.79	0.39	0.43	0.46
					2.50	2.35	1.80	1.28	5.77	0.76	0.40	5.75	
801	273.	2.92	25.1	2.80	2.50	2.38	1.86	1.40	5.81	5.81	0.36	0.40	0.44
					2.49	2.34	1.79	1.27	5.78	0.75	0.37	5.76	
802	207.	1.89	24.0	1.81	1.62	1.54	1.25	1.02	5.80	5.80	0.32	0.35	0.38
					1.60	1.52	1.20	0.93	5.77	0.58	0.34	5.76	
803	209.	1.88	23.9	1.80	1.61	1.53	1.24	1.01	5.80	5.80	0.30	0.32	0.36
					1.59	1.50	1.19	0.91	5.77	0.56	0.31	5.76	
804	167.	1.52	24.4	1.47	1.27	1.20	1.00	0.85	5.79	5.80	0.25	0.27	0.32
					1.26	1.19	0.96	0.79	5.77	0.52	0.26	5.75	
805	49.	1.66	63.9	1.62	1.51	1.47	1.30	1.13	5.82	5.82	0.20	0.22	0.25
					1.50	1.46	1.27	1.08	5.80	0.78	0.22	5.78	
[i]806	219.	1.84	23.7	1.75	1.53	1.44	1.12	0.80	0.50	0.46	0.31	0.33	0.37
					1.52	1.40	1.06	0.72	0.48	0.53	0.31	0.34	
[i]807	224.	1.84	23.4	1.75	1.52	1.43	1.11	0.79	0.49	0.45	0.29	0.31	0.35
					1.51	1.40	1.06	0.71	0.47	0.52	0.30	0.33	
[i]808	121.	1.51	31.9	1.47	1.25	1.18	0.97	0.75	0.52	0.50	0.26	0.27	0.31
					1.24	1.16	0.93	0.70	0.51	0.56	0.27	0.28	
[i]809	57.	1.61	78.1	1.56	1.45	1.40	1.22	0.99	0.70	0.68	0.22	0.20	0.23
					1.44	1.39	1.19	0.96	0.70	0.74	0.26	0.24	
[i]810	217.	2.43	31.2	2.34	2.10	2.00	1.64	1.29	0.99	0.95	0.45	0.34	0.40
					2.09	1.98	1.60	1.23	0.98	1.03	0.51	0.34	
[i]811	196.	2.18	31.1	2.10	1.89	1.80	1.51	1.22	0.97	0.94	0.42	0.31	0.37
					1.88	1.78	1.48	1.17	0.96	1.01	0.48	0.32	
[i]812	169.	1.89	31.4	1.83	1.66	1.59	1.37	1.14	0.92	0.92	0.37	0.28	0.34
					1.65	1.57	1.34	1.11	0.94	0.97	0.43	0.29	
[i]813	43.	1.37	65.2	1.33	1.22	1.18	1.02	0.83	0.59	0.58	0.19	0.18	0.22
					1.20	1.17	0.99	0.80	0.59	0.64	0.22	0.21	
[i]814	205.	3.55	41.5	3.45	3.17	3.06	2.57	2.03	1.43	1.43	0.59	0.42	0.50
					3.18	3.04	2.54	1.95	1.48	1.55	0.68	0.42	
[i]815	178.	3.05	40.4	2.96	2.72	2.63	2.24	1.80	1.33	1.33	0.53	0.36	0.44
					2.72	2.61	2.21	1.74	1.36	1.42	0.60	0.37	
[i]816	103.	2.46	46.7	2.39	2.20	2.13	1.84	1.50	1.08	1.09	0.39	0.31	0.36
					2.20	2.12	1.81	1.45	1.12	1.17	0.45	0.32	
[i]817	65.	1.60	93.6	1.56	1.43	1.39	1.20	0.97	0.69	0.69	0.22	0.19	0.23
					1.42	1.38	1.17	0.95	0.70	0.74	0.26	0.21	

[a]Top value, P_{5j} (90°); bottom value, P_{5k} (270°).
[i]Without helium injection; mass flow $\dot{w}$ data seem 12 percent low.

TABLE III.—Continued.

(d) Concluded.

Run	$\dot{w}$, g/s	P_o, MPa	T_o, K	P_0, MPa	Pressure at pressure tap locations 1 to 7, MPa								P_e, MPa
					P_1	P_2	P_3	P_4	P_5	(a)	P_6	P_7	
[i]818	265.	3.28	31.8	3.15	2.84	2.69	2.10	1.54	1.09	1.04	0.53	0.41	0.48
					2.83	2.66	2.06	1.46	1.08	1.15	0.60	0.42	
[i]819	240.	2.86	31.6	2.75	2.46	2.34	1.87	1.41	1.05	1.01	0.49	0.37	0.44
					2.46	2.31	1.83	1.35	1.04	1.10	0.56	0.38	
[i]820	199.	2.30	31.3	2.21	2.00	1.90	1.57	1.25	0.99	0.96	0.43	0.32	0.38
					1.99	1.88	1.53	1.21	0.99	1.03	0.50	0.32	
[i]821	57.	1.70	70.0	1.66	1.53	1.47	1.28	1.03	0.72	0.72	0.23	0.21	0.25
					1.52	1.47	1.25	1.00	0.74	0.78	0.27	0.23	
822	265.	3.16	31.0	3.04	2.73	2.59	2.07	1.64	5.79	5.79	0.40	0.45	0.48
					2.71	2.54	2.02	1.57	5.77	1.10	0.43	5.75	
823	241.	2.78	30.8	2.68	2.40	2.28	1.84	1.50	5.80	5.80	0.36	0.40	0.43
					2.38	2.24	1.80	1.44	5.78	1.04	0.40	5.76	
824	198.	2.28	31.0	2.21	1.97	1.88	1.57	1.34	5.82	5.82	0.32	0.35	0.38
					1.96	1.85	1.54	1.29	5.79	1.00	0.37	5.77	
825	59.	1.75	79.5	1.70	1.58	1.53	1.35	1.18	5.83	5.84	0.20	0.22	0.25
					1.56	1.52	1.31	1.15	5.81	0.81	0.22	5.80	
826	245.	3.14	33.7	3.03	2.75	2.62	2.18	1.83	5.79	5.80	0.47	0.47	0.51
					2.74	2.58	2.13	1.73	5.77	1.29	0.49	5.76	
827	220.	2.71	33.1	2.62	2.37	2.27	1.91	1.64	5.80	5.80	0.41	0.41	0.45
					2.36	2.23	1.87	1.57	5.77	1.21	0.45	5.76	
828	192.	2.32	32.8	2.25	2.04	1.96	1.68	1.48	5.80	5.81	0.35	0.36	0.39
					2.03	1.93	1.65	1.43	5.78	1.14	0.40	5.76	
829	58.	1.71	68.2	1.67	1.54	1.49	1.32	1.18	5.83	5.83	0.20	0.23	0.26
					1.52	1.48	1.29	1.15	5.80	0.80	0.22	5.79	

[a]Top value, P_{5j} (90°); bottom value, P_{5k} (270°).
[i]Without helium injection; mass flow $\dot{w}$ data seem 12 percent low.

TABLE IV.—FLOW RATE AND PRESSURE DROP DATA FOR STRAIGHT CYLINDRICAL SEAL, FULLY ECCENTRIC POSITION

[Where two values are given, the top value is for the 0° circumferential position (minimum clearance) and the bottom value is for the 180° circumferential position (maximum clearance).][a]

(a) Nitrogen

Run	$\dot{w}$, g/s	P_o, MPa	T_o, K	P_0, MPa	Pressure at pressure tap locations 1 to 7, MPa								P_e, MPa
					P_1	P_2	P_3	P_4	P_5	(b)	P_6	P_7	
864	193.	3.24	262.4	3.15	3.14	3.11	2.66	1.87	1.17	1.49	0.40	0.41	0.43
					2.86	2.76	2.35	1.91	1.62	1.49	0.91	0.22	
865	332.	5.62	274.4	5.48	5.56	5.52	4.86	3.40	1.96	2.53	0.69	0.70	0.71
					5.08	4.91	4.19	3.36	2.82	2.62	1.60	0.39	
866	298.	4.87	265.2	4.73	4.75	4.71	4.11	2.89	1.72	2.19	0.61	0.62	0.64
					4.35	4.20	3.58	2.88	2.43	2.28	1.38	0.35	
867	269.	4.35	260.0	4.24	4.25	4.21	3.64	2.56	1.55	1.97	0.55	0.56	0.58
					3.89	3.75	3.20	2.58	2.18	2.05	1.23	0.32	
868	242.	3.90	256.7	3.80	3.79	3.75	3.23	2.27	1.40	1.78	0.49	0.50	0.52
					3.46	3.34	2.85	2.30	1.95	1.82	1.10	0.28	
869	156.	2.52	244.5	2.45	2.43	2.40	2.02	1.42	0.93	1.17	0.33	0.34	0.37
					2.21	2.14	1.83	1.48	1.26	1.19	0.71	0.20	
870	113.	1.88	247.6	1.83	1.81	1.78	1.50	1.07	0.71	0.88	0.26	0.27	0.29
					1.64	1.59	1.36	1.10	0.94	0.89	0.53	0.18	
871	71.	1.27	261.3	1.24	1.21	1.19	1.00	0.72	0.49	0.59	0.20	0.21	0.22
					1.11	1.07	0.92	0.74	0.64	0.60	0.35	0.14	
872	135.	2.39	276.2	2.33	2.32	2.28	1.92	1.32	0.83	1.10	0.15	0.16	0.11
					2.10	2.04	1.74	1.41	1.20	1.12	0.68	0.12	
873	329.	5.54	281.6	5.39	5.47	5.43	4.81	3.40	1.97	2.42	0.32	0.34	0.18
					5.01	4.82	4.11	3.29	2.76	2.59	1.58	0.27	
874	308.	5.06	274.7	4.93	4.97	4.92	4.33	3.04	1.78	2.23	0.29	0.32	0.17
					4.54	4.37	3.73	3.00	2.51	2.38	1.44	0.22	
875	254.	4.20	268.0	4.09	4.11	4.07	3.54	2.45	1.44	1.90	0.23	0.26	0.15
					3.74	3.60	3.07	2.47	2.08	1.96	1.18	0.20	
876	236.	3.85	263.2	3.75	3.75	3.71	3.20	2.22	1.32	1.75	0.22	0.24	0.14
					3.41	3.28	2.80	2.26	1.91	1.80	1.08	0.18	
877	195.	3.17	256.7	3.09	3.08	3.04	2.60	1.81	1.12	1.46	0.18	0.20	0.13
					2.80	2.70	2.30	1.87	1.58	1.49	0.89	0.15	
878	101.	1.68	244.5	1.63	1.60	1.57	1.33	0.93	0.62	0.78	0.12	0.13	0.11
					1.46	1.41	1.20	0.98	0.83	0.79	0.47	0.07	
879	73.	1.26	249.6	1.23	1.20	1.17	0.99	0.70	0.47	0.59	0.10	0.12	0.11
					1.09	1.06	0.90	0.74	0.63	0.60	0.35	0.04	
880	57.	1.03	253.2	1.00	0.97	0.95	0.80	0.58	0.40	0.48	0.10	0.11	0.11
					0.88	0.86	0.73	0.60	0.51	0.49	0.28	0.05	
881	505.	3.52	84.2	3.30	3.21	3.11	2.21	1.04	0.49	0.48	0.18	0.18	0.14
					2.57	2.31	1.47	0.81	0.51	0.49	0.24	0.21	
882	418.	2.99	84.1	2.81	2.71	2.62	1.85	0.91	0.46	0.44	0.17	0.18	0.14
					2.16	1.95	1.26	0.72	0.47	0.45	0.23	0.18	

[a]As logged, 180° = minimum clearance, as presented in this table, 180° = maximum clearance.
[b]Top value, P_{5j} (90°); bottom value, P_{5k} (270°).

TABLE IV.—Continued.

(a) Continued.

Run	$\dot{w}$, g/s	P_o, MPa	T_o, K	P_0, MPa	Pressure at pressure tap locations 1 to 7, MPa								P_e, MPa
					P_1	P_2	P_3	P_4	P_5	(b)	P_6	P_7	
883	320.	2.38	84.3	2.24	2.15	2.07	1.47	0.75	0.40	0.39	0.16	0.16	0.13
					1.71	1.56	1.03	0.61	0.41	0.41	0.23	0.19	
884	217.	1.69	83.9	1.59	1.52	1.45	1.04	0.56	0.33	0.32	0.14	0.15	0.12
					1.19	1.11	0.75	0.47	0.34	0.34	0.21	0.17	
885	151.	1.24	84.3	1.17	1.11	1.06	0.78	0.44	0.28	0.28	0.13	0.14	0.12
					0.88	0.83	0.58	0.39	0.30	0.30	0.21	0.16	
886	112.	1.00	86.2	0.94	0.89	0.84	0.64	0.39	0.26	0.27	0.13	0.14	0.12
					0.71	0.68	0.50	0.37	0.30	0.28	0.22	0.13	
887	1274.	3.91	85.0	3.66	3.54	3.43	2.38	1.05	0.47	0.49	0.17	0.18	0.15
					2.78	2.50	1.60	0.86	0.53	0.52	0.23	0.18	
888	1171.	3.34	85.1	3.13	3.01	2.92	2.03	0.94	0.44	0.45	0.16	0.17	0.14
					2.35	2.12	1.38	0.77	0.49	0.48	0.22	0.20	
889	1025.	2.66	85.2	2.50	2.39	2.31	1.61	0.78	0.40	0.39	0.15	0.16	0.14
					1.86	1.69	1.12	0.66	0.43	0.43	0.22	0.19	
890	869.	2.01	85.5	1.89	1.80	1.73	1.21	0.62	0.34	0.34	0.14	0.15	0.13
					1.38	1.28	0.87	0.54	0.37	0.37	0.21	0.16	
891	770.	1.61	84.9	1.52	1.45	1.39	0.98	0.51	0.29	0.30	0.12	0.14	0.13
					1.11	1.04	0.71	0.46	0.32	0.33	0.20	0.17	
925	1359.	4.67	89.9	4.39	4.27	4.14	2.75	1.18	0.59	0.68	0.26	0.24	0.17
					3.50	3.13	2.05	1.11	0.70	0.73	0.35	0.26	
926	1325.	4.49	90.2	4.22	4.09	3.96	2.66	1.18	0.60	0.67	0.26	0.23	0.17
					3.35	3.00	1.97	1.08	0.69	0.71	0.35	0.25	
927	1242.	4.04	90.4	3.80	3.66	3.55	2.45	1.15	0.61	0.63	0.25	0.22	0.16
					3.00	2.69	1.80	1.02	0.66	0.66	0.35	0.24	
928	1128.	3.42	90.5	3.21	3.07	2.96	2.06	1.03	0.57	0.58	0.24	0.21	0.16
					2.50	2.26	1.53	0.90	0.60	0.60	0.34	0.23	
929	1384.	4.69	87.5	4.40	4.28	4.15	2.71	1.09	0.51	0.60	0.21	0.21	0.16
					3.51	3.12	2.03	1.06	0.63	0.66	0.29	0.26	
930	1206.	3.68	87.3	3.46	3.30	3.19	2.17	1.00	0.50	0.52	0.20	0.19	0.15
					2.68	2.41	1.60	0.88	0.55	0.55	0.27	0.21	
931	1063.	2.96	87.4	2.78	2.64	2.55	1.75	0.85	0.46	0.46	0.19	0.18	0.14
					2.12	1.93	1.30	0.75	0.49	0.49	0.26	0.20	
932	917.	2.33	87.7	2.18	2.05	1.98	1.37	0.71	0.41	0.41	0.17	0.16	0.14
					1.64	1.52	1.04	0.63	0.43	0.44	0.26	0.21	
933	751.	1.65	87.5	1.55	1.46	1.40	0.99	0.55	0.34	0.35	0.15	0.14	0.13
					1.17	1.09	0.77	0.50	0.36	0.38	0.24	0.16	
934	627.	1.28	89.2	1.19	1.11	1.06	0.78	0.46	0.31	0.33	0.13	0.13	0.13
					0.90	0.85	0.62	0.44	0.35	0.36	0.25	0.18	
935	1312.	4.51	92.5	4.24	4.06	3.93	2.60	1.15	0.61	0.71	0.28	0.24	0.18
					3.35	3.00	2.00	1.12	0.73	0.76	0.41	0.28	

[b]Top value, P_{5j} (90°); bottom value, P_{5k} (270°).

TABLE IV.—Continued.

(a) Concluded.

Run	$\dot{w}$, g/s	P_o, MPa	T_o, K	P_0, MPa	Pressure at pressure tap locations 1 to 7, MPa								P_e, MPa
					P_1	P_2	P_3	P_4	P_5	(b)	P_6	P_7	
936	1227.	4.05	92.9	3.81	3.67	3.55	2.42	1.15	0.63	0.69	0.28	0.24	0.17
					3.01	2.72	1.84	1.07	0.71	0.73	0.41	0.27	
937	1133.	3.54	92.9	3.33	3.19	3.08	2.13	1.06	0.61	0.65	0.27	0.22	0.17
					2.62	2.37	1.63	0.98	0.67	0.68	0.40	0.26	
938	982.	2.81	92.9	2.64	2.50	2.42	1.70	0.91	0.56	0.59	0.25	0.20	0.15
					2.05	1.88	1.32	0.84	0.61	0.61	0.38	0.23	
939	807.	2.06	93.0	1.94	1.83	1.76	1.27	0.74	0.49	0.52	0.21	0.18	0.14
					1.49	1.40	1.01	0.70	0.54	0.54	0.36	0.21	
940	642.	1.46	93.2	1.37	1.29	1.24	0.92	0.58	0.42	0.45	0.18	0.15	0.13
					1.06	1.01	0.76	0.58	0.47	0.48	0.33	0.18	
[c]941	734.	5.94	140.3	5.76	5.77	5.67	4.67	3.11	1.91	2.99	0.37	0.34	0.22
					5.26	5.13	4.44	3.77	3.38	3.11	1.87	0.36	
[c]942	653.	5.58	141.0	5.42	5.40	5.30	4.40	2.99	1.90	2.75	0.34	0.30	0.20
					4.94	4.83	4.18	3.54	3.06	2.85	1.70	0.32	
[c]943	553.	4.89	138.8	4.75	4.71	4.61	3.85	2.67	1.78	2.38	0.31	0.27	0.18
					4.32	4.23	3.67	3.11	2.60	2.45	1.47	0.29	
[c]944	398.	3.97	139.4	3.86	3.80	3.72	3.13	2.25	1.60	1.92	0.27	0.21	0.15
					3.48	3.40	2.91	2.38	2.02	1.96	1.20	0.20	
[c]945	288.	3.26	146.8	3.16	3.11	3.03	2.54	1.82	1.31	1.53	0.20	0.17	0.13
					2.84	2.77	2.36	1.91	1.60	1.55	0.86	0.16	
[c]946	210.	2.60	154.4	2.52	2.46	2.39	2.01	1.44	1.05	1.21	0.16	0.14	0.12
					2.24	2.18	1.85	1.50	1.26	1.21	0.67	0.14	
[c]947	173.	2.17	148.2	2.10	2.04	1.98	1.66	1.19	0.88	1.00	0.13	0.13	0.12
					1.85	1.81	1.53	1.25	1.05	1.02	0.56	0.08	
[c]948	116.	1.56	161.2	1.50	1.44	1.39	1.17	0.84	0.63	0.71	0.09	0.11	0.12
					1.30	1.27	1.07	0.89	0.74	0.73	0.39	0.10	
[c]949	84.	1.16	159.5	1.10	1.04	1.01	0.84	0.61	0.46	0.52	0.07	0.10	0.12
					0.94	0.92	0.78	0.64	0.53	0.54	0.28	0.06	

(b) Hydrogen

950	34.	2.27	260.4	2.23	2.19	2.14	1.81	1.28	0.91	1.04	0.27	0.30	0.34
					2.01	1.94	1.67	1.32	1.11	1.05	0.58	0.26	
951	63.	4.20	271.1	4.14	4.10	4.05	3.41	2.31	1.53	1.92	0.46	0.53	0.56
					3.77	3.65	3.14	2.46	2.06	1.96	1.12	0.36	
952	53.	3.60	272.3	3.55	3.51	3.46	2.90	1.99	1.34	1.67	0.39	0.46	0.50
					3.23	3.12	2.68	2.11	1.77	1.68	0.95	0.32	
953	46.	3.15	270.3	3.10	3.06	3.00	2.53	1.75	1.20	1.46	0.34	0.40	0.44
					2.80	2.71	2.33	1.84	1.54	1.45	0.83	0.27	

[b]Top value, P_{5j} (90°); bottom value, P_{5k} (270°).

[c]Warm gas or liquid was heated by passing pressurant gas through it with controlled venting. When warm gas was run through the eccentric seal, there seemed to be a region where temperature became uncontrollable (around $P_R = P_o/P_c = 0.8$ for the eccentric seal).

TABLE IV.—Continued.

(b) Continued.

Run	$\dot{w}$, g/s	P_o, MPa	T_o, K	P_0, MPa	Pressure at pressure tap locations 1 to 7, MPa								P_e, MPa
					P_1	P_2	P_3	P_4	P_5	(b)	P_6	P_7	
954	28.	1.95	260.3	1.91	1.86	1.81	1.54	1.09	0.78	0.90	0.22	0.26	0.30
					1.70	1.65	1.41	1.13	0.95	0.90	0.49	0.23	
955	16.	1.17	255.0	1.14	1.09	1.04	0.89	0.64	0.47	0.54	0.16	0.19	0.23
					0.99	0.97	0.83	0.67	0.55	0.55	0.28	0.19	
956	226.	2.07	25.7	1.97	1.87	1.77	1.35	0.89	0.67	0.67	0.36	0.41	0.48
					1.58	1.47	1.11	0.83	0.66	0.71	0.42	0.44	
957	250.	2.47	27.5	2.35	2.23	2.12	1.60	1.01	0.75	0.77	0.36	0.42	0.50
					1.88	1.75	1.32	0.96	0.76	0.81	0.47	0.44	
958	285.	2.82	25.8	2.68	2.54	2.42	1.77	1.03	0.71	0.71	0.37	0.43	0.51
					2.12	1.95	1.41	0.94	0.70	0.76	0.41	0.46	
959	283.	2.83	26.2	2.69	2.54	2.43	1.78	1.04	0.72	0.72	0.35	0.40	0.49
					2.12	1.96	1.42	0.96	0.71	0.77	0.42	0.43	
960	217.	1.72	24.1	1.62	1.51	1.43	1.07	0.68	0.50	0.49	0.30	0.35	0.43
					1.25	1.16	0.85	0.62	0.48	0.54	0.31	0.40	
961	195.	1.45	23.9	1.36	1.26	1.18	0.91	0.59	0.45	0.45	0.25	0.30	0.38
					1.04	0.97	0.72	0.55	0.43	0.50	0.28	0.35	
962	225.	1.79	23.7	1.69	1.57	1.49	1.10	0.68	0.49	0.48	0.29	0.34	0.42
					1.30	1.20	0.87	0.62	0.47	0.53	0.30	0.39	
963	200.	1.46	23.5	1.37	1.26	1.19	0.91	0.58	0.44	0.43	0.24	0.29	0.37
					1.05	0.97	0.71	0.54	0.41	0.48	0.27	0.34	
964	184.	1.29	22.9	1.20	1.10	1.04	0.79	0.52	0.40	0.39	0.24	0.29	0.37
					0.91	0.85	0.62	0.48	0.37	0.44	0.26	0.34	
965	173.	1.16	22.9	1.08	0.98	0.92	0.72	0.48	0.38	0.37	0.22	0.26	0.34
					0.82	0.76	0.57	0.45	0.35	0.43	0.24	0.31	
966	153.	0.99	23.2	0.93	0.84	0.78	0.63	0.44	0.36	0.36	0.19	0.24	0.31
					0.70	0.66	0.50	0.42	0.34	0.41	0.23	0.29	
967	153.	0.99	22.4	0.92	0.84	0.78	0.62	0.43	0.34	0.34	0.22	0.08	0.34
					0.69	0.64	0.48	0.40	0.31	0.39	0.24	0.24	
968	134.	0.81	22.5	0.74	0.67	0.62	0.51	0.37	0.31	0.31	0.18	0.08	0.30
					0.55	0.52	0.40	0.35	0.29	0.36	0.21	0.28	
969	239.	1.98	23.9	1.86	1.74	1.64	1.21	0.73	0.52	0.51	0.28	0.34	0.42
					1.42	1.29	0.94	0.66	0.49	0.56	0.30	0.38	
970	214.	1.65	23.5	1.55	1.43	1.35	1.01	0.63	0.46	0.45	0.24	0.29	0.37
					1.16	1.07	0.79	0.58	0.44	0.51	0.28	0.33	
971	261.	2.32	24.5	2.18	2.05	1.94	1.42	0.84	0.58	0.57	0.29	0.34	0.43
					1.69	1.55	1.11	0.76	0.56	0.63	0.33	0.38	
972	279.	2.67	25.3	2.52	2.39	2.27	1.67	0.98	0.67	0.67	0.35	0.41	0.50
					1.91	1.82	1.31	0.88	0.65	0.72	0.39	0.45	
973	251.	3.00	32.0	2.87	2.74	2.64	2.01	1.34	1.04	1.12	0.36	0.44	0.52
					2.31	2.24	1.75	1.33	1.11	1.16	0.75	0.41	

[b]Top value, P_{5j} (90°); bottom value, P_{5k} (270°).

TABLE IV.—Concluded.

(b) Concluded.

Run	$\dot{w}$, g/s	P_o, MPa	T_o, K	P_0, MPa	Pressure at pressure tap locations 1 to 7, MPa								P_e, MPa
					P_1	P_2	P_3	P_4	P_5	(b)	P_6	P_7	
974	224.	2.64	32.1	2.53	2.41	2.31	1.80	1.25	0.99	1.09	0.32	0.38	0.47
					2.05	1.99	1.60	1.27	1.09	1.13	0.74	0.38	
975	186.	2.15	31.8	2.06	1.96	1.87	1.50	1.10	0.85	1.02	0.26	0.33	0.41
					1.69	1.65	1.38	1.16	1.03	1.06	0.65	0.36	
976	206.	3.39	39.3	3.27	3.17	3.07	2.42	1.66	1.23	1.50	0.40	0.49	0.51
					2.77	2.77	2.26	1.80	1.54	1.52	0.97	0.40	
977	181.	2.87	38.0	2.77	2.67	2.58	2.08	1.47	1.07	1.37	0.34	0.42	0.51
					2.35	2.35	1.96	1.63	1.43	1.39	0.82	0.35	
978	148.	2.30	36.3	2.22	2.12	2.05	1.67	1.21	0.88	1.09	0.30	0.34	0.43
					1.88	1.89	1.61	1.39	1.20	1.11	0.63	0.31	
979	138.	3.30	49.6	3.20	3.12	3.03	2.45	1.69	1.20	1.40	0.39	0.46	0.54
					2.82	2.78	2.30	1.82	1.48	1.43	0.74	0.42	
980	120.	2.84	47.8	2.76	2.67	2.59	2.11	1.49	1.08	1.22	0.34	0.40	0.49
					2.40	2.38	1.97	1.57	1.28	1.26	0.67	0.38	
981	88.	2.26	47.7	2.19	2.10	2.03	1.68	1.21	0.91	0.98	0.27	0.32	0.40
					1.89	1.87	1.55	1.26	1.03	1.04	0.55	0.32	
982	287.	2.71	25.0	2.55	2.42	2.30	1.69	0.98	0.67	0.65	0.35	0.42	0.50
					1.88	1.86	1.29	0.87	0.63	0.71	0.37	0.47	
983	275.	2.47	24.4	2.32	2.18	2.07	1.52	0.89	0.61	0.59	0.31	0.38	0.47
					1.70	1.67	1.15	0.79	0.57	0.65	0.34	0.43	
984	249.	2.06	23.8	1.93	1.79	1.70	1.26	0.75	0.52	0.51	0.28	0.34	0.43
					1.39	1.38	0.95	0.67	0.49	0.57	0.30	0.40	
985	224.	1.71	23.0	1.60	1.47	1.39	1.04	0.65	0.47	0.45	0.28	0.33	0.42
					1.16	1.16	0.79	0.58	0.43	0.51	0.28	0.40	
986	203.	1.44	22.7	1.34	1.23	1.16	0.88	0.56	0.41	0.40	0.24	0.29	0.37
					0.97	0.97	0.67	0.51	0.38	0.46	0.25	0.35	

[b]Top value, P_{5j} (90°); bottom value, P_{5k} (270°).

TABLE V.—FLOW RATE AND PRESSURE DROP DATA FOR STRAIGHT CYLINDRICAL SEAL WITH BACKPRESSURE CONTROL, PARTIALLY ECCENTRIC POSITION[a]

[Where two values are given, the top value is for the 0° circumferential position and the bottom value is for the 180° circumferential position.]

(a) Nitrogen

Run	$\dot{w}$, g/s	P_o, MPa	T_o, K	P_0, MPa	Pressure at pressure tap locations 1 to 7, MPa								P_e, MPa
					P_1	P_2	P_3	P_4	[b]P_5	(c)	P_6	P_7	
514	1386.	5.43	85.8	5.13	4.72	4.53	3.16	1.48	0.78	0.71	0.28	0.44	0.46
					4.37	4.06	2.88	1.72	~~2.77~~	0.64	0.29	0.43	
515	1368.	5.27	87.0	4.98	4.60	4.41	3.01	1.37	0.74	0.69	0.34	0.49	0.51
					4.27	3.95	2.79	1.66	~~2.70~~	0.66	0.33	0.48	
516	1308.	4.83	86.7	4.57	4.16	3.99	2.71	1.26	0.69	0.65	0.31	0.44	0.46
					3.86	3.58	2.53	1.53	~~2.47~~	0.63	0.30	0.44	
517	1377.	5.26	84.6	4.97	4.57	4.38	2.97	1.31	0.68	0.62	0.27	0.42	0.44
					4.24	3.93	2.77	1.61	~~2.68~~	0.60	0.26	0.41	
518	876.	2.32	84.4	2.19	1.94	1.89	1.29	0.69	0.43	0.40	0.23	0.30	0.32
					1.80	1.69	1.21	0.77	~~1.21~~	0.40	0.23	0.29	
519	1290.	4.61	84.5	4.36	3.91	3.73	2.52	1.14	0.69	0.55	0.37	0.40	0.44
					3.67	3.38	2.37	1.38	~~0.08~~	0.56	0.27	0.42	
520	1188.	4.52	85.2	4.30	3.90	3.76	2.75	1.65	1.28	1.15	1.02	1.03	1.09
					3.67	3.44	2.56	1.71	~~0.09~~	1.06	0.96	1.06	
521	1110.	4.61	86.9	4.42	4.06	3.92	3.05	2.10	1.78	1.67	1.56	1.58	1.61
					3.85	3.64	2.88	2.15	~~0.09~~	1.60	1.50	1.59	
522	123.	2.46	295.1	2.41	2.28	2.26	1.84	1.36	1.04	1.05	0.29	0.23	0.28
					2.22	2.16	1.82	1.46	~~0.00~~	1.14	0.40	0.19	
523	227.	4.29	288.9	4.19	4.00	3.93	3.28	2.39	1.84	1.86	0.56	0.47	0.52
					3.91	3.79	3.27	2.58	~~0.00~~	2.00	0.76	0.40	
524	300.	5.52	286.9	5.39	5.18	5.08	4.28	3.08	2.34	2.37	0.75	0.65	0.69
					5.09	4.91	4.26	3.34	~~0.00~~	2.53	1.01	0.56	
525	1282.	4.69	89.2	4.43	4.03	3.88	2.62	1.26	0.69	0.62	0.41	0.52	0.54
					3.72	3.42	2.41	1.33	~~0.00~~	0.58	0.37	0.51	
526	1005.	2.99	89.1	2.83	2.51	2.42	1.61	0.83	0.49	0.45	0.23	0.31	0.35
					2.31	2.13	1.49	0.89	~~0.00~~	0.45	0.24	0.32	
527	723.	1.68	89.1	1.59	1.39	1.37	0.92	0.54	0.35	0.33	0.19	0.21	0.25
					1.28	1.19	0.85	0.57	~~0.00~~	0.34	0.20	0.22	

(b) Hydrogen

496	38.	3.05	299.9	2.98	2.87	2.81	2.38	1.74	1.34	1.38	0.42	0.37	0.40
					2.77	2.68	2.29	1.77	1.47	1.44	0.61	0.29	
497	78.	4.87	306.2	4.76	4.60	4.52	3.85	2.76	2.10	2.16	0.68	0.60	0.64
					4.46	4.32	3.71	2.84	2.33	2.25	0.98	0.49	
498	63.	4.88	304.9	4.78	4.62	4.53	3.86	2.77	2.11	2.18	0.77	0.99	1.01
					4.47	4.33	3.72	2.85	2.34	2.27	1.01	0.98	

[a]Data in these tables were taken *after* the data in previous tables (as a new run), and they should really be listed as 1514, 1515, ..., rather than 514, 515, ...

[b]P_5 values for the 180° circumferential position are questionable at best and should not be used.

[c]Top value, P_{5j} (90°); bottom value, P_{5k} (270°).

TABLE V.—Concluded.

(b) Concluded.

Run	$\dot{w}$, g/s	P_o, MPa	T_o, K	P_0, MPa	Pressure at pressure tap locations 1 to 7, MPa								P_e, MPa
					P_1	P_2	P_3	P_4	P_5	(c)	P_6	P_7	
499	51.	4.00	303.1	3.92	3.78	3.71	3.16	2.30	1.77	1.82	0.56	0.49	0.53
					3.66	3.54	3.05	2.35	1.94	1.89	0.81	0.39	
500	24.	1.91	287.2	1.86	1.77	1.75	1.48	1.10	0.86	0.88	0.27	0.26	0.28
					1.72	1.67	1.44	1.11	0.92	0.92	0.38	0.21	
501	351.	4.60	28.3	4.39	4.07	3.89	2.87	1.60	1.05	1.04	0.54	0.58	0.61
					3.75	3.46	2.51	1.46	1.04	0.98	0.51	0.56	
502	333.	4.54	28.2	4.34	4.04	3.88	2.96	1.88	1.42	1.36	1.18	1.26	1.29
					3.75	3.48	2.62	1.69	1.30	1.27	1.08	1.29	
503	405.	6.03	29.6	5.75	5.39	5.18	3.94	2.15	1.35	1.28	0.64	0.70	0.73
					5.03	4.65	3.41	1.93	1.32	1.20	0.61	0.67	
504	356.	6.17	49.1	5.94	5.59	5.39	4.20	2.57	1.81	1.76	1.14	1.32	1.32
					5.27	4.94	3.80	2.41	1.78	1.68	1.08	1.33	
505	400.	5.94	29.3	5.68	5.29	5.07	3.80	2.15	1.50	1.41	1.20	1.31	1.34
					4.93	4.59	3.37	1.91	1.35	1.29	1.07	1.34	
506	272.	3.45	26.6	3.32	3.07	2.94	2.21	1.46	1.05	0.88	0.48	0.48	0.52
					2.27	2.23	1.75	1.07	0.78	0.77	0.42	0.49	
507	256.	3.64	26.1	3.52	3.29	3.17	2.53	1.92	1.61	1.44	1.27	1.29	1.32
					2.64	2.60	2.13	1.54	1.30	1.29	1.17	1.30	
508	227.	2.33	24.8	2.23	2.04	1.94	1.43	0.95	0.69	0.59	0.33	0.34	0.37
					1.53	1.51	1.15	0.71	0.52	0.52	0.30	0.34	
509	190.	2.44	24.5	2.37	2.23	2.16	1.81	1.51	1.35	1.25	1.16	1.17	1.20
					1.86	1.84	1.61	1.31	1.18	1.18	1.11	1.18	
510	281.	3.49	26.2	3.35	3.09	2.92	2.16	1.38	0.97	0.83	0.44	0.45	0.49
					2.41	2.38	1.74	1.02	0.74	0.72	0.39	0.46	
511	322.	6.32	39.8	6.12	5.80	5.55	4.42	3.00	2.24	2.01	1.10	0.66	0.75
					5.29	5.11	3.89	2.51	1.89	1.82	1.06	0.61	
512	310.	6.02	40.1	5.83	5.49	5.26	4.19	2.88	2.17	1.96	1.25	1.40	1.43
					5.17	4.90	3.72	2.44	1.86	1.80	1.13	1.42	
513	250.	4.77	41.8	4.63	4.35	4.18	3.40	2.49	1.96	1.81	0.97	0.54	0.63
					4.13	3.94	3.10	2.21	1.77	1.71	1.01	0.48	

[c]Top value, P_{5j} (90°); bottom value, P_{5k} (270°).

TABLE VI.—HYDROGEN CHOKED-FLOW DATA[a]

Data											Calculated parameters				
Run	P_o, MPa	$P_{R,o}$ MPa	T_o, K	$T_{R,o}$	P_t/P_o	G, g/cm^2 s	G/G^*	$\dot{w}$	P_t, MPa	$\frac{P_t/P_o}{(P_t/P_o)_{PG}}$	P_t/P_o	$(P_t/P_o)_R$	G, g/cm^2 s	G/G^*	$1 + \psi_Q(T_{R,o})$
1183	3.45	2.669	288	8.73	0.524	251	0.217	0.0373	1.8	0.994	0.5316	1.008	214	0.185	----
1184	3.47	2.684	288	8.73	.524	256	.221	.0381	1.82	.994	.5320	1.009	216	.186	----
1185	4.611	3.567	288	8.73	.515	341	.294	.0507	2.38	.976	.5304	1.006	286	.247	----
1186	3.024	2.339	272.1	8.25	.531	228	.199	.0339	1.6	1.007	.5326	1.010	193	.167	----
1187	2.976	2.302	270.3	8.2	.536	227	.196	.0337	1.6	1.016	.533	1.011	191	.164	----
1188	4.314	3.337	273	8.28	.524	326	.282	.0484	2.26	.994	.5304	1.006	275	.237	----
1189	2.561	1.981	268	8.13	.545	198	.171	.0294	1.4	1.033	.5333	1.011	165	.142	----
1190	2.631	2.035	276.6	8.39	.536	167	.144	.0249	1.41	1.016	.5330	1.011	167	.144	----
1191	3.755	2.905	277.3	8.41	.524	238	.206	.0354	1.97	.994	.5319	1.008	238	.205	----
1192	3.692	2.856	278.8	8.45	.5216	231	.199	.0344	1.93	.989	.5319	1.008	233	.201	----
1193	4.701	3.636	281.2	8.53	.516	292	.252	.0434	2.427	.978	.5304	1.006	295	.255	----
1194	2.017	1.56	269.9	8.18	.546	135	.116	.0201	1.101	1.035	.5338	1.012	129	.112	----
1195	2.972	2.299	33.49	1.015	.2746	1467	1.267	.2174	.816	.521	.2969	.5630	1459	1.259	1.035
1196	3.871	2.994	40.34	1.223	.3126	1339	1.156	.199	1.21	.593	----	----	----	----	1.257
1197	1.192	.922	30.72	.932	.3939	892	.77	.1326	.47	.747	.7121	1.350	605	.522	.987
1198	2.090	1.617	28.95	.878	.2433	1398	1.208	.208	.508	.461	.2553	.4840	1355	1.170	.969
1199	2.832	2.19	27.81	.843	.1475	1696	1.465	.252	.418	.280	.1409	.2671	1731	1.493	.961
1200	3.3	2.552	27.25	.826	.116	1871	1.616	.278	.384	.22	.1034	.1960	1926	1.662	.957
1201	2.84	2.196	32.23	.977	.261	1418	1.224	.21	.74	.495	.2768	.5248	1482	1.2784	1.01
1202	2.00	1.547	70.0	2.122	.508	285.8	.247	.042	1.02	.963	.4776	.9056	279	.241	1.12
1203	4.202	3.25	284.5	8.63	.517	260	.224	.0387	2.17	.980	.5317	1.008	262	.226	----
1204	5.216	4.034	285.8	8.67	.511	321.8	.278	.0478	2.67	.969	.53	1.006	325	.280	----
1205	2.583	1.998	273.5	8.29	.532	166.6	.144	.0247	1.375	1.009	.5332	1.011	165	.142	----
1206	3.505	2.711	29.45	.893	.1898	1853	1.6	.275	.665	.360	.1379	.262	1894	1.634	.974
1207	2.779	2.15	30.32	.919	.2278	1566	1.352	.2327	.633	.432	.2170	.411	1577	1.361	.983
1208	2.488	1.924	37.37	1.133	.274	953.8	.824	.141	.682	.520	----	----	----	----	1.127
1209	2.034	1.573	65.31	1.98	.4664	307.6	.268	.0457	.949	.884	.4754	.901	298	.257	1.127
1210	4.614	3.569	28.65	.869	.1003	2207	1.906	.328	.463	.190	.0821	.1557	2277	1.965	.967
1211	4.123	3.189	29.1	.882	.1122	2050	1.770	.305	.463	.212	.1043	.1978	2124	1.833	.971
1212	4.216	3.261	28.75	.872	.1065	2088	1.803	.31	.449	.202	.0951	.1803	2155	1.859	.968
1213	3.461	2.677	29.46	.893	.1429	1835	1.58	.273	.494	.271	.1406	.2665	1878	1.620	.974
1214	2.137	1.653	31.04	.941	.2884	1266	1.093	.188	.616	.547	.3455	.6551	1240	1.070	.991
1215	1.571	1.215	32.25	.978	.4762	896.7	.774	.133	.748	.903	.6303	1.195	756	.653	1.01
1216	5.797	4.484	28.57	.866	.0766	2506	2.164	.375	.444	.145	.0576	.1093	2599	2.242	.966
1217	4.114	3.182	30.32	.919	.1309	1989	1.718	.296	.538	.248	.1253	.2375	2049	1.768	.981
1218	2.752	2.127	32.34	.981	.2692	1425	1.231	.212	.74	.510	.2937	.5569	1435	1.238	.987
1219	3.602	2.786	30.56	.928	.1581	1833	1.583	.272	.57	.3	.1567	.2971	1869	1.613	.983
1220	2.805	2.17	31.32	.95	.2326	1517	1.310	.225	.652	.441	.2431	.4705	1528	1.318	.995
1221	2.117	1.638	32.21	.977	.312	1185	1.023	.176	.6606	.592	.4145	.7859	1132	0.977	1.01
1222	5.724	----	28.07	.851	.0754	2502	2.161	.372	.431	.143	.0539	.1023	2601	2.245	.963
1223	4.154	3.213	29.79	.903	.1222	2020	1.744	.3	.508	.232	.1143	.2168	2087	1.801	.977
1224	2.709	2.095	31.28	.948	.2398	1495	1.291	.222	.65	.455	.2589	.4909	1490	1.286	.995

[a]From reference 10.

[b]Thermodynamic critical values: pressure, P_c, 1.2928 MN/m^2; density, ρ_c, 0.03143 g/cm^3; temperature, T_c, 32.976 K. Critical value ratio, $\sqrt{P_c \rho_c z_c}$ = 1158 g/cm^2 s (16.44 lbm/in.^{2} s).

1. Report No.	2. Government Accession No.	3. Recipient's Catalog No.
NASA TP-1850		

4. Title and Subtitle	5. Report Date
Straight Cylindrical Seal for High-Performance Turbomachines	June 1987
	6. Performing Organization Code 505-62-21
7. Author(s) Robert C. Hendricks	8. Performing Organization Report No. E-3184
	10. Work Unit No.
9. Performing Organization Name and Address National Aeronautics and Space Administration Lewis Research Center Cleveland, Ohio 44135	11. Contract or Grant No.
	13. Type of Report and Period Covered Technical Paper
12. Sponsoring Agency Name and Address National Aeronautics and Space Administration Washington, D.C. 20546	14. Sponsoring Agency Code

15. Supplementary Notes

The data and information contained herein were released for general use in May 1977.

16. Abstract

A straight cylindrical seal configuration representing the seal for a high-performance turbopump (e.g., the space shuttle main engine fuel pump) was tested under static (*nonrotating*) conditions. The test data included critical mass flux and pressure profiles over a wide range of inlet temperatures and pressures for fluid nitrogen and fluid hydrogen with the seal in concentric and fully eccentric positions. The critical mass fluxes (or leakage rates) for the concentric and fully eccentric configurations were nearly the same when based on stagnation conditions upstream of the seal. The fully eccentric configuration pressure profiles of the gas and liquid were different. Further, the pressure differences between the maximum- and minimum-clearance positions were highly dependent on the geometric conditions, the temperature, and the absolute pressure at both the inlet and the exit. The pressure differences were greatest in the inlet region. The results, although complex, tend to follow the corresponding-states principles for critical flows. Gaseous injection near the seal exit plane significantly altered the pressure profiles and could be used to control turbomachine instabilities. High-pressure, high-temperature hydrogen gas could be used for this purpose in an alternative design.

17. Key Words (Suggested by Author(s))	18. Distribution Statement
Seals; Turbomachines; Fluid mechanics; Space shuttle main engine; Dynamics; Instability	Unclassified–unlimited STAR Category 34

19. Security Classif. (of this report)	20. Security Classif. (of this page)	21. No of pages	22. Price*
Unclassified	Unclassified	75	A04

*For sale by the National Technical Information Service, Springfield, Virginia 22161

NASA-Langley, 1987